UNIVERSITY OF PAVIA

Ph.D. School in Chemical and Pharmaceutical Sciences

XXXII Cycle

Coordinator: Prof. Mauro Freccero

DEVELOPMENT OF BIOCOMPATIBLE MATERIALS FOR THE IMMOBILIZATION OF MACROMOLECULES OF PHARMACEUTICAL INTEREST

Tutor: Prof. Enrica Calleri

Co-tutor: Prof. Giuseppe Tripodo

Ph.D. Thesis by

Marco Corti

2016-2019

SUMMARY

General Introduction……..... **1**
1. Porous Materials and Porous Polymers…… 2
2. Hierarchical Porous Structure……. 4
3. Applicative Fields of Porous Polymers……... 6
4. Polymerized High Internal Phase Emulsions……... 9
5. References……. 22

Project Aims…….. **30**

Chapter 1 – PolyHIPEs Synthesis and DoE Approach……. **33**
1. Introduction…… 35
2. Experimental section…… 38
3. Results and Discussion…… 46
4. Conclusions…… 61
5. References……. 62

Chapter 2 – Polymeric IMERs for Biocatalysis…… **65**
1. Introduction…… 67
2. Experimental section…… 69
3. Results and Discussion…… 76
4. Conclusions…… 83
5. References……. 84

Chapter 3 – Biomedical Applications…… **86**
1. Introduction…… 88
2. Experimental section…… 90
3. Results and Discussion…… 99
4. Conclusions…… 112
5. References……. 113

General Conclusions and Perspective……..... **116**

GENERAL INTRODUCTION

1. Porous materials and porous polymers

According to the most recent literature, porous materials covered a central role in the development of innovative technological tools and scientific signs of progress are often associated with the exploitation of these materials. Moreover, with the emerging of nanomaterials, the fundamental role of the porosity in determining materials properties has emerged. Therefore, porous materials have an essential role in several applications and emerging technological fields due to their numerous advantages such as high superficial areas, open internal structure, and possible tunable pore environment[1, 2]. Considering the diameter, the International Union of Pure and Applied Chemistry (IUPAC) classify the pores of porous materials in three categories: micropores (smaller than 2 nm), mesopores (2-50 nm) and macropores (larger than 50 nm)[3]. Another possible classification of porous materials concerns the chemical nature of pore walls leading to the three distinct classes of skeleton: i) the organic skeleton, including porous polymers and supermolecular organic frameworks among the others; ii) the inorganic skeleton such as porous carbons or mesoporous silica and, iii) the hybrid skeleton of metallorganic frameworks. Porous polymers, as a class of porous material, gained increasing interest from researchers due to their potential to integrate the features of both porous materials and polymers[4, 5]. Porous polymers could be defined as polymeric supports with one or more pores. Even if they typically show more the one pore, polymers with one pore (termed hollow polymers) can be included in this definition[4]. Indeed, compared to other porous materials, porous polymers show relevant advantages including chemical diversity and ease to be processed. Porous polymers can be synthesized in a versatile manner and can be exploited in agreement with the concept of rational materials design. Moreover, different chemical moieties can be incorporated into the polymeric structure by presynthetic modification or by post-production functionalization. Porous polymers could also be modeled into various macroscopical structures by controlling shapes and dimensions more easily compared with other materials. Furthermore, porous polymers are typically associated with good chemical stability because of the covalent bonds in the structure. Therefore, porous polymers have been observed to show very promising properties to be exploited as multifunctional tools to be used as “game-changers” platforms for existing applications and also as innovative materials[6, 7]. Porous polymers have been used since the 1930s in many industrial and scientific fields (ion-exchange resins, food industry, pharmaceutical industry, synthetic chemistry among, in Li-ion batteries, etc.). Besides these, porous polymers show promising potential to be used in developing fields such as gas adsorption capture[8-10], molecular separation[11-13], catalysis[14],

electrochemical energy storage[15], drug delivery[16], sensors[17], enantioseparation[18], proton conduction[19], photoenergy conversion in solar cells[20], and many others[1]. There are several important features that may affect the applications of these materials such as pore structure, size and, geometry, surface functionalities and polymeric framework structure including starting monomer composition. Moreover, to be considered an actual valuable source, the porous polymer should be scalable and cheap by using more sustainable raw materials while retaining high performances[1]. The applicative fields of this kind of materials are described more intensively in the following paragraph.

Table i-1: Properties of porous polymers, zeolites, porous carbons, and MOF[1].

Properties	Porous polymers	Zeolites	Porous carbons	MOFs
Pore size	Micro-, meso- and macropores	Micro-, meso- and macropores	Micro-, meso- and macropores	Micro-, meso- and macropores
Cristallinity	Amorphous	Typically high	Typically amorphous	Typically high
Thermal stability	Medium to high	High	High	Low to medium
Chemical stability	Medium to excellent	Good (acid/base sensitive)	Excellent	Poor to good
Chemical diversity	Very high	Medium	Low to medium	Very high
Structural diversity	Very high	High	High	Very high
Processing	Good	Insoluble, but technologies for films, pellets etc.	Insoluble, but technologies for films, pellets etc.	Insoluble, but technologies for films, pellets etc.
Unique selling points	Low density, simultaneous synthesis and processing, commercially proven technology	Low cost, widely used	Good conductivity, commercially proven technology	Structural and chemical control for a diverse range of materials

2. Hierarchical porous structure

An important feature of porous polymers and porous materials, in general, is represented by the possible hierarchical structure of pores. Indeed, in recent years, many important efforts have been made to develop a hierarchical porous structure to be exploited in several applications with several advantages. Porous materials with integrated multiple levels of porosity are defined hierarchically structured porous materials in which a porous structure with more than one length scale from micro to macropores are represented[21]. Usually, the multiple levels of porosity are achieved by the development of bimodalities such as micro–meso, meso–macro, and micro-macro, or even trimodalities such as micro–meso–macro and meso–meso–macro[22]. The advantages gained by this particular interconnected network are i) high number of pores, ii) high surface area, iii) large accessible space, iv) low density, v) variable chemical compositions leading to good performances to be exploited in many fields such as energy storage, catalysis, gas sensing, separation and biomedicine among the others[23,24]. The most favorable features associated with porous polymers with a hierarchical internal network of pores can be summarized in five categories:

- Several synthesis procedures. Different strategies have been developed to obtain hierarchical porous materials including dual surfactant templating, colloidal crystal templating, polymer templating, bioinspired process, emulsion templating, SCFs, freeze-drying, BFs, phase separation, selective leaching, replication, zeolitization, sol-gel controlling, post-treatment, and spontaneous formation.
- Controllable porous properties. The porous structural features can be controlled by different approaches leading to great progress in the design and production of hierarchical internal morphologies, even if precise control is still not completely accomplished.
- Tunable macroscopic morphologies. Shapes and dimensions of hierarchically porous materials can be easily controlled by using different strategies (self-formation to a 0D sphere, polymer-templating to 1D fiber, biotemplating to 2D film and phase-separation to a 3D monolith).
- Adjustable multiple functions. Materials characterized by hierarchical porosities are attractive for the development of new functioning systems due to their high activity and selectivity. Indeed, by the introduction of new functionalities, nanounits and, bioentities, hierarchical porous polymers will express several different properties.

Also, it will be possible to develop platforms showing hybrid functions in order to create material extremely versatile

- A vast array of utilization. The obtained porous structures and morphologies could be employed for applications in several fields.

.

3. Applicative fields of Porous Polymers

As already mentioned, different applications of porous polymers have been explored, taking advantage of the hierarchical porous structure, such as gas absorption, water treatment, heterogeneous catalysis, and electrochemical energy storage[25]. Besides these important fields, the hierarchical porous polymers have gained increasing interest in two specific application fields i.e. the separation science and biomedicine.

3.1. Biomedicine

The achievement of innovative strategies as alternative diagnostic tools and innovative therapeutic approaches is related to the fast development of biomedicine towards years. In this context, porous polymers with tunable hierarchical pores and functionality present promising properties to be exploited in biomedical applications and many works have been published concerning this topic[26, 27]. In particular, porous polymers have been exploited in diagnosis[27], immobilization of enzymes[28, 29], and drug delivery[30, 31]. Indeed, several scientific papers have been published describing porous polymer applied as biomedical tools. For instance, Ibrahim and coworkers described in a recent review the effective preparation of drug delivery systems based on metal-organic frameworks to be used as carriers of antineoplastic molecules[32]. Moreover, porous titanium scaffolds have been developed as polymeric sponges. In cellular tests, these Ti-based scaffolds were able to improve the growth and proliferation of mesenchymal stem cells[33]. Tissue regeneration is a key biomedical application of porous material as reported by the numerous studies found in the literature concerning engineered bone graft substitutes[34, 35], wound dressing[36, 37] and regenerative therapy in general[38].

3.2. Separation

Separation is a process aimed to isolate pure compounds from complex matrices and it represents an essential step in many industrial processes, mainly in pharmaceutical and chemical industries. Therefore, many efforts have been made to develop innovative and effective separation techniques/materials. In recent years, several porous materials with different internal morphology have been achieved for separation purposes such as zeolites, activated carbons, carbon molecular sieves, aluminophosphates, polymeric resins, and MOFs. Porous polymers showing high energy efficiency, low cost, ease of processing, controllable pores and other tunable surface functionalities represent very promising candidates for the development of suitable tools for separation aims. In order to achieve

diverse separation applications, porous polymers can be modeled in different macroscopic shapes including membranes, powders, and monoliths[1, 39]. Specifically, monolithic materials express very peculiar features in separation sciences. Monolithic supports are defined as single pieces of macroporous material and their first use can be traced back to the 1960s. One of the first applications of monolithic materials was in high performance liquid chromatography as an alternative to packed column[40]. Indeed, in the 1980s, the HPLC suffered major limitations due to the utilization of particle-based stationary phases characterized by a slow diffusive process thought the inter-particulate voids. Obviously, monoliths, also termed continuous beds, allowed a significant decrease in the void volume of interparticle leading to a more efficient chromatographic separation. The excellent properties of continuous chromatographic beds are related to their macroporous structure. Indeed, the mobile phase flush through the macropores with consequent improvement of mass transport allowing more rapid and more efficient separation[41-43]. In 1989, Hjerten and coworkers developed a chromatographic column based on a solvent-swollen hydrophilic monolith composed by poly(acrylic acid-co-methylenebisacrylamide (MBAA)) suitable for HPLC application with high flow rates[44]. An important step in the development of chromatographic columns based on continuous beds was achieved in 1992 by Svec and Frechet who described an efficient method for the production of a macroporous polymer as high performance liquid chromatography separation phase obtained by an acrylate-based polymeric backbone[45]. Throughout years other kinds of monolithic materials have been developed such as carbon-based monoliths[46, 47], hybrid organosilica monoliths[48, 49], nano-particle-integrated monoliths[50, 51] and so on. In most recent years further progress has been made by developing polymeric monoliths exhibiting better performances in separation sciences. According to chemical nature, monolithic can be classified into diverse groups such as inorganic supports (comprising silica, celite and zeolites), organic polymer (both synthetic and natural) hybrid monoliths, metal-based monoliths and carbon-based monoliths[39]. The properties of these categories are summarized in the Table i-2.

Table i-2: Classification of monolithic materials based on their chemical backbone[39].

Classification	Fabrication approaches	Advantages	Disadvantages
Organic monoliths	Free radical polymerization	Wide pH range	Low surface area
	Ring-opening polymerization	Good biocompatibility	Shortening lifetime
	Living radical polymerization	Good Thermal stability	Low solvent stability
	Thiol-based click polymerization	Easy-to-modify	
Silica-based monoliths	Sol-gel	Good solvent stability	Complex and long preparation cycle
		High stability	Low reproducibility
		High surface area	Narrow pH range
		Large and adjustable porosity	
Hybrid monoliths	Sol-gel	Good mechanical stability	Low reproducibility
	Free radical polymerization	Wide pH range	Low surface area
	ROMP	Simple preparation process	
	Thiol-based click polymerization	High column efficiency	
Carbon-based monoliths	Templating around silica beads	Good solvent stability	Mechanical fragility
	Melting method	High chemical stability	Low peak efficency
	Dip coating	High thermal stability	
	Chemical vapor deposition		
Metal-based monoliths	Sol-gel	High surface area	Not easy-to-modify
	Templating process	High pH and mechanical stability	
	Coating of Silica monoliths	Good solvent stability	
	Microwave prepration	Good thermal conductivity	
	Electro-deposition	Good electrical conductivity	

4. Polymerized High Internal Phase Emulsions

As already mentioned above, many different approaches could be applied to the production of porous polymers. Among these methodologies, emulsion templating has emerged as an effective technique to obtain a hierarchical porous structure, with tunable properties and functionalities included in polymeric backbone. Initially, the emulsion templating technique was applied to synthesize hydrophobic crosslinked polymers termed “polyHIPEs” (polymerized high internal phase emulsion). These materials are achieved by the polymerization of monomers in the external phase (continuous phase) of water-in-oil emulsions (w/o) termed HIPEs (high internal phase emulsions). HIPEs are paste-like, highly viscous emulsions with a volume of internal phase (droplet phase) higher than 74.05% of the total volume. This value represents the maximum occupiable space by monodisperse, uniform and undeformable spheres (i.e. by the droplet composing the internal phase[52-54]). The biphasic structure of emulsion is exploited as a template for the final polymeric material with a resulting porous structure, hence the definition of “emulsion templating”. Progress in this technique throughout the years led to the publication of several review articles indicating the vast array of possibilities for polyHIPEs[55-59]. Moreover, HIPEs have been known in the literature for many years, in particular in cosmetic and food applications[60]. In the 1960s, the preparation of polymeric foams has been described[59].

4.1. PolyHIPEs morphology and pores structure

The unique macroporous structure of polyHIPE materials is generated by several physicochemical processes leading to an internal morphology with a hierarchical pore distribution (Fig i-1). The materials are characterized by spherical macropores (typically from 1 to a few hundred µm in diameter) generated through the removal of the internal phase. The evaporation of the water phase leads to the evacuation of droplets leaving air-filled “voids”. This process is governed by the thermodynamic equilibrium between emulsion phase separation and droplet stabilization. The polymerization of the external phase composed by lipophilic monomers results in a thin polymeric layer surrounding the spherical pores thereby forming the polymeric “skeleton” of the polyHIPE. These macropores are cavities representing the first level of porosity in the materials. Nomenclature of polyHIPE-pores is an important issue, because, throughout literature, several terms have been proposed for the first level of pores, namely cells, voids or simply cavities. In this work, we adopted the term “voids”, in agreement with most of the authors publishing in this field, even if IUPAC refers to voids as inter-particle spaces. Indeed, the name “cell” tends to be avoided,

mainly for the ambiguous meaning if polyHIPEs are applied for biomedical purposes (tissue engineering or cell cultures for instance). Since the size of the cavities reflects the droplet size of the HIPE, the most important factors influencing the cavity size relate to variables that influence the HIPE's kinetic stability, which include surfactant(s), surfactant concentration, the presence of other stabilizers, and the energy input during HIPE preparation (stirring or shearing of emulsion)[59]. In order to achieve a highly porous material, voids need to be interconnected by the second level of pores which determine convective mass transfer through a polyHIPE material. The most probable mechanism for the formation of the secondary interconnecting pores was firstly proposed by Cameron[54] who hypothesized that these pores are crated during the polymerization and crosslinking processes. In this theory, pores are formed due to shrinkage and contraction phenomena that occur at the interface causing ruptures in the polymeric thin film at its thinnest points. Also for this second level of pores, many names are found in the literature ("holes", "channels" and "throats" among the others) and, for this work, we selected "throats". Both the first and second levels of pores are in the macropores region, indeed the average diameter of throats (typically above a few nanometers) can be really close to the voids' one leading to the obtainment fibrillar mesh morphology. However, a smaller third order of pores may be identified in polyHIPE materials belonging to the mesopores region (2-50 nm) if a porogenic solvent is applied for the synthesis of polyHIPEs or if a high degree of crosslinking is achieved in the polymeric matrix. Due to the presence of three levels of pores, a "macroreticular" internal structure is achieved[61]. The porous structure of polyHIPEs is defined by several factors such as void and throats size, void shape (spherical or polyhedral) and interconnectivity. Obviously, different synthetic parameters have a strong influence on these factors and, consequently may affect the internal morphology of pores. These parameters are listed below.

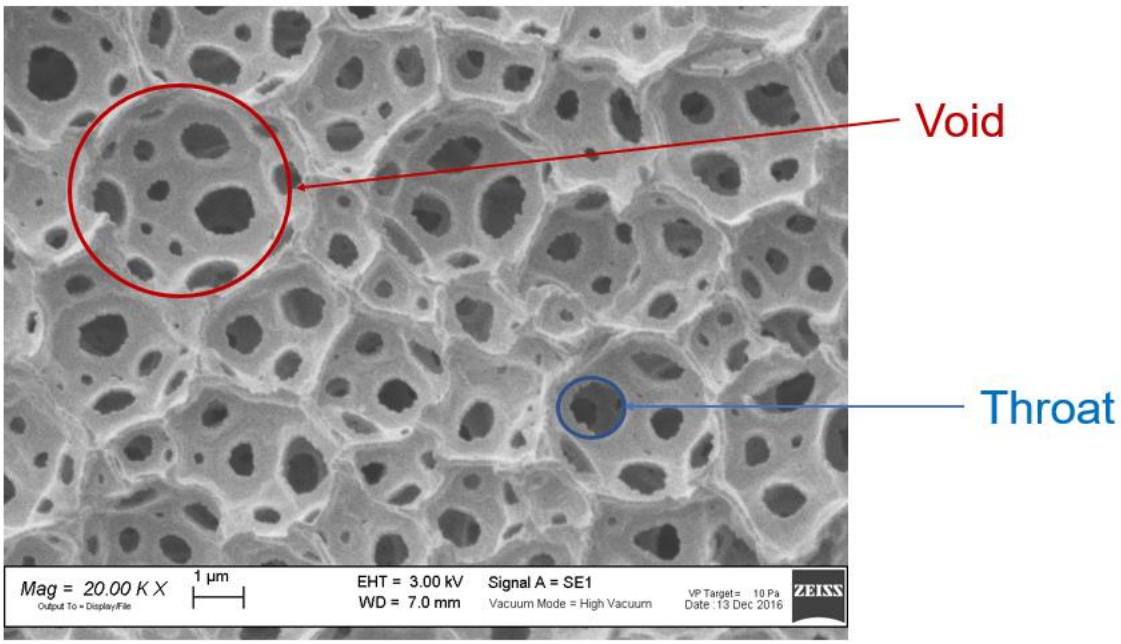

Figure i-1: typical polyHIPE-structure with the two levels of pores termed as “voids" and "throats"

4.1.1. Emulsion stabilization strategies

Being the emulsions thermodynamically unstable systems, suitable stabilization approaches are required (these approaches will be deeply described in the following paragraph). The strategies used most frequently to stabilize HIPEs are the use of molecular surfactants or amphiphilic particles and the use of either these approaches has an important effect on voids' diameter. In fact, polyHIPEs from surfactant-stabilized emulsions show voids with an average diameter from 1 to 20 µm in those obtained by Pickering HIPEs voids diameter is typically in a range from 200 to 700 µm[62]. Also voids interconnectivity is influenced by the stabilization procedure. For polyHIPEs obtained by surfactant-stabilized HIPEs, voids interconnectivity is often affected by the surfactant amount, the internal phase volume and the presence of porogenic solvents. Although the void interconnectivity does not seem to be sensitive to the monomer amount in the external phase, there is a strong influence of the surfactant/monomer ratio on the interconnectivity[63]. For instance, low surfactant content (5%) in the continuous phase allows the obtainment of non-porous structures, while small interconnecting throats are achieved from emulsions containing 7-10 % surfactant. Therefore, by increasing the surfactant amount further than 10% determine the typical highly interconnected network of polyHIPEs, while emulsion templated monoliths are usually not generated with a surfactant amount greater than 50% in the external phase[63]. On the other hand, the droplets in amphiphilic particles-stabilized HIPEs (Pickering HIPEs) are usually

larger than those in surfactant-stabilized emulsions leading to a polymer film significantly thicker with a consequent impediment in the formation of interconnecting pores. Moreover, the stabilizing particles might be strongly absorbed in the o/w interface preventing the droplet coalescence with a consequent formation of closed structures. Indeed, porous polyHIPEs structure from Pickering emulsions has been produced only under specific conditions. The formation of interconnecting pores is subordinated to a strong interaction between the monomer and the stabilizing particles or to a modification of the amphiphilicity of stabilizing particles. In this context, Zheng and coworkers described the development of hydrophobic interconnected macroporous polymers from HIPEs using n-octadecyltrimethoxysilane (ODS)-modified silica particles[64].

4.1.2. Locus of initiation of polymerization

PolyHIPEs have been produced from w/o HIPEs by using different types of initiator systems such as free radical polymerization (FRP) or electron transfer for atom transfer radical polymerization (AGET ATRP). The different polymerization systems can include external-phase initiation, interfacial initiation, and nanoparticles-based initiation and the locus of initiation can significantly affect the macromolecular structure of pores as summarized by Fig i-2[65]. In general, external-phase initiation tends to produce porous structures, while interfacial initiation tends to produce closed structures.

4.1.3. Monomers composing the external phase.

Obviously, the properties of polyHIPEs are strictly related to the nature of monomers composing the external phase which may also influence void interconnectivity. For instance, when styrene was used as the predominant monomer, close polyHIPEs were fabricated. On the other hand, an interconnected morphology was achieved when n-butyl acrylate (nBA) was used instead of styrene[66].

4.2. Stabilization of HIPEs

As already mentioned, emulsions are unstable systems, therefore, HIPE stabilization is an essential step for the polyHIPEs synthesis. Typically, HIPE stability is enabled by the utilization of suitable stabilizers, which are usually surfactants but can also be particles or gels. Indeed, the development of stabilization strategies has recently attracted significant attention (Fig i-3).

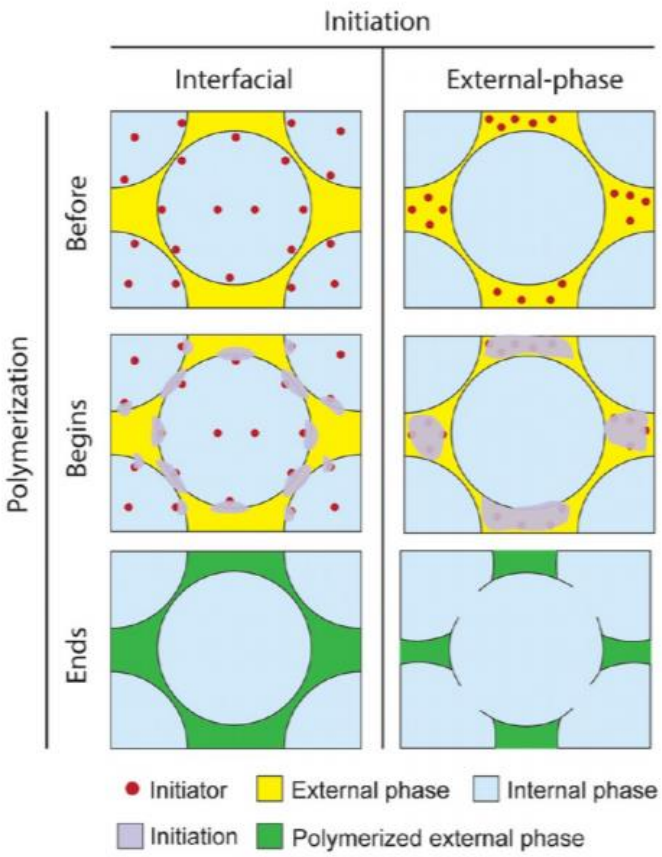

***Figure i-2**: Schematic illustration showing the possible effects of the locus of initiation on internal morphology. The picture was taken from ref. 25.*

4.2.1. Surfactants.

As the most conventional technique, surfactants are common HIPE stabilizers, but not all surfactants are able to stabilize high internal phase emulsions. Commonly used surfactants for w/o HIPEs include sorbitan monooleate (SMO or Span 80) and polyglycerol polyricinoleate (PGPR). According to the Bancroft rule, due to the great volume of the dispersed phase, to prevent phase inversion, surfactants should only be soluble in the minor, external phase[67]. In order to produce stable HIPEs, large content of surfactants (typically between 20 and 50% of the external phase) is required. This represents a significant drawback because of the need for removing these relatively large amounts of surfactant following polyHIPE synthesis. Recently, in the literature different solution were proposed including the enhancement of the surfactant efficiency by the introduction of macromolecular surfactants (that are less likely to leach), and reactive surfactants (covalently linked to polyHIPE polymeric skeleton). Indeed, macromolecular surfactants have proven to be excellent HIPE stabilizers[68-70]. For instance, amphiphilic BCPs were used successfully to stabilized w/o HIPEs: the hydrophobic fraction included polystyrene (PS) and poly(1,4-butadiene) (PBD), while the hydrophilic blocks included PEO and poly(acrylic acid) (PAA)

were found to link their hydrophobic blocks in the continuous phases of the resulting polyHIPEs[71]. Moreover, reactive surfactants are promising alternatives to solve the problems associated with surfactant leaching because of the covalent incorporation of these stabilizers into the polyHIPE network. For instance, in a work published in 2015[72], a stable w/o HIPE was achieved by the incorporation of span 80 into a polyHIPE network via a chain transfer reaction during the ring-opening metathesis polymerization (ROMP) of cyclooctene. Another promising and emerging strategy is represented by block copolymer surfactants as the sole monomer. Indeed, polyHIPEs based only on monomeric BCP surfactant, namely F-127 dimethacrylate (used as a stabilizer, sole monomer and, crosslinking agent) were recently reported[73].

4.2.2. Particles

Particle-stabilized emulsions are also defined as Pickering emulsions[74]. This stabilization strategy has not reached the same success at stabilizing HIPEs leading to emulsions that are more likely to reach out a phase inversion. By the way, Pickering HIPEs have been developed successfully over the past decade by using both inorganic and organic particles[75, 76]. For example, Yi and coworkers used polymeric Janus nanoparticles (consisting of a linear poly(methyl methacrylate) “tail” and a cross-linked poly(4-vinylpyridine) “head”) for the stabilization of w/o emulsions and the synthesis of macroporous polymer foams[77].

4.2.3. Emulsion gel

Gel particles showed outstanding properties to be exploited as HIPE stabilizers[78]. The most common gel particles included several different entities such as i) thermosensitive monomers, such as N-isopropylacrylamide, ii) ionic monomers, such as methacrylic acid poly(urethane urea)s iii) polymers functionalized with groups determining strong intermolecular hydrogen bonding, such as 2-ureido-4[1H]pyrimidinone, and iv) star polymers with crosslinked cores.

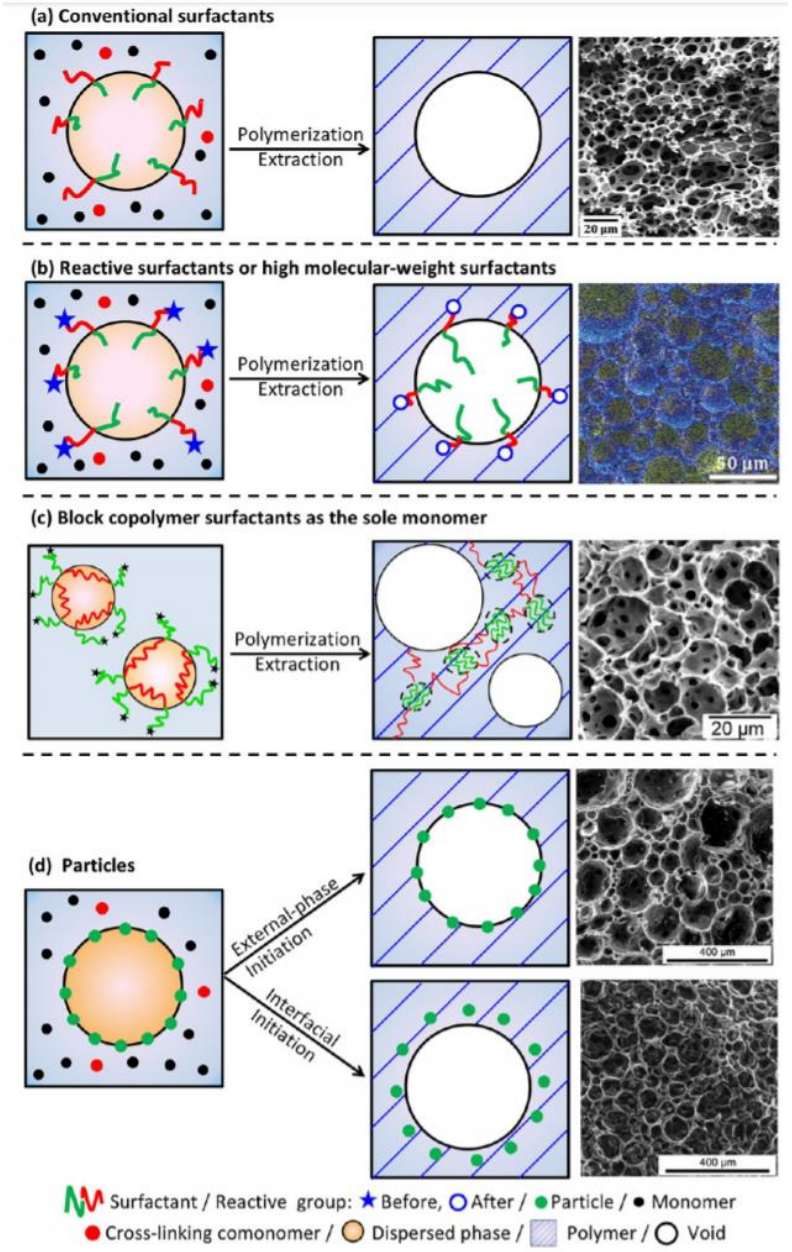

Figure i-3: PolyHIPEs fabricated from HIPEs that were formed by adopting a variety of stabilization strategies (with illustrative micrographs from the literature): (a) conventional surfactants; (b) reactive surfactants and high molecular weight surfactants; (c) BCP surfactants as the sole monomer; (d) particles (showing both external-phase initiation and interfacial initiation). The picture was taken from ref. 25.

4.3. Polymerization techniques

PolyHIPEs' macromolecular structure and its control through synthetic conditions is a fundamental task for the application of these polymeric materials. A wide range of polymerization techniques was applied for a rational design of polyHIPEs for the development of optimized properties. The most used method is represented by the conventional free radical polymerization (FRP). Indeed, polyHIPEs are usually obtained by

thermally initiated FRP, a generally simple reaction that is easy to carry out, convenient and applicable to several vinyl monomers. Typically, mild conditions are required to perform FRP and this usually represents a requirement when polyHIPEs are intended to be applied as biomedical tools. For instance, the polymerization of styrene and MMA were achieved by the rapid decomposition of an initiator (2,2′-azobis(isobutyronitrile)) in the presence of a suitable catalyst (cetyltrimethylammonium bromide) at room temperature and 40°C, respectively[79, 80]. Furthermore, several redox systems were developed to determine a faster polymerization reaction occurring at moderate temperature (benzoyl peroxide with trimethylaniline[81], ammonium persulfate with tetramethylethylene diamine[82], and ascorbic acid/iron(II) sulfate heptahydrate/hydrogen peroxide[83]). In fact, high temperatures could affect the emulsion stability leading to an incorrect polymerization step. Besides these considerations, FRP showed certain drawbacks to be applied as a polymerization protocol for high internal phase emulsions. This technique is limited to monomers with reactive double bonds (styrenics and acrylates) and is typically only applied for the control on the homogeneity of the final polymeric network. and limited reaction conditions can be applied. Therefore, even if FRP is still the most common technique, in order to overcome some of these limitations, a variety of controlled radical polymerizations (CRPs) have emerged for the synthesis of polyHIPEs. Indeed, few works concerning the polymerization of HIPEs by atom transfer radical polymerization (ATRP) approaches have been reported in the literature[75, 84] even if many efforts are required to adapt ATRP for the polyHIPEs synthesis. Reversible addiction-fragmentation chain-transfer (RAFT) is a well-established polymerization technique typically used to prepared polymers. The polyHIPEs synthesized via RAFT show good features, such as porous structure more controllable by synthetic conditions, good mechanical properties and easily tailorable functional groups[85, 86]. Besides the radical polymerizations, other methods have been applied for the polymerizations of HIPEs such as step-growth polymerization[87, 88], Diels−Alder polymerization[89], ring-opening metathesis polymerization (ROMP)[72, 90], and the thiol−ene/thiol−yne click reactions[91]. In Fig i-4 a schematic representation of the most common polymerizations used for polyHIPEs synthesis is reported.

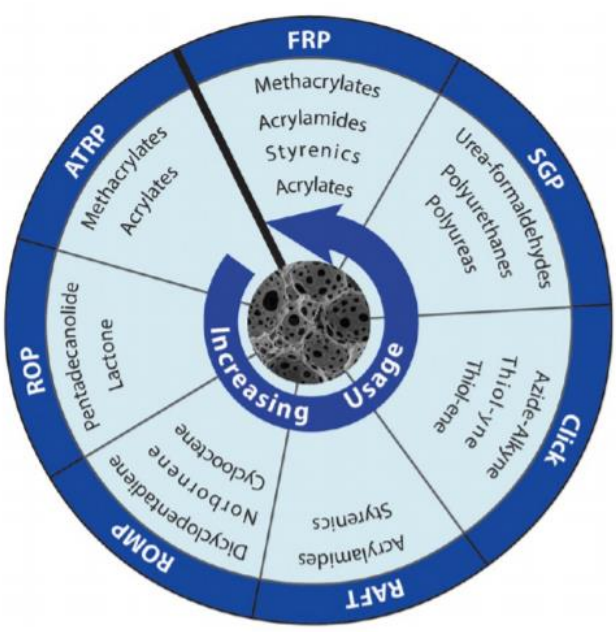

Figure i-4: Most used polymerization techniques used for the synthesis of polyHIPEs. The picture was taken from ref. 25

4.4. PolyHIPEs shape

PolyHIPEs are extremely versatile polymers and they can be produced in several external structures and different shapes (for example beads, rods or fibers). Indeed, polyHIPE shape can be moduled by numerous approaches and complex networks have been fabricated by using such methods.

4.4.1. Double emulsion

In this kind of approach, a double emulsion system (triphasic system) is achieved when a HIPE has been dispersed as droplets within a continuous phase (typically, a w/o HIPE is dispersed in an aqueous phase). By the polymerization of the external phase of the HIPE "droplets", polyHIPE-based beads are typically fabricated and a wide range of double emulsions have been developed for this purpose[92, 93]. The double emulsion approach can also be used for the fabrication of polyHIPE-based monoliths. For instance, Lei and coworkers developed a polyHIPE monolith by the addition of a water-soluble monomer to a water-in-toluene-in-water HIPE as reported in a report published in 2016[92].

4.4.2. Control on polymerization environment/frozen polymerization and sedimentation polymerization

Other effective methods for the preparation of polyHIPE-based beads are frozen polymerization and sedimentation polymerization. Both these approaches generate beads that are usually a few milliliters in diameter. Frozen polymerization of HIPE was applied for the synthesis of aligned porous beads through directional freezing, and frozen ultraviolet (UV) initiation of an oil-in-water (o/w) HIPE[94]. On the other hand, sedimentation polymerization has been used for the preparation of emulsion-templated polymer beads based on acrylamide and N, N‘-methylenebisacrylamide as starting monomers[95].

4.4.3. Electrospinning

PolyHIPE shape can also be controlled by the application of novel manufacturing techniques. For instance, electrospinning is an effective method for the fabrications of nanofibers. In order to obtain satisfactory materials, this technique requires viscous, polar and visco-elastic solutions with constant viscosity. Therefore, HIPEs showing these features can be used as a template to produce fibrous polymers via electrospinning. For example, bicontinuous polymers in the form of fibers have been fabricated starting from w/o HIPEs consisting of aqueous poly(vinyl alcohol) (PVA) solutions dispersed within PCL-in-toluene solutions[96].

4.4.4. Microfluidics

Microfluidics was observed as an effective and very advantageous approach for the generation of homogeneous high internal phase emulsions. Indeed, microfluidics has been exploited for the production of highly ordered HIPEs leading to the synthesis of polyHIPEs monoliths with well-controlled pore sizes and porous structure[97]. Moreover, recent improvements in this technique allowed also the production of polyHIPE-based beads, rods, and fibers[98].

4.4.5. 3D printing

Nowadays, 3D printing is probably the most powerful tool for manufacturing objects in complicated shapes. 3D printing allows polyHIPEs to be obtained in complex shapes and in always more complicated architecture. By using this technique a precise control on the polymeric structure is possible. Indeed, polyHIPEs with several different shapes have been fabricated by using the starting emulsions as inks[99].

4.4.6. PolyHIPE-based membranes

Another important shape in which polyHIPEs could be modeled is flatform polymers leading to the obtainment of polyHIPE-based membranes. Actually, the production of these membranes is achieved by simply casting thin HIPE films on flat surfaces where the polymerization step can occur. For example, an acrylate-based polyHIPE membrane was easily achieved and applied for protein purification[100].

4.5. Alternative emulsion types

Typically, polyHIPEs have been obtained by using reversed emulsion (water-in-oil) as a template. In this conventional approach, monomers are oil-soluble while the water phase droplets serve as a template for the first level of porosity. However, in some cases, alternative approaches can be used. For instance, the utilization of direct emulsions (oil-in-water) is necessary for the development of polyHIPEs based on water-soluble monomers. According to many reports, the preparation of o/w HIPEs is often associated with difficulties in the obtainment of a sufficiently stable emulsion. Obviously, if in reverse HIPEs, surfactants must have low HLB values (hydrophilic-lipophilic balance value) for o/w HIPEs' stabilization surfactants that are soluble in water (high HLB values) are needed[59, 101]. An efficient method for the preparation of a stable monolith based on poly-acrylic acid templated from an o/w HIPE was described by Kranjc at coworkers.[38] In some cases, for the preparation of suitable HIPEs, water should be avoided and nonaqueous emulsion must be used. In order to stabilize nonaqueous high internal phase emulsions, polymeric surfactants (such as Synperonic) seem to be the most effective tools[102, 103]. Therefore, some strategies have been applied including i) use of two immiscible organic liquids; ii) use of monomers, without any solvent, forming the external phase; iii) use of ionic liquids as droplet phase[104]. Sometimes, the use of organic solvents is not recommended (typically, organic solvents are hazardous for human health and environment) and their removal could result in a critical step and traces of solvents could affect the applicability of polyHIPEs in the field of interest (in particular for materials intended to be applied in biological area). Therefore, the use of supercritical fluids as the droplets phase in HIPEs represents an appealing approach. Indeed, it is considered a "green" technology due to the absence of organic solvents and the removal of the droplets is simply achieved by depressurization (typically, CO_2 in supercritical conditions is used). On the other hand, supercritical fluids technology is associated with many drawbacks as well. First of all, a specific and expensive apparatus is required and then high pressures are required for the formation of such HIPEs. Moreover,

the emulsion stabilization is reported to be quite difficult by using supercritical fluids. For these reasons, only a few works have been published concerning this topic[105, 106]. Another important alternative emulsion type is achieved by comprising monomers in both oil and aqueous phase leading to the formulation of a specific class of porous materials with special properties including responsivity to the environmental changes or specific separation characteristics. For example, Kovacic et al. were able to yield responsive poly(acrylic acid) and poly(N-isopropylacrylamide) polyHIPE-base monoliths showing varying degrees of resistance to flow depending on pH and temperature[107].

4.6. Functionalization of polyHIPEs

Usually, to provide functional polyHIPE materials, the emulsion's starting composition comprises functional agents (i.e. functional monomers). Then, typically, further chemistry steps following the polyHIPE synthesis occur. More recently, many efforts have been made to improve the applicability of polyHIPEs in various scientific and technological fields by the exploitation of post-production functionalization[25]. For this purpose, different approaches have been evaluated such as changing the surface chemistry[57], creating meso or microporosity or by the fabrication of other porous materials (porous carbons) from the polyHIPE polymeric structures[108]. On the other hand, many drawbacks are related to post-synthesis polyHIPE functionalization including the need for numerous synthesis steps for the obtainment of a suitable functionalization and negative effects on materials' properties such as the mechanical properties. Surface modifications and surface enrichment represent effective methods for the functionalization of polyHIPEs. The modifications can be obtained by removing unreacted portions after synthesis of polyHIPEs or porogenic solvents, changing the hydro-lipophilicity or by changing the surface roughness values[109, 110]. Another fundamental topic regarding the functionalization of polyHIPEs concerns the increase of the specific surface area (SSA) of these polymers. SSA is a property of solid materials defined by IUPAC as a total surface area per mass unit[3]. High values of SSA are required for porous polymers that are intended to be applied, for example, as chromatographic stationary phases or absorbents. Regrettably, polyHIPEs materials do not show high SSAs (typically of 10 m^2/g)[111]. For this reason, some strategies have been applied to enhance the polyHIPEs SSAs such as the use of porogenic solvents or hyper-crosslinking. In particular, hyper-cross-linking via Friedel−Crafts reactions allowed to obtain emulsion templated polymers with SSAs of up to 1600 m^2/g [55]. However, the main drawback related to the hyper-crosslinking approach is the significant negative influence on the mechanical properties of the final

material. In this context, many works focused on the preparation of polyHIPEs hyper-crosslinked with high SSA while lowering the deterioration of mechanical features[112].

4.7. Applications

Due to their extreme versatility, polyHIPE-based supports represent promising tools for both industrial and research fields. Indeed, the development of emulsion templated polymers is typical “application-driven”. The transfer to an industrial scale of such technology represents a very challenging process due to many issues related to the instability of starting emulsions (high internal phase volumes and the consequent high amount of surfactants required) and to the tricky developments of effective polymerization procedures[25]. Therefore, many efforts have been made to apply polyHIPEs in several fields, in particular as “flow-through” supports, column packing, and membranes[113, 114]. The advantages of polyHIPEs in these applications are related to the possibility to polymerize in any shapes including inside a column, the low back-pressure values when continuous flow is applied and the wide range of surface modifications easily reachable. Adsorption, absorption, and catalysis are the most commonly investigate applications, followed by polyHIPE-based scaffolds for tissue engineering and controlled release. Furthermore, some recent studies highlighted new interesting exploitations for polyHIPEs such as heat and sound insulation[25]. In general, the most appealing application fields are i) adsorption and absorption: by the development of absorbents for body fluids[115], contaminants from water[116] and, in general of broad-spectrum absorbent[73]; ii) flow-through reaction and catalysis[117-120]; iii) tissue engineering scaffolds[121, 122] due to the macroporous structure showing numerous advantages in biomedical fields (even for 3D cell cultures and controlled release)[25]; iv) release and encapsulation (the hierarchical and tortuous porous structure had a significant effect on the release behavior)[56, 123]; and v) shape memory material[38, 124].

5. References

1. Wu, J.; Xu, F.; Li, S.; Ma, P.; Zhang, X.; Liu, Q.; Fu, R.; Wu, D., Porous Polymers as Multifunctional Material Platforms toward Task-Specific Applications. *Adv Mater* **2019,** *31* (4), e1802922.

2. Pandey, N.; Pandey-Rai, S., Updates on artemisinin: an insight to mode of actions and strategies for enhanced global production. *Protoplasma* **2016,** *253* (1), 15-30.

3. Sing, K. S. W.; Everett, D. H.; Haul, R. A. W.; Moscou, L.; Pierotti, R. A.; Rouquerol, J.; Siemieniewska, T., International union of pure and applied chemistry, IUPAC. *Pure Appl. Chem* **1985,** *57*, 603.

4. Wu, D.; Xu, F.; Sun, B.; Fu, R.; He, H.; Matyjaszewski, K., Design and preparation of porous polymers. *Chem Rev* **2012,** *112* (7), 3959-4015.

5. Sun, J.-K.; Antonietti, M.; Yuan, J., Nanoporous ionic organic networks: from synthesis to materials applications. *Chemical Society Reviews* **2016,** *45* (23), 6627-6656.

6. Dalapati, S.; Jin, S.; Gao, J.; Xu, Y.; Nagai, A.; Jiang, D., An azine-linked covalent organic framework. *Journal of the American Chemical Society* **2013,** *135* (46), 17310-17313.

7. Jin, Y.; Hu, Y.; Zhang, W., Tessellated multiporous two-dimensional covalent organic frameworks. *Nature Reviews Chemistry* **2017,** *1*.

8. Zou, L.; Sun, Y.; Che, S.; Yang, X.; Wang, X.; Bosch, M.; Wang, Q.; Li, H.; Smith, M.; Yuan, S.; Perry, Z.; Zhou, H. C., Porous Organic Polymers for Post-Combustion Carbon Capture. *Advanced Materials* **2017,** *29* (37).

9. Zeng, Y.; Zou, R.; Zhao, Y., Covalent organic frameworks for CO<inf>2</inf> capture. *Advanced Materials* **2016,** *28* (15), 2855-2873.

10. Xie, Y.; Wang, T. T.; Liu, X. H.; Zou, K.; Deng, W. Q., Capture and conversion of CO<inf>2</inf> at ambient conditions by a conjugated microporous polymer. *Nature Communications* **2013,** *4*.

11. Sekizkardes, A. K.; Kusuma, V. A.; Dahe, G.; Roth, E. A.; Hill, L. J.; Marti, A.; Macala, M.; Venna, S. R.; Hopkinson, D., Separation of carbon dioxide from flue gas by mixed matrix membranes using dual phase microporous polymeric constituents. *Chemical Communications* **2016,** *52* (79), 11768-11771.

12. Kim, S.; Lee, Y. M., Rigid and microporous polymers for gas separation membranes. *Progress in Polymer Science* **2015,** *43*, 1-32.

13. Carta, M.; Malpass-Evans, R.; Croad, M.; Rogan, Y.; Jansen, J. C.; Bernardo, P.; Bazzarelli, F.; McKeown, N. B., An efficient polymer molecular sieve for membrane gas separations. *Science* **2013,** *339* (6117), 303-307.

14. Zhang, Y.; Riduan, S. N., Functional porous organic polymers for heterogeneous catalysis. *Chemical Society Reviews* **2012,** *41* (6), 2083-2094.

15. Alahakoon, S. B.; Thompson, C. M.; Occhialini, G.; Smaldone, R. A., Design Principles for Covalent Organic Frameworks in Energy Storage Applications. *ChemSusChem* **2017,** *10* (10), 2116-2129.

16. Fang, Q.; Wang, J.; Gu, S.; Kaspar, R. B.; Zhuang, Z.; Zheng, J.; Guo, H.; Qiu, S.; Yan, Y., 3D Porous Crystalline Polyimide Covalent Organic Frameworks for Drug Delivery. *Journal of the American Chemical Society* **2015,** *137* (26), 8352-8355.

17. Dong, J.; Zhang, K.; Li, X.; Qian, Y.; Zhu, H.; Yuan, D.; Xu, Q. H.; Jiang, J.; Zhao, D., Ultrathin two-dimensional porous organic nanosheets with molecular rotors for chemical sensing. *Nature Communications* **2017,** *8* (1).

18. Han, X.; Zhang, J.; Huang, J.; Wu, X.; Yuan, D.; Liu, Y.; Cui, Y., Chiral induction in covalent organic frameworks. *Nature Communications* **2018,** *9* (1).

19. Meng, X.; Wang, H. N.; Song, S. Y.; Zhang, H. J., Proton-conducting crystalline porous materials. *Chemical Society Reviews* **2017,** *46* (2), 464-480.

20. Gu, C.; Huang, N.; Chen, Y.; Zhang, H.; Zhang, S.; Li, F.; Ma, Y.; Jiang, D., Porous Organic Polymer Films with Tunable Work Functions and Selective Hole and Electron Flows for Energy Conversions. *Angewandte Chemie - International Edition* **2016,** *55* (9), 3049-3053.

21. Sun, M.-H.; Huang, S.-Z.; Chen, L.-H.; Li, Y.; Yang, X.-Y.; Yuan, Z.-Y.; Su, B.-L., Applications of hierarchically structured porous materials from energy storage and conversion, catalysis, photocatalysis, adsorption, separation, and sensing to biomedicine. *Chemical Society Reviews* **2016,** *45* (12), 3479-3563.

22. Bae, W. G.; Kim, H. N.; Kim, D.; Park, S. H.; Jeong, H. E.; Suh, K. Y., 25th anniversary article: scalable multiscale patterned structures inspired by nature: the role of hierarchy. *Adv Mater* **2014,** *26* (5), 675-700.

23. Yang, X. Y.; Leonard, A.; Lemaire, A.; Tian, G.; Su, B. L., Self-formation phenomenon to hierarchically structured porous materials: design, synthesis, formation mechanism and applications. *Chem Commun (Camb)* **2011,** *47* (10), 2763-86.

24. Fang, B.; Kim, J. H.; Kim, M. S.; Yu, J. S., Hierarchical nanostructured carbons with meso-macroporosity: design, characterization, and applications. *Acc Chem Res* **2013,** *46* (7), 1397-406.

25. Zhang, T.; Sanguramath, R. A.; Israel, S.; Silverstein, M. S., Emulsion Templating: Porous Polymers and Beyond. *Macromolecules* **2019,** *52* (15), 5445-5479.

26. Wang, H.; Zhu, W.; Liu, J.; Dong, Z.; Liu, Z., PH-Responsive Nanoscale Covalent Organic Polymers as a Biodegradable Drug Carrier for Combined Photodynamic Chemotherapy of Cancer. *ACS Applied Materials and Interfaces* **2018,** *10* (17), 14475-14482.

27. Lee, S.; Barin, G.; Ackerman, C. M.; Muchenditsi, A.; Xu, J.; Reimer, J. A.; Lutsenko, S.; Long, J. R.; Chang, C. J., Copper Capture in a Thioether-Functionalized Porous Polymer Applied to the Detection of Wilson's Disease. *Journal of the American Chemical Society* **2016,** *138* (24), 7603-7609.

28. Sun, Q.; Fu, C. W.; Aguila, B.; Perman, J.; Wang, S.; Huang, H. Y.; Xiao, F. S.; Ma, S., Pore Environment Control and Enhanced Performance of Enzymes Infiltrated in Covalent Organic Frameworks. *Journal of the American Chemical Society* **2018,** *140* (3), 984-992.

29. Kandambeth, S.; Venkatesh, V.; Shinde, D. B.; Kumari, S.; Halder, A.; Verma, S.; Banerjee, R., Self-templated chemically stable hollow spherical covalent organic framework. *Nature Communications* **2015,** *6*.

30. Bai, L.; Phua, S. Z. F.; Lim, W. Q.; Jana, A.; Luo, Z.; Tham, H. P.; Zhao, L.; Gao, Q.; Zhao, Y., Nanoscale covalent organic frameworks as smart carriers for drug delivery. *Chemical Communications* **2016,** *52* (22), 4128-4131.

31. Vyas, V. S.; Vishwakarma, M.; Moudrakovski, I.; Haase, F.; Savasci, G.; Ochsenfeld, C.; Spatz, J. P.; Lotsch, B. V., Exploiting Noncovalent Interactions in an Imine-Based Covalent Organic Framework for Quercetin Delivery. *Advanced Materials* **2016,** *28* (39), 8749-8754.

32. Ibrahim, M.; Sabouni, R.; Husseini, G. A., Anti-cancer Drug Delivery Using Metal Organic Frameworks (MOFs). *Curr Med Chem* **2017,** *24* (2), 193-214.

33. Wang, C.; Chen, H.; Zhu, X.; Xiao, Z.; Zhang, K.; Zhang, X., An improved polymeric sponge replication method for biomedical porous titanium scaffolds. *Mater Sci Eng C Mater Biol Appl* **2017,** *70* (Pt 2), 1192-1199.

34. Ogueri, K. S.; Jafari, T.; Escobar Ivirico, J. L.; Laurencin, C. T., POLYMERIC BIOMATERIALS FOR SCAFFOLD-BASED BONE REGENERATIVE ENGINEERING. *Regen Eng Transl Med* **2019,** *5* (2), 128-154.

35. Wang, Z.; Wang, K.; Lu, X.; Li, C.; Han, L.; Xie, C.; Liu, Y.; Qu, S.; Zhen, G., Nanostructured Architectures by Assembling Polysaccharide-Coated BSA Nanoparticles for Biomedical Application. *Adv Healthc Mater* **2015,** *4* (6), 927-37.

36. Chaudhari, A. A.; Vig, K.; Baganizi, D. R.; Sahu, R.; Dixit, S.; Dennis, V.; Singh, S. R.; Pillai, S. R., Future Prospects for Scaffolding Methods and Biomaterials in Skin Tissue Engineering: A Review. *Int J Mol Sci* **2016,** *17* (12).

37. Garg, T.; Goyal, A. K., Biomaterial-based scaffolds--current status and future directions. *Expert Opin Drug Deliv* **2014,** *11* (5), 767-89.

38. Wang, J.; Brasch, M. E.; Baker, R. M.; Tseng, L. F.; Pena, A. N.; Henderson, J. H., Shape memory activation can affect cell seeding of shape memory polymer scaffolds designed for tissue engineering and regenerative medicine. *J Mater Sci Mater Med* **2017,** *28* (10), 151.

39. Ma, S.; Li, Y.; Ma, C.; Wang, Y.; Ou, J.; Ye, M., Challenges and Advances in the Fabrication of Monolithic Bioseparation Materials and their Applications in Proteomics Research. *Advanced Materials* **2019**.

40. Buchmeiser, M. R., Polymeric monolithic materials: Syntheses, properties, functionalization and applications. *Polymer* **2007,** *48* (8), 2187-2198.

41. Orr, V.; Zhong, L.; Moo-Young, M.; Chou, C. P., Recent advances in bioprocessing application of membrane chromatography. *Biotechnology Advances* **2013,** *31* (4), 450-465.

42. Tennikova, T. B.; Reusch, J., Short monolithic beds: History and introduction to the field. *Journal of Chromatography A* **2005,** *1065* (1), 13-17.

43. Tennikova, T. B.; Freitag, R., An introduction to monolithic disks as stationary phases for high performance biochromatography. *Journal of Separation Science* **2000,** *23* (1), 27-38.

44. Hjertén, S.; Liao, J. L.; Zhang, R., High-performance liquid chromatography on continuous polymer beds. *Journal of Chromatography A* **1989,** *473* (C), 273-275.

45. Svec, F.; Frechet, J. M. J., Continuous rods of macroporous polymer as high-performance liquid chromatography separation media. *Analytical Chemistry* **1992,** *64* (7), 820-822.

46. Liang, C.; Dai, S.; Guiochon, G., A graphitized-carbon monolithic column. *Analytical Chemistry* **2003,** *75* (18), 4904-4912.

47. Eltmimi, A. H.; Barron, L.; Rafferty, A.; Hanrahan, J. P.; Fedyanina, O.; Nesterenko, E.; Nesterenko, P. N.; Paull, B., Preparation, characterisation and modification of carbon-based monolithic rods for chromatographic applications. *Journal of Separation Science* **2010,** *33* (9), 1231-1243.

48. Colón, H.; Zhang, X.; Murphy, J. K.; Rivera, J. G.; Colón, L. A., Allyl-functionalized hybrid silica monoliths. *Chemical Communications* **2005,** (22), 2826-2828.

49. Zheng, M. M.; Lin, B.; Feng, Y. Q., Hybrid organic-inorganic octyl monolithic column for in-tube solid-phase microextraction coupled to capillary high-performance liquid chromatography. *Journal of Chromatography A* **2007,** *1164* (1-2), 48-55.

50. Cao, Q.; Xu, Y.; Liu, F.; Svec, F.; Fréchet, J. M. J., Polymer monoliths with exchangeable chemistries: Use of gold nanoparticles as intermediate ligands for capillary columns with varying surface functionalities. *Analytical Chemistry* **2010,** *82* (17), 7416-7421.

51. Krenkova, J.; Lacher, N. A.; Svec, F., Control of selectivity via nanochemistry: Monolithic capillary column containing hydroxyapatite nanoparticles for separation of proteins and enrichment of phosphopeptides. *Analytical Chemistry* **2010,** *82* (19), 8335-8341.

52. Todd, E. M.; Hillmyer, M. A., Porous Polymers from Self-Assembled Structures. In *Porous Polymers*, 2011; pp 31-78.

53. Cameron, N. R.; Krajnc, P.; Silverstein, M. S., Colloidal Templating. In *Porous Polymers*, 2011; pp 119-172.

54. Cameron, N. R.; Sherrington, D. C., High Internal Phase Emulsions (HIPEs) - Structure, Properties and Use in Polymer Preparation. In *Advances in Polymer Science*, 1996; Vol. 126, pp 162-214.

55. Silverstein, M. S., Emulsion-templated polymers: Contemporary contemplations. *Polymer* **2017,** *126*, 261-282.

56. Silverstein, M. S., PolyHIPEs: Recent advances in emulsion-templated porous polymers. *Progress in Polymer Science* **2014,** *39* (1), 199-234.

57. Cameron, N. R., High internal phase emulsion templating as a route to well-defined porous polymers. *Polymer* **2005,** *46* (5), 1439-1449.

58. Pulko, I.; Krajnc, P., Porous Polymer Monoliths by Emulsion Templating. Encyclopedia of Polymer Science and Technology. *Encyclopedia of Polymer Science and Technology* **2017**, 1-28.

59. Pulko, I.; Krajnc, P., High internal phase emulsion templating--a path to hierarchically porous functional polymers. *Macromol Rapid Commun* **2012,** *33* (20), 1731-46.

60. Lissant, K., *Emulsions and emulsion technology*. CRC Press: 1974; Vol. 3.

61. Sherrington, D. C.; Hodge, P., *Syntheses and Separations Using Functional Polymers* **1988**.

62. Wong, L. L. C.; Ikem, V. O.; Menner, A.; Bismarck, A., Macroporous polymers with hierarchical pore structure from emulsion templates stabilised by both particles and surfactants. *Macromolecular Rapid Communications* **2011,** *32* (19), 1563-1568.

63. Williams, J. M.; Wrobleski, D. A., Spatial distribution of the phases in water-in-oil emulsions. open and closed microcellular foams from cross-linked polystyrene. *Langmuir* **1988,** *4* (3), 656-662.

64. Zheng, X.; Zhang, Y.; Wang, H.; Du, Q., Interconnected Macroporous Polymers Synthesized from Silica Particle Stabilized High Internal Phase Emulsions. *Macromolecules* **2014,** *47* (19), 6847-6855.

65. Gurevitch, I.; Silverstein, M. S., One-pot synthesis of elastomeric monoliths filled with individually encapsulated liquid droplets. *Macromolecules* **2012,** *45* (16), 6450-6456.

66. Zhang, T.; Xu, Z.; Guo, Q., Closed-cell and open-cell porous polymers from ionomer-stabilized high internal phase emulsions. *Polymer Chemistry* **2016,** *7* (48), 7469-7476.

67. Williams, J. M., High Internal Phase Water-in-Oil Emulsions: Influence of Surfactants and Cosurfactants on Emulsion Stability and Foam Quality. *Langmuir* **1991,** *7* (7), 1370-1377.

68. Kovačič, S.; Silverstein, M. S., Superabsorbent, High Porosity, PAMPS-Based Hydrogels through Emulsion Templating. *Macromolecular Rapid Communications* **2016,** *37* (22), 1814-1819.

69. Zhang, T.; Xu, Z.; Wu, Y.; Guo, Q., Assembled Block Copolymer Stabilized High Internal Phase Emulsion Hydrogels for Enhancing Oil Safety. *Industrial and Engineering Chemistry Research* **2016,** *55* (16), 4499-4505.

70. Zhang, T.; Xu, Z.; Cai, Z.; Guo, Q., Phase inversion of ionomer-stabilized emulsions to form high internal phase emulsions (HIPEs). *Physical Chemistry Chemical Physics* **2015,** *17* (24), 16033-16039.

71. Viswanathan, P.; Johnson, D. W.; Hurley, C.; Cameron, N. R.; Battaglia, G., 3D surface functionalization of emulsion-templated polymeric foams. *Macromolecules* **2014,** *47* (20), 7091-7098.

72. Kovačič, S.; Preishuber-Pflügl, F.; Pahovnik, D.; Žagar, E.; Slugovc, C., Covalent incorporation of the surfactant into high internal phase emulsion templated polymeric foams. *Chemical Communications* **2015,** *51* (36), 7725-7728.

73. Zhang, T.; Silverstein, M. S., Microphase-separated macroporous polymers from an emulsion-templated reactive triblock copolymer. *Macromolecules* **2018,** *51* (10), 3828-3835.

74. Menner, A.; Ikem, V.; Salgueiro, M.; Shaffer, M. S. P.; Bismarck, A., High internal phase emulsion templates solely stabilised by functionalised titania nanoparticles. *Chemical Communications* **2007,** (41), 4274-4276.

75. Gurevitch, I.; Silverstein, M. S., Nanoparticle-based and organic-phase-based AGET ATRP polyHIPE synthesis within pickering HIPEs and surfactant-stabilized HIPEs. *Macromolecules* **2011,** *44* (9), 3398-3409.

76. Gurevitch, I.; Silverstein, M. S., Shape memory polymer foams from emulsion templating. *Soft Matter* **2012,** *8* (40), 10378-10387.

77. Yi, F.; Xu, F.; Gao, Y.; Li, H.; Chen, D., Macrocellular polymer foams from water in oil high internal phase emulsion stabilized solely by polymer Janus nanoparticles: preparation and their application as support for Pd catalyst. *RSC Advances* **2015,** *5* (50), 40227-40235.

78. Li, Z.; Ming, T.; Wang, J.; Ngai, T., High internal phase emulsions stabilized solely by microgel particles. *Angewandte Chemie - International Edition* **2009,** *48* (45), 8490-8493.

79. Zhang, T.; Xu, G.; Li, Z. F.; Regev, O.; Maddumaarachchi, M.; Blum, F. D., PS/CTAB/silica composites from room temperature polymerization of high internal phase emulsion gels. *Journal of Colloid and Interface Science* **2015,** *451*, 161-169.

80. Zhang, T.; Xu, G.; Regev, O.; Blum, F. D., Low-temperature polymerization of methyl methacrylate emulsion gels through surfactant catalysis. *Journal of Colloid and Interface Science* **2016,** *461*, 128-135.

81. Moglia, R. S.; Whitely, M.; Dhavalikar, P.; Robinson, J.; Pearce, H.; Brooks, M.; Stuebben, M.; Cordner, N.; Cosgriff-Hernandez, E., Injectable polymerized high internal phase emulsions with rapid in situ curing. *Biomacromolecules* **2014,** *15* (8), 2870-2878.

82. Butler, R.; Hopkinson, I.; Cooper, A. I., Synthesis of Porous Emulsion-Templated Polymers Using High Internal Phase CO2-in-Water Emulsions. *Journal of the American Chemical Society* **2003,** *125* (47), 14473-14481.

83. Wu, R.; Menner, A.; Bismarck, A., Macroporous polymers made from medium internal phase emulsion templates: Effect of emulsion formulation on the pore structure of polyMIPEs. *Polymer* **2013,** *54* (21), 5511-5517.

84. Lamson, M.; Epshtein-Assor, Y.; Silverstein, M. S.; Matyjaszewski, K., Synthesis of degradable polyHIPEs by AGET ATRP. *Polymer* **2013,** *54* (17), 4480-4485.

85. Khodabandeh, A.; Arrua, R.; Desire, C.; Rodemann, T.; Bon, S.; Thickett, S.; Hilder, E., Preparation of inverse polymerized high internal phase emulsions using an amphiphilic macro-RAFT agent as sole stabilizer. *Polym. Chem.* **2016,** *7*.

86. Streifel, B. C.; Parker, J. F.; Giles, S. L.; Williams, S. J.; Duncan, J. H.; Wynne, J. H., Porosity control in high internal phase emulsion templated polyelectrolytes via ionic crosslinking. *Journal of Polymer Science Part A: Polymer Chemistry* **2016,** *54* (16), 2486-2492.

87. David, D.; Silverstein, M. S., Porous polyurethanes synthesized within high internal phase emulsions. *Journal of Polymer Science Part A: Polymer Chemistry* **2009,** *47* (21), 5806-5814.

88. Moglia, R. S.; Robinson, J. L.; Muschenborn, A. D.; Touchet, T. J.; Maitland, D. J.; Cosgriff-Hernandez, E., Injectable PolyMIPE Scaffolds for Soft Tissue Regeneration. *Polymer (Guildf)* **2014,** *56* (1), 426-434.

89. Xiao, C.; Zhang, S.; Chen, J., Synthesis of Emulsion-templated Porous Polycaprolactone. *MATEC Web of Conferences* **2016,** *67*, 06108.

90. Mert, E., Tailoring the mechanical and thermal properties of dicyclopentadiene polyHIPEs with the use of a comonomer. *Express Polymer Letters* **2015,** *9*, 344-353.

91. Lovelady, E.; Kimmins, S. D.; Wu, J.; Cameron, N. R., Preparation of emulsion-templated porous polymers using thiol–ene and thiol–yne chemistry. *Polymer Chemistry* **2011,** *2* (3), 559-562.

92. Lei, L.; Zhang, Q.; Shi, S.; Zhu, S., High internal phase emulsion with double emulsion morphology and their templated porous polymer systems. *J Colloid Interface Sci* **2016,** *483*, 232-240.

93. Li, Z.; Liu, H.; Zeng, L.; Yang, S.; Wang, Y., Preparation of high internal water-phase double emulsions stabilized by a single anionic surfactant for fabricating interconnecting porous polymer microspheres. *Langmuir* **2014,** *30* (41), 12154-63.

94. Lu, Z.; Zhang, S.; Chen, J., Aligned Porous Beads Prepared by Frozen Polymerization of Emulsion-Templates Involving Tiny Emulsifier. *MATEC Web of Conferences* **2016,** *67*, 03045.

95. Zhang, H.; Cooper, A. I., Synthesis of Monodisperse Emulsion-Templated Polymer Beads by Oil-in-Water-in-Oil (O/W/O) Sedimentation Polymerization. *Chemistry of Materials* **2002,** *14* (10), 4017-4020.

96. Samanta, A.; Nandan, B.; Srivastava, R. K., Morphology of electrospun fibers derived from High Internal Phase Emulsions. *Journal of Colloid and Interface Science* **2016,** *471*, 29-36.

97. Costantini, M.; Colosi, C.; Guzowski, J.; Barbetta, A.; Jaroszewicz, J.; Święszkowski, W.; Dentini, M.; Garstecki, P., Highly ordered and tunable polyHIPEs by using microfluidics. *Journal of Materials Chemistry B* **2014,** *2* (16), 2290-2300.

98. Lafleur, J. P.; Senkbeil, S.; Novotny, J.; Nys, G.; Bogelund, N.; Rand, K. D.; Foret, F.; Kutter, J. P., Rapid and simple preparation of thiol-ene emulsion-templated monoliths and their application as enzymatic microreactors. *Lab Chip* **2015,** *15* (10), 2162-72.

99. Johnson, D. W.; Sherborne, C.; Didsbury, M. P.; Pateman, C.; Cameron, N. R.; Claeyssens, F., Macrostructuring of emulsion-templated porous polymers by 3D laser patterning. *Adv Mater* **2013,** *25* (23), 3178-81.

100. Pulko, I.; Smrekar, V.; Podgornik, A.; Krajnc, P., Emulsion templated open porous membranes for protein purification. *Journal of Chromatography A* **2011,** *1218* (17), 2396-2401.

101. Krajnc, P.; Štefanec, D.; Pulko, I., Acrylic Acid "Reversed" PolyHIPEs. *Macromolecular Rapid Communications* **2005,** *26* (16), 1289-1293.

102. Cameron, N. R.; Sherrington, D. C., High internal phase emulsions (HIPEs)—Structure, properties and use in polymer preparation. In *Biopolymers liquid crystalline polymers phase emulsion*, Springer: 1996; pp 163-214.

103. Cameron, N. R.; Sherrington, D. C., Synthesis and Characterization of Poly (aryl ether sulfone) PolyHIPE Materials. *Macromolecules* **1997,** *30* (19), 5860-5869.

104. Shirshova, N.; Bismarck, A.; Steinke, J. H. G., Ionic Liquids as Internal Phase for Non-Aqueous PolyHIPEs. *Macromolecular rapid communications* **2011,** *32* (23), 1899-1904.

105. Lee, J.-Y.; Tan, B.; Cooper, A. I., CO2-in-water emulsion-templated poly (vinyl alcohol) hydrogels using poly (vinyl acetate)-based surfactants. *Macromolecules* **2007,** *40* (6), 1955-1961.

106. Tan, B.; Lee, J.-Y.; Cooper, A. I., Synthesis of emulsion-templated poly (acrylamide) using CO2-in-water emulsions and poly (vinyl acetate)-based block copolymer surfactants. *Macromolecules* **2007,** *40* (6), 1945-1954.

107. Kovačič, S.; Jeřabek, K.; Krajnc, P., Responsive poly (acrylic acid) and poly (N-isopropylacrylamide) monoliths by high internal phase emulsion (HIPE) templating. *Macromolecular Chemistry and Physics* **2011,** *212* (19), 2151-2158.

108. Mazaj, M.; Logar, N. Z.; Žagar, E.; Kovačič, S., A facile strategy towards a highly accessible and hydrostable MOF-phase within hybrid polyHIPEs through in situ metal-oxide recrystallization. *Journal of Materials Chemistry A* **2017,** *5* (5), 1967-1971.

109. Pakeyangkoon, P.; Magaraphan, R.; Malakul, P.; Nithitanakul, M. In *Effect of soxhlet extraction and surfactant system on morphology and properties of poly (DVB) polyHIPE*, 2008; Wiley Online Library: pp 149-156.

110. Sergienko, A. Y.; Tai, H.; Narkis, M.; Silverstein, M. S., Polymerized high internal-phase emulsions: Properties and interaction with water. *Journal of applied polymer science* **2002,** *84* (11), 2018-2027.

111. Jerábek, K.; Pulko, I.; Soukupova, K.; Štefanec, D.; Krajnc, P., Porogenic solvents influence on morphology of 4-vinylbenzyl chloride based PolyHIPEs. *Macromolecules* **2008,** *41* (10), 3543-3546.

112. Woodward, R. T.; Jobbe-Duval, A.; Marchesini, S.; Anthony, D. B.; Petit, C.; Bismarck, A., Hypercrosslinked polyHIPEs as precursors to designable, hierarchically porous carbon foams. *Polymer* **2017,** *115*, 146-153.

113. Choudhury, S.; Connolly, D.; White, B., Supermacroporous polyHIPE and cryogel monolithic materials as stationary phases in separation science: A review. *Analytical Methods* **2015,** *7* (17), 6967-6982.

114. Kovačič, S.; Krajnc, P., Macroporous monolithic poly (4-vinylbenzyl chloride) columns for organic synthesis facilitation by in situ polymerization of high internal phase emulsions. *Journal of Polymer Science Part A: Polymer Chemistry* **2009,** *47* (23), 6726-6734.

115. Clear, S. C.; Parthasarathy, R. V.; Sura, R. K.; Soo, P. P., High internal phase emulsion foams containing polyelectrolytes. Google Patents: 2005.

116. Sergienko, A. Y.; Tai, H.; Narkis, M.; Silverstein, M. S., Polymerized high internal phase emulsions containing a porogen: specific surface area and sorption. *Journal of applied polymer science* **2004,** *94* (5), 2233-2239.

117. Kovačič, S.; Mazaj, M.; Ješelnik, M.; Pahovnik, D.; Žagar, E.; Slugovc, C.; Logar, N. Z., Synthesis and Catalytic Performance of Hierarchically Porous MIL-100 (Fe)@ polyHIPE Hybrid Membranes. *Macromolecular rapid communications* **2015,** *36* (17), 1605-1611.

118. Yin, D.; Guan, Y.; Gu, H.; Jia, Y., Polymerized high internal phase emulsion monolithic material: a novel stationary phase of thin layer chromatography. *Rsc Advances* **2017,** *7* (12), 7303-7309.

119. Tripodo, G.; Marrubini, G.; Corti, M.; Brusotti, G.; Milanese, C.; Sorrenti, M.; Catenacci, L.; Massolini, G.; Calleri, E., Acrylate-based poly-high internal phase emulsions for effective enzyme immobilization and activity retention: From computationally-assisted synthesis to pharmaceutical applications. *Polymer Chemistry* **2018,** *9* (1), 87-97.

120. Choudhury, S.; Connolly, D.; White, B., Application of polymeric high-internal-phase-emulsion-coated stationary-phase columns in open-tubular capillary electrochromatography. *Journal of Applied Polymer Science* **2016,** *133* (48).

121. Hu, Y.; Gao, H.; Du, Z.; Liu, Y.; Yang, Y.; Wang, C., Pickering high internal phase emulsion-based hydroxyapatite–poly (ε-caprolactone) nanocomposite scaffolds. *Journal of Materials Chemistry B* **2015,** *3* (18), 3848-3857.

122. Wang, A.-j.; Paterson, T.; Owen, R.; Sherborne, C.; Dugan, J.; Li, J.-m.; Claeyssens, F., Photocurable high internal phase emulsions (HIPEs) containing hydroxyapatite for additive manufacture of tissue engineering scaffolds with multi-scale porosity. *Materials Science and Engineering: C* **2016,** *67*, 51-58.

123. Gitli, T.; Silverstein, M. S., Emulsion templated bicontinuous hydrophobic-hydrophilic polymers: loading and release. *Polymer* **2011,** *52* (1), 107-115.

124. Lendlein, A., *Shape-memory polymers*. Springer: 2010; Vol. 226.

PROJECT AIMS

The origin of the present research project can be traced back to the past experiences gained at the Pharmaceutical Analysis Laboratory (PAL) (University of Pavia) with different chromatographic supports such as particle silica columns, monolithic silica column or synthetic polymers. The need for innovative and versatile solid supports, suitable for biocompatible studies, led to the investigation of new materials in order to carry out different bioanalytical studies.

The main aim of this Ph.D. project was to build-up a biocompatible polymeric platform with functional groups for the immobilization of biomolecules. Therefore, analytical tools have been set up to be used under continuous flow in order to develop devices for pharmaceutical applications. Moreover, we were also interested in the development of polymeric supports with suitable properties for biomedical applications. Therefore, polyHIPEs have been considered for this project due to the macroporous and hierarchical pore structure typical for these emulsion templated polymers. Therefore, the applications of the materials developed within this Ph.D. project can be divided into two main fields:

1. Biocatalysis.

   Biocatalytic tools may be achieved by the immobilization of enzymes to provide the synthesis of valuable chemicals. Therefore, by the obtainment of a polyHIPE monolithic column and the immobilization of a suitable enzyme, an immobilized enzyme reactor (IMER) has been achieved and applied in in-flow synthesis procedures.

2. Biomedicine.

   Due to the biocompatibility and the porous structure, acrylate-based polyHIPEs represent appealing supports for biomedical applications. Indeed, the potentialities of these materials to be used as scaffolds for drug delivery applications have been evaluated.

According to these aims, some modifications of the monomers mixture and of the polymerization parameters were necessary in order to develop new polymeric systems suitable for the different applications. In this context, a mathematical method has been used to predict the effect of several parameters on the final materials' properties in order to provide a reliable and efficient approach for studying the reaction.

The project is expected to achieve new functionalized PolyHIPEs, optimized in order to be fabricated in different shapes, such as monolithic columns, scaffolds, and membranes. One of the most interesting advantages of these materials is the extreme versatility and ease of

curing them in any shapes. In fact, the selected materials can be formulated in different forms, shapes, and dimensions in order to develop several devices useful in a wide range of scientific and technological fields. For example, monolithic columns, obtained by in situ polymerization are useful in biocatalysis studies as HPLC column.

CHAPTER 1

PolyHIPEs Synthesis and DoE approach

Acrylate-based poly-high internal phase emulsions for effective enzyme immobilization and activity retention: from computationally-assisted synthesis to pharmaceutical applications

Tripodo, G.[a], Marrubini, G.[a], Corti, M.[a], Brusotti, G.[a], Milanese, C.[b], Sorrenti, M.[a], Catenacci, L.[a], Massolini, G.[a], Calleri, E.[a]

[a]Department of Drug Sciences, University of Pavia, Viale Taramelli 12, Pavia, 70131, Italy

[b]C.S.G.I. - Department of Chemistry, Physical-Chemistry Section, University of Pavia, Viale Taramelli 16, Pavia, 70131, Italy

*Polymer Chemistry, **2018**, 9, 87-97*

This paper focuses on the synthesis of innovative functional materials prepared by the polymerization of high internal phase emulsions (HIPEs) for the bioconjugation of active molecules. By applying a computational method, this paper demonstrates how to produce materials with tailored features, such as pore dimensions (on the nano-micro scale), swelling in water and organic solvents and bulk densities. To this aim, starting from different emulsion compositions, ten materials are synthesized and fully characterized. Six different outputs (i.e. swelling in water and THF, mass loss in water and THF, throat and void diameters) are modeled using D-optimal mixture experimental designs. A clear correlation between the applied synthetic conditions and the final properties of the materials is demonstrated. The responses allow the selection of a single material for the development of a bioreactor prototype. Thus, the selected material is loaded into a glass column and polymerized in situ. An in-column procedure is also used for the covalent binding of horseradish peroxidase (HRP) as a model enzyme. A standard substrate is selected to test the activity of the immobilized enzyme. To conclude, the experimental design models allow one to obtain different materials with different features that could find applications in the fields such as biocatalysis/biochromatography, drug delivery or diagnostics. To the best of our knowledge, for the first time, an acrylate-based polyHIPE material is used for the binding of enzymes in the active form and successfully applied under flow conditions.

1. Introduction

The aim of this first part of my Ph.D. study is to produce new materials and to establish their potential applications. In particular, these materials should be able to immobilize proteins or enzymes of pharmaceutical interest by retaining the biomolecule's activity. Ideally, these materials should be characterized by (i) an interconnected structure, to ensure solvent and substance exchanges within the material and the surrounding environment; (ii) mechanical stability, to support flow, pressure, and friction; (iii) a predominant hydrophobic nature with partial water affinity, to avoid water over-swelling while ensuring an effective wettability to allow water spreading within the material and (iv) the presence of functionalities for biomolecule linkages. In the literature, there are several methods to produce porous materials, not necessarily showing interconnected pores. Porous materials have been obtained by vapor phase polymerization of metal-organic frameworks[1], by spray-drying[2], after post-production solubilization of water-soluble polymers blended into another polymer network[3], through a layer-by-layer process using a uniform polystyrene (PS) latex fabricated by dispersion polymerization[4], by phase separation of cellulose acetate and subsequent hydrolysis[5], or by common salt leaching of NaCl[6]. These methods are effective but it is not clear how to obtain interconnected pores within the matrix or tailorable dimensions of the micro-structures. It is also true that the shape and morphology of the final macro-structure could not be accurately controlled by applying some of these methods. Based on these premises, we focused our attention on the preparation of materials using the high internal phase emulsion (HIPE) technique to obtain polymerized materials [poly(HIPEs)] with easy to control shape and functions. HIPEs are water in oil emulsions with higher than 70% (w/w or v/v) content in the internal phase. With this technique by polymerizing the external phase, the thin and stretched film surrounding the internal phase droplets polymerizes and, eventually, crosslinks to form monoliths with an internally interconnected structure with voids which are the results of internal phase droplets. The porosity of these materials is given by throats which are the result of polymer contraction upon polymerization and crosslinking[7]. Obviously, the polymerization and crosslinking take place at the interface of W/O. PolyHIPEs can be molded, 3D printed and obtained in any shape. Furthermore, differently from other foam-like synthetic materials, they can be obtained as porous material with highly flexible topological characteristics with different porosities (74–99%), pore sizes (1–300 μm), interconnecting pores (0.1–20 μm) and compressive moduli up to 60 MPa[8]. These properties can be simply modulated by varying the process parameters such as the stirring rate, mixing time and temperature or changing the composition parameters such as different monomer

rates, the concentration of surfactant and nature of the monomers. Recently, as already described before, different polyHIPEs have been proposed for different applications: chromatography[9, 10], scaffolds for regenerative medicine[11], catalysis[12], biocatalysis[13], or 3D printing[14]. This versatility justifies and demonstrates that polyHIPEs are effective tools that can be used for different applications. Among the most used monomers in polyHIPE formation, styrene and divinylbenzene are found in several examples. However, this composition could not lead to materials with effective biocompatibility, biodegradation and post-production functionalization. Other approaches exploit the use of preformed polymers, biodegradable polyesters[15, 16], polyurethane[17] or polysaccharides[18, 19]. In this field, several complete and exhaustive reviews have been published[7, 20, 21]. The strategy of using pre-formed polymers could be of interest but the possibility of choosing different structural/functional monomers in our scope is fundamental. These premises led us to propose an acrylate system[22]. As a starting backbone monomer, the first choice was butyl acrylate because of its hydrophobicity. As the crosslinker, a trifunctional crosslinker such as trimethylolpropane triacrylate was evaluated since it would form a strictly interconnected polymeric structure ensuring a good resistance of the final material to mechanical stresses such as flow and friction. Last but not least, the selected functionalized monomer was the epoxy bearing glycidyl methacrylate because the epoxy groups can be further exploited for post-production immobilization of macromolecules such as enzymes, proteins or antibodies. Moreover, after hydrolysis, the epoxy groups lead to the consequent formation of hydroxyl groups (i.e., spontaneous hydrolysis or upon functionalization), that allows the material to gain a certain affinity for water. The hydrophobic nature of the main components is taken into specific account to reduce the swelling of the material in water. Only a few examples of butyl acrylate-based polyHIPEs are shown in the literature[15, 23, 24]. All these examples describe the use of butyl acrylate in combination with other monomers such as divinyl benzene (as a crosslinker) or as acrylate endcapping of poly(ε-caprolactone). On the other hand, butyl acrylate has found applications in the preparation of nanoparticles or biomaterials[25, 26]. Only few or no example of polyHIPEs bearing GMA functional groups for post-production functionalization are found in the literature. At the same time, only a few examples of enzymes chemically conjugated to a polyHIPE can be found in the literature and are based on styrene divinylbenzene systems[27, 28]. In the literature we did not find examples of acrylate-based polyHIPEs used to chemically immobilized enzymes retaining the catalytic activity under continuous flow conditions. For the pharmaceutical industry, biocatalysis is one of the key technologies in the area of “white biotechnology”. From another

perspective, flow reactor technology shows many advantages compared with batch methods, including increased safety, high control of reaction parameters, the possibility of automation and inline purifications. The combined use of continuous flow systems in biocatalyzed processes can overcome the main limitations associated with batch biotransformations that, at present, limit wider use of biocatalysis for industrial applications[29]. Biocatalyzed reactions performed in flow chemistry reactors can benefit from improved mass transfer, excellent temperature control and, importantly, continuous substrate feed and product removal, thus limiting the possible substrate/product inhibition of the enzyme activity. The use of continuous flow technologies also offers the possibility to implement enzymatic cascade reactions by confining different enzymatic activities in different environments. Despite these benefits, the potential of biocatalysis in flow reactors is far from being fully exploited. A key advantage of such a technology is clearly the availability of appropriate supports for enzyme immobilization to be used for different scopes: microscale, lab-scale or production scale synthesis[30, 31]. To accomplish the main aim of obtaining materials able to develop a bioreactor to be used under flow conditions, a property prediction tool, that could guide parameter selection and enable access to polyHIPEs possessing any desired morphology, could be useful. To this aim, a computational model by applying a design of experiment (DoE) approach was followed. Firstly, a set of HIPEs was prepared within an established range of parameters, then, different outputs from the obtained materials, such as swelling, mass loss, etc., were used to validate the model. A correlation between the applied synthetic conditions and the final properties of the materials was found. One of the materials from the computational model was selected and successfully used for the preparation of a bioreactor based on horseradish peroxidase.

2. Experimental section

2.1. Materials

Trimethylpropanetriacrylate (TMPT), butyl acrylate (BA), potassium persulfate (KPS), glycidyl methacrylate (GMA), N,N,N′,N′-tetramethylethylenediamine (TEMED), horseradish peroxidase (HRP), O-phenylenediamine (OPD), monobasic potassium phosphate (KH2PO4), anhydrous citric acid, ammonium sulfate, glycine, tetrahydrofuran (THF), absolute ethanol (EtOH), methanol (MeOH) and acetonitrile (ACN) used in this study were obtained from Sigma-Aldrich (Milan, Italy). Hydrogen peroxide solution (30%) was obtained from Belinka Perkemija. Synperonic PE/L 121™ was kindly provided by Croda Italiana Spa. All the materials were used as received. 30 mL Syringe PP/PE without a needle luer lock tip and female luer coupler in polypropylene were obtained from Sigma-Aldrich (Milan, Italy). Water used in this study was double deionized water (DDW), obtained by a Milli-q system from Millipore. An Omnifit® empty glass column (6.6 ID × 100 mm) was used in the bioreactor preparation.

2.2. Apparatus

Scanning electron microscopy (SEM) analyses were performed on a Zeiss EVO MA10 instrument (Carl Zeiss, Oberkochen, Germany) on gold-sputtered samples. Images were acquired from different sides of the samples. ATR-FTIR analyses were carried out using a Spectrum One PerkinElmer FTIR spectrophotometer (resolution: 4 cm^{-1}) (Monza, Italy) equipped with a MIRacle™ ATR device. All the liquid chromatography operations (enzyme immobilization and bioreactor characterization) were carried out using an Agilent Technologies HP-1100 HPLC instrument (Palo Alto, CA, USA) provided with a quaternary pump, a Rheodyne injection valve (20 µL loop), a degasser, a UV-Vis detector and thermostat oven (25 ± 0.5 °C). For HPLC analyses an Agilent Technologies LiChrospher 100 RP-18 5 µm (250 × 4.6 mm ID) column was used. The spectrophotometric analyses were performed by using a Shimadzu UV-1601 spectrophotometer.

2.3. Experimental design calculation

All calculations were performed using Microsoft Excel 2010 and R version 3.1.0 (2014-04-10) Copyright(C) 2014 The R Foundation for Statistical Computing. R-based chemometric software routines were used for DoE calculations. The R-based software has been developed by the Group of Chemometrics of the Italian Chemical Society

[http://gruppochemiometria.it/ gruppo-lavoro-r-in-chemiometria.html]. Simplex graphs and response surface plots were obtained by using Design-Expert® version 7.0.0 software (Stat-Ease Inc., MN, USA).

2.4. Methods

2.4.1. Synthesis of poly-high internal phase emulsion materials.

The polyHIPE preparation was carried out by mixing two distinct phases in a two-neck round bottom flask purged with nitrogen following a procedure described in the previous work[19]. The general procedure for all the prepared materials was carried out as follows: the oil phase was achieved with a total volume of 8 mL, while the water phase had a total volume of 32 mL. Indeed, a w/o emulsion 80/20 v/v was formed. The oil phase was prepared by mixing established amounts of two different lipophilic monomers: butyl acrylate as a backbone monomer and glycidyl methacrylate as a functional monomer. The oil phase comprised Synperonic PE/L 121 as the surfactant for the thermodynamic stabilization of the emulsion, and TMPT as a trifunctional crosslinker. The water phase was prepared by dissolving 272 mg of potassium persulfate in nitrogen degassed water. One of the necks of the round bottom flask was provided with a 50 mL dropping funnel with a PTFE stopcock filled with the water phase. The water phase was added drop by drop to the oil phase by manually regulating the dropping funnel stopcock under stirring at 300 rpm by an overhead stirrer supplied with a PTFE D-shaped paddle. The water phase was added over almost 20 min and the system was maintained under stirring and under nitrogen. When all the water phase was added to the oil phase, the stirring speed was increased to 400 rpm and the system was maintained under nitrogen during the complete stirring period. The material obtained at the end of the established stirring time (1 hour) is a highly viscous cream-like emulsion. After the mixing time, the obtained emulsion was added with 272 µL of TEMED and the mixture was stirred for further 2 min at 400 rpm. The material obtained was quickly poured into a Petri dish and allowed to polymerize for 24 h at room temperature. After the 24 h polymerization reaction, a white and lightweight solid was achieved. The polyHIPE obtained was transferred into a 200 mL crystallizer and washed as follows: two times in water (2 × 100 mL), one time in EtOH (1 × 100 mL), two times in MeOH (2 × 100 mL) and, eventually, in THF (2 × 100 mL). After washing, the polyHIPEs were dried in an oven at 40 °C for 24 h. Finally, the materials were characterized.

2.4.2. Experimental design for polyHIPEs and validation of the computational model.

The starting composition of the mixture of the HIPEs was selected from a previous study that established the domain of HIPE formation[22]. In particular, it has been seen that two formulations well-performed in terms of thermodynamic stability and polyHIPE formation. These compositions were as follows: (i) HIPE 2.0 BA + GMA 0.7, surfactant 0.15, TMPT 0.15 and (ii) HIPE 2.8.1 BA + GMA 0.75, surfactant 0.10, TMPT 0.15. The three factors considered to build up the computational model and, subsequently, to assess the output after the polymerization reaction, were: the amount of BA + GMA (factor A ranging from 0.7–0.8), the surfactant amount (factor B ranging from 0.05–0.2), and the crosslinker TMPT amount (factor C ranging from 0.09–0.15). The amounts of the three considered factors were constrained and are given in Table 1-1.

Table 1-3: Factors, experimental domain, and concentration levels considered for the

Factor	Units	Low level	High level
u1: BA + GMA	% w/w	0.7	0.8
u2: Surfactant	% w/w	0.05	0.2
u3: TMPT	% w/w	0.09	0.15

Constraint: u1+u2+u3 = 1

The experimental domain defined by the constrained concentrations of the three factors is the irregular polygon shown in Fig. 1-1. Therefore, a D-optimal design for the mixture ought to be used for studying the reaction[2, 3]. Under the hypothesis that all the responses could be modeled by special cubic mixture models, the plan of the experiments was computed as illustrated in Fig. 1-1. Ten experiments were selected and carried out; the compositions of the studied mixtures are summarized in Table 1-2 and Fig. 1-1.

Table 1-4: A, B, and C are the real values of the tested composition mixtures, expressed as the component ratio. u1, u2, and u3 are the upper-bound pseudocomponent values of the same mixtures, used for model computation. Both types of mixture representations respect the constraint that their sum per row equals 1

	A	B	C			
Experiment #	BA+GMA	SURFACTANT	TMPT	u_1	u_2	u_3
1	0.800	0.110	0.090	0.000	0.600	0.400
2	0.700	0.150	0.150	0.667	0.333	0.000
3	0.755	0.155	0.090	0.300	0.300	0.400
4	0.800	0.080	0.120	0.000	0.800	0.200
5	0.750	0.100	0.150	0.333	0.667	0.000
6	0.752	0.128	0.120	0.317	0.483	0.200
7	0.710	0.200	0.090	0.600	0.000	0.400
8	0.800	0.050	0.150	0.000	1.000	0.000
9	0.700	0.175	0.125	0.667	0.167	0.167
10	0.700	0.200	0.100	0.667	0.000	0.333

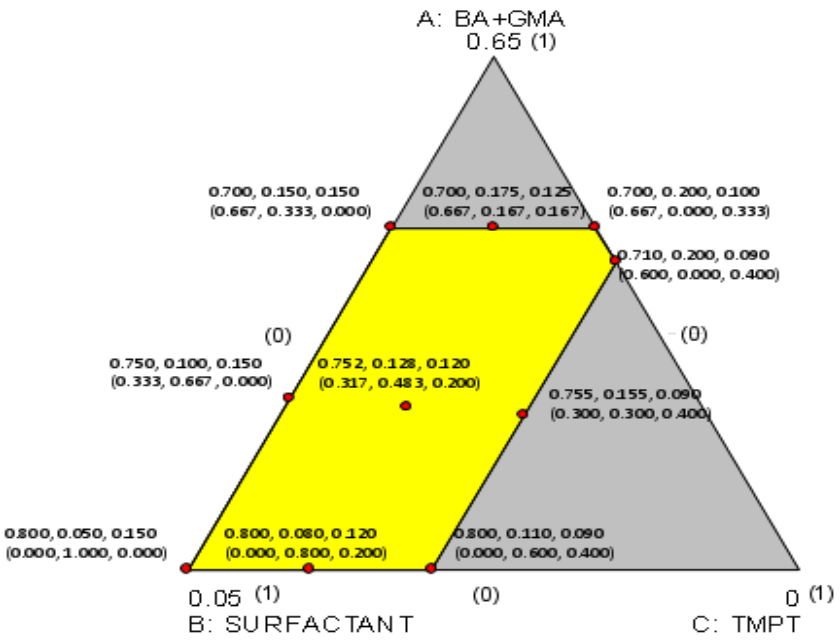

Figure 1-1: Experimental domain and compositions of the mixtures used in the polymerization reactions. The actual (real compositions), expressed as proportions, are shown together with the compositions coded as upper limit-bound pseudocomponents (compositions in brackets).

The ten experiments were those that provided the best compromise between the selection of a limited number of experiments and minimized log(normalized determinant) of the

dispersion matrix[32, 33]. As can be seen in Fig. 1-1, the ten experiments have been selected at the vertices of the polygon, at the midpoints of four of the five sides, and in the centroid of the polygon. The choice of performing ten experiments and postulate special cubic models a priori instead of simpler models such as the linear or the quadratic model was made by considering that the simpler models could be computed and validated anyway since they have a greater number of degrees of freedom (e.g. 4 degrees of freedom for the quadratic model and 7 for the linear model, respectively) and the estimate of the coefficients would be of better quality[32]. Actually, one of the encountered problems was that of collinearity between the factors which is expected for mixture designs, especially in highly constrained experimental domains[34], such as the one studied here. Therefore, in order to reduce the level of collinearity, all model computations were carried out using upper level-bound pseudocomponents (ui, i = 1, 2, 3) of the factors (A, B, and C). Once the pseudocomponent model predictive capacity had been defined and found acceptable, the equations in terms of the real values for the factors could be computed by substituting the relationships between A, B, and C and the corresponding ui, for a clearer understanding of the model results. The upper-bound pseudocomponents were computed using the following equation:

$$ui = \frac{Ui - Xi}{\sum_{i=1}^{3} Ui - 1}$$

where Ui is the upper-level value of the i-th factor, and Xi is the real value of the factor in the mixture. Therefore, for example, u1 for the upper level value of A = X1 will be equal to (0.8 − 0.8)/(0.8 + 0.2 + 0.15 − 1) = 0, whereas u1 for the lower level of A will be equal to (0.8 − 0.7)/(0.8 + 0.2 + 0.15 − 1) = 0.667. The outputs from the characterization of the polymers under examination used for the validation of the model were the polymer swelling in water (SWaq, Y1) and in THF (SWthf, Y2), the weight loss after wetting with water (WLaq, Y3) and THF (WLthf, Y4), and the material porosity (measured by the throat internal diameters, PID, Y5, and by the void diameters, VD, Y6). In order to validate this model, a single experiment, with 4 replicates, was conducted. Therefore, an eleventh HIPE (11.a) was achieved to confirm the obtainment of a material with the expected properties as: BA + GMA = 0.788; TMPT = 0.150 and surfactant = 0.062.

2.4.3. Weight loss and swelling studies in water and organic solvents.

The obtained polyHIPEs were characterized in terms of weight loss and swelling in water and organic solvents. The dried material was evaluated in terms of extractable matter in water and in organic solvents after polymerization. To do this, the polyHIPEs obtained after the synthetic procedure (as described above) were subjected or not to the THF last washing procedure to assess the mass loss in THF which is a good solvent for the soluble portions (not crosslinked) of the acrylate material. Small samples of dried polyHIPEs (≈ 15 mg) were cut and the starting weights (Ws) were recorded. The small monoliths were placed in a 50 mL beaker containing 20 mL of water or THF. The solvents were replaced with fresh ones at least 2 times in 24 h. Then the weights of wet samples (Wfw), after having been quickly dried on the surface with filter paper, were recorded. The samples were transferred into an oven at 40 °C to constant weight (24 h). Then the final weights (Wfd) of the dried materials were recorded. The weight loss (WL) and swelling (SW) values were calculated as follows:

$$WL = \frac{Ws - Wfd}{Ws} \times 100 \qquad SW = \frac{Wfw - Wfd}{Wfd}$$

where Ws is the starting dry weight, Wfw is the weight of the wet sample and Wfd is the final weight of the dried sample.

2.4.4. Semiquantitative analysis by ATR-FTIR of epoxy group hydrolysis during polyHIPE formation as a function of the composition.

ATR-FTIR spectra were obtained by using a Spectrum One PerkinElmer FTIR spectrophotometer (Monza, Italy) equipped with a MIRacle™ ATR device which allowed to collect spectra in the range of 4000–400 cm^{-1} (resolution: 4 cm^{-1}) directly on the polyHIPE samples. The semi-quantitative analysis of the epoxy groups in the polyHIPEs was performed by using the software provided with the ATR-FTIR equipment. It allows us to calculate the area of the selected bands. In particular, the bands at 908 and 847 cm^{-1} and at 1720 cm^{-1}, due to the vibrational bands attributed to the epoxy group ring and to the stretching of the carbonyl group, respectively, were used. The band at 1720 cm^{-1} was considered invariable with respect to the epoxy signals.

2.4.5. Preparation of a monolithic polyHIPE column.

For the preparation of a polyHIPE monolithic column, an optimized and fully characterized material was selected. A suitable composition (#6) was chosen in order to achieve the selected emulsion. HIPE was prepared as described above in the section Synthesis of poly-high internal phase emulsion materials. After 1 hour mixing of the oil/water mixture the obtained emulsion has been used for the preparation of a monolithic polyHIPE column. Therefore, approximately 10 mL of the white creamlike HIPE was placed in a 40 mL PE syringe. 68 µl of TEMED were added to the emulsion using a second syringe connected, with a polypropylene female luer coupler, to the pre-filled HIPE syringe. Indeed, the HIPE and TEMED were mixed by using a “syringe-to-syringe” method where the two components were stirred by a continuous extrusion from one syringe to the other until a complete mixing was achieved (12 extruding procedures were found to be convenient). To prepare a monolithic polyHIPE column, the obtained emulsion after the “syringe-to-syringe” method was rapidly transferred into the Omnifit® empty glass column to yield a 10 × 6.6 mm I.D. chromatographic bed using one of the two syringes allowing an in situ polymerization performed for 24 hours at room temperature. The obtained monolithic column was washed by flushing 13.5 mL of water, ethanol, and THF at 0.3 mL min^{-1} in order to remove the non-crosslinked material and side products. After washing, the monolithic column was stored at room temperature in THF.

2.4.6. Immobilization of a model enzyme on the monolithic bed

Enzyme immobilization was carried out following a well-established in situ immobilization procedure[35, 36]. Ten mL of a 0.5 mg mL^{-1} solution of horseradish peroxidase in 50 mM phosphate buffer (pH 7.0) containing 1.875 M ammonium sulfate was prepared. Before the immobilization, the monolithic column was equilibrated with 50 mM phosphate buffer (pH 7.0). The immobilization was carried out at 0.3 mL min^{-1} for 24 hours in a recycling system. The column was backflushed every 20 min. Then the enzymatic column was washed with 10 mL of 50 mM phosphate buffer (pH 7.0). After the immobilization process, an end-capping step with 13.5 mL of a 1 M glycine solution was used to block the remaining epoxy groups. The glycine eluate was collected, for the spectrophotometric assay. As the last step, the enzymatic column was washed with 13.5 mL of 50 mM phosphate buffer (pH 7.0). Finally, the enzymatic column was stored at 2–8 °C in 50 mM phosphate buffer (pH 7.0).

2.4.7. Evaluation of the immobilization yield.

The immobilization yield was calculated spectrophotometrically. The spectrophotometric analysis was carried out at 280 nm. A calibration curve was obtained with 5 different known

concentrations of HRP solution in 50 mM phosphate buffer (pH 7.0) and 1.875 M ammonium sulfate. The calibration range was 0.0675–0.25 mg mL^{-1}. Then a spectrophotometric analysis of the HRP solution was carried out before and after the immobilization step. The analysis was also carried out to estimate the concentration of HRP in the glycine eluate. The same experiment was performed on a polyHIPE column prepared without epoxy groups (no GMA which was substituted with BA) to verify the concentration of both HRP and glycine after the column treatment.

2.4.8. Evaluation of HRP activity after immobilization.

A 10 mg mL^{-1} solution of O-phenylenediamine (OPD), which is a standard substrate for HRP producing a soluble product, solubilized in a buffer solution at pH 5.0 (anhydrous citric acid 0.053 M and monobasic potassium phosphate 0.103 M) was prepared[37]. From this stock solution, different dilutions were prepared (0.25, 0.5, 1.0, 2.0, 2.5, 5.0, and 10.5 mg mL^{-1}). Before the inflow activity assay, the column containing the immobilized enzyme was equilibrated with a 50 mM phosphate buffer solution (pH 7.0). The HPLC analysis was carried out with the injections of 20 µL of the different dilutions. The flow-rate was 0.2 mL min^{-1}, the mobile phase applied was 50 mM phosphate buffer (pH 7.0) and the specific detection was performed at 441 nm. After the in-flow activity assay, the column was washed by the application of 13.5 mL of 50 mM phosphate buffer (pH 7.0). When not in use the column was stored at 2–8 °C in 50 mM phosphate buffer (pH 7.0).

3. Results and discussion

In this project, we demonstrate that functionalized polyHIPEs are effective materials for the development of enzyme bioreactors. The main goal of this work is to prove that by varying the HIPE compositions, it is possible to obtain materials with predictable behaviors in terms of pore dimensions (e.g. to optimize back pressure) and/or water/solvent affinity (e.g. to enhance biocatalyst activity). This prerequisite is fundamental for the application of these materials as functionalized supports for the immobilization of biocatalysts.

3.1. PolyHIPE experimental design, synthesis, and characterization

For the rational design of the materials to be selected for a specific application, a computational approach has been used to (i) establish the composition range for the HIPE formation; (ii) link the outputs from the characterization to the compositions; and (iii) validate the models by performing a random experiment within the established composition range and evaluate if this composition, within four replicated (different) batches (reproducibility), shows similar outputs within the expected ranges. The monomer used for the polyHIPE synthesis was BA, as the backbone, because of the presence of the C4 chain which can modify the water affinity of the material and improve the separation behaviors of the chromatographic systems. The structural stability was also improved by a high crosslinking density achieved by TMPT as the tri-functional crosslinker. GMA was selected as a functional monomer in order to guarantee the conjugation reaction between the nucleophilic groups of the enzyme (mostly –NH2 groups) and the epoxy groups from GMA in the polyHIPE. An important advantage provided by these formulations is that the polymerization reactions were carried out at room temperature since a KPS/TEMED system was used as the radical initiator. As shown in Table 1-2, ten different polyHIPEs were synthesized and characterized. To morphologically characterize the obtained polyHIPEs, all the samples were subjected to SEM analysis. The images were taken from different sides of the samples and those from the internal side were used for the calculation of void and throat diameter. In particular, images were acquired from the upper, lower and lateral (internal) sides of the samples. As shown in Fig. 1-2, the typical open-cell structure of the polyHIPE materials was achieved for some of the formulations selected by the computational model. In particular, the polyHIPE open-cell typical structure was achieved for 6 materials (1, 2, 4, 5, 6 and 8). The other compositions (3, 7, 9 and 10) did not allow a polyHIPE typical morphology. Actually, the samples with the highest concentration of surfactant (3, 7, 9 and 10) did not lead to the typical polyHIPE structure. The effect of the surfactant concentration on the

formation of polyHIPEs was previously observed. In particular, it has been shown that by increasing the surfactant concentration, thinner monomer films separating adjacent emulsion droplets are produced with consequent phase separation[7, 38]. Throat and void diameters were evaluated from SEM images and are given in Table 1-3. As from Table 1-3 void and throat diameters can be modulated by varying the composition of the polyHIPE. In particular, throat diameters can be varied between 400–1700 nm while voids can range from 1.5–7.7 µm. This is an important feature because it could lead to the selection of the material based on its behavior.

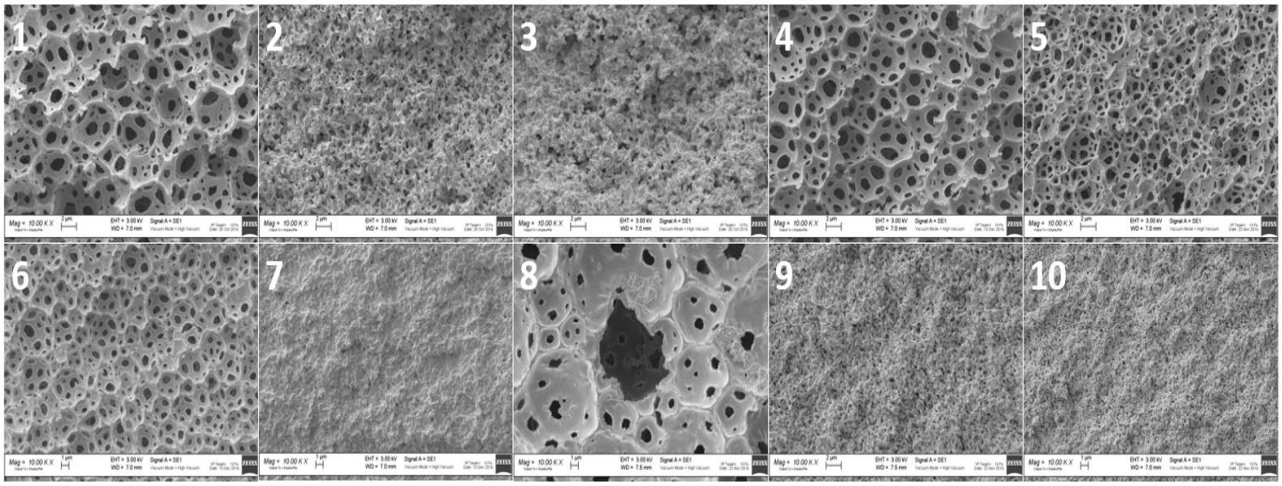

Figure 1-5: SEM images of polyHIPEs from 1 to 10, all the shown samples are at a magnification of 10000 x

Table 1-5: Throats and void diameters of each polyHIPEs expressed as average values ± SD (n=25)

polyHIPE	Throats diameter (µM)	Voids diameter (µM)
1	1.5 ± 0.5	3.9 ± 0.5
2	0.4 ± 0.1	1.5 ± 0.3
4	1.4 ± 0.3	3.9 ± 1.0
5	0.7 ± 0.2	2.1 ± 0.8
6	0.7 ± 0.2	2.4 ± 0.7
8	1.7 ± 0.3	7.7 ± 0.8

All the materials were also characterized in terms of weight loss and swelling in water and THF. Moreover, a semiquantitative analysis by ATR-FTIR of epoxy group hydrolysis was

carried out. The results are shown in Table 1-4. From the data shown in Table 1-4 different considerations arise. First, samples not characterized by an open-cell structure show the lowest ability to swell in both water and THF. This is not surprising because the material being less interconnected will not allow good penetration of the solvent inside the material.

Table 1-6: Weight loss and swelling in water and THF and semiquantitative analysis by ATR-FTIR of epoxy group hydrolysis of the obtained materials (1–10). The values were expressed as average values ± SD (n = 3) ***** The ATR-FTIR semiquantitative analysis was performed by calculating the rate of the areas epoxy/ester 908/1720 cm^{-1} (A) and 847/1720 cm^{-1} (B). These values are adimensional and higher values correspond to lower hydrolysis.

Sample	WL in H_2O	WL in THF	SW in H_2O	SW in THF	Peak area rate A/B*
1	13.50 % ± 8.15 %	3.98 % ± 0.93 %	4.16 ± 0.54	6.33 ± 0.27	0.075/0.153
2	8.90 % ± 5.09 %	14.14 % ± 0.40 %	2.13 ± 0.19	3.95 ± 0.33	0.066/0.140
3	6.11 % ± 0.59 %	13.87 % ± 1.94 %	1.11 ± 0.09	1.86 ± 0.19	0.094/0.176
4	10.38 % ± 2.19 %	9.21 % ± 1.80 %	5.56 ± 0.08	5.05 ± 0.57	0.075/0.143
5	15.11% ± 2.86 %	10.98 % ± 1.03 %	4.27 ± 0.10	4.89 ± 0.12	0.076/0.152
6	10,04 % ± 3.77 %	14.86 % ± 0.47 %	2.88 ± 0.08	4.43 ± 0.24	0.074/0.150
7	7.11 % ± 0.63 %	18.28 % ± 0.25 %	0.55 ± 0.01	1.32 ± 0.04	0.102/0.161
8	13.17 % ± 3.39 %	10.46 % ± 0.36 %	4.79 ± 0.98	7.10 ± 0.85	0.074/0.164
9	4.81 % ± 0.32 %	16.70 % ± 3.62 %	0.86 ± 0.01	1.27 ± 0.03	0.084/0.188
10	8.76 % ± 0.34 %	29.80 % ± 0.05 %	0.80 ± 0.09	1.46 ± 0.28	0.103/0.169

On the other side, materials 1, 2, 4, 5, 6 and 8 show swelling values related to the void diameter. This is particularly true for the swelling in THF. In particular, samples 2, 5 and 6 with void diameters of 1.5–2.4 µm had swelling values of 3.95–4.89 in THF. Samples 1, 4 and 8 which show void diameters of 3.9–7.7 µm had higher swelling values of 5.05–7.10 in THF. The swelling in water could not follow the same order as in THF and this is not surprising because of the predominantly hydrophobic nature of the material. So, a “leveling effect” of the material itself on the swelling behavior in water could be predictable as also confirmed by the computational analysis (see below). However, some slight differences (even if not statistically significant) could be noted among the samples so we thought that the reason could be a different hydrolysis yield of the epoxy group during the synthesis (leading to the formation of hydrophilic OH groups) based on the formulation. Even, for this

reason, we performed a semi-quantitative ATR-FTIR analysis to study the hydrolysis of epoxy groups during the process. In particular, we compared the area of the band at 1720 cm^{-1} which is related to the stretching vibration of the carbonyl ester group (chosen as a quantitatively "fixed" band) with those related to the epoxy group at 908 and 847 cm^{-1}. The semiquantitative analysis was performed by calculating the ratio of the areas 908/1720 cm^{-1} (A) and 847/1720 cm^{-1} (B). These values are adimensional and are given in Table 1-4. The higher the value of the found rates, the lower the hydrolysis of the epoxy groups (being a rate epoxy/ester). It was not possible to find the highest value of the ratio (no hydrolysis) because of problems in handling the liquid monomers (BA + GMA + TMPT) for ATR-FTIR analysis. Obviously, the absence of bands related to the epoxy groups will indicate full hydrolysis; we previously demonstrated that by formulating the polyHIPE without the GMA, the indicated bands were not present[22]. The results from the semiquantitative analysis indicate that epoxy group hydrolysis is independent by the polyHIPE composition (i.e. samples 1, 2, 4, 5, 6 and 8) while the hydrolysis yield was lower for samples 3, 7, 9 and 10, which did not show any open-cell morphology, with the epoxy groups being less exposed to the environment. One could also speculate that the "no-hydrolysis values" are those found for samples 3, 7, 9 and 10 (no open-cell morphology) which are close to the values found for the other samples, indicating low general hydrolysis during the polyHIPE formation. Obviously, this is a fundamental result because it ensures that the integrity of the epoxy groups is independent by the chosen composition. The last step in the synthesis of the polyHIPEs was the selection of a random composition within the established domain which was prepared in 4 different batches to test the reproducibility of the materials and the prediction ability (validity) of the model. In this manner, the mixtures A: BA + GMA 0.788, B: surfactant 0.062, C: TMPT 0.15 were prepared and the resulting polyHIPEs were characterized as described before. Fig. 1-3 shows the SEM images of the new polyHIPE material. The SEM images were acquired for composition 11 (4 replicates) showing a porous network for all the four materials which consequently were recognized as polyHIPEs. The throat and void diameters were then calculated and expressed as average diameter ± SD, Table 1-5.

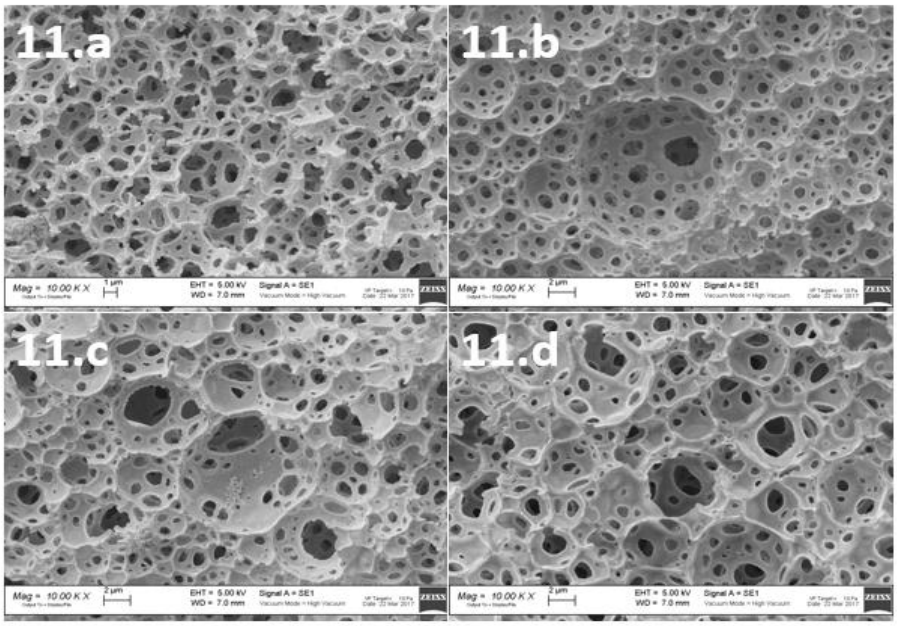

Figure 1-6: SEM images of polyHIPE 11.a; 11.b; 11.c; 11.d at 10000 x magnification

Table 1-7: Throats and void diameter of polyHIPEs 11.a, 11.b, 11.c and 11.d expressed as average values ± SD (n=25).

polyHIPE	Throats diameter (µM)	Voids diameter (µM)
11.a	1.2 ± 0.1	4.7 ± 0.5
11.b	1.1 ± 0.1	4.7 ± 0.5
11.c	1.2 ± 0.1	4.6 ± 0.4
11.d	1.2 ± 0.1	4.7 ± 0.5

As is shown, all the diameters for throats or voids are comparable in the four repeated samples, within a range of 0.1 µm, indicating an effective reproducibility of the adopted experimental method for the material preparation. Table 1-6 summarizes the main results from the performed characterization on sample 11. Also, in this case, considering the possibly large experimental error for water loss or swelling determination, the found experimental values show comparable values for the four prepared samples. The results from all the characterized compositions (samples 1–10) were used to compute the model equations and are given in Table 1-7. Some selected diagnostic parameters for appraising the quality of the model computed are listed. As far as the fitting of the experimental points is concerned, the R^2 and the adjusted R^2 are given in Table 1-1 and 1-7. The model statistical significance computed using the ANOVA of the regression is described by the F parameter

together with the model probability level (p-value). The Root Mean Square Error in Cross-Validation (RMSECV) is an indicator of the model prediction ability. The RMSECV is computed by processing as many models as experiments, and excluding each time one experiment, whose response was then predicted based on the remaining experiments. Ideally, the lower the RMSECV the better is the model in prediction. The equation for computing the RMSECV is:

$$RMSECV = \sqrt{\frac{\sum_{i=1}^{N}(Yi - yi)^2}{N}}$$

Except for WLaq, all the responses were described by Scheffé polynomial models that showed sufficient quality in the fitting. The minimum R^2 and the adjusted R^2 were 0.834 and 0.787, respectively. The least statistical significance for the models computed using the ANOVA of the regression was at the level of probability of p = 0.027 (Table 1-8, model for WLthf). The model prediction ability was investigated first by computing the Root Mean Square Error in Cross-Validation (RMSECV). All models showed RMSECV in agreement with the experimental standard deviation (compare the data of RMSECV of Table 1-8 with confidence intervals given in Table 1-9).

Table 1-8: Weight loss and swelling in water and THF and semiquantitative analysis by ATR-FTIR of epoxy groups hydrolysis of the obtained materials (11a-11d). The values were expressed as average values ± SD (n=3).

Sample	WL in H2O	WL in THF	SW in H2O	SW in THF
11.a	8.10 % ± 2.56 %	6.77 % ± 0.74 %	4.42 ± 0.16	7.42 ± 0.70
11.b	8.46 % ± 2.66 %	4.92 % ± 0.68 %	3.86 ± 0.28	6.47 ± 0.25
11.c	6.35 % ± 1.54 %	5.75 % ± 0.64 %	4.85 ± 0.58	6.56 ± 0.45
11.d	6.97 % ± 2.08 %	6.25 % ± 0.98 %	4.11 ± 0.83	6.37 ± 0.35

Table 1-9: Model equations and diagnostics. SWaq is the swelling of the polymer in water, SWthf is the swelling of the polymer in THF, WLaq is the weight loss after polymer wetting with water, and WLthf is the weight loss after polymer wetting with THF measured in %; PID, polymer throat internal diameter, and VD, polymer void diameter measured in μm. C.I.(95%, n = 10) is the confidence interval at the 95% probability level for the mean of n = 10 observations collected in duplicate measurements. NA, not applicable.

Models equations	R^2	Adj. R^2	F (p-value)	RMSECV
SWaq = -2.02·u_1 + 4.81·u_2 –11.10·u_3 + 8.07·u_1·u_2 + 26.01·u_1·u_3 + 24.04·u_2·u_3 – 57.94·u_1·u_2·u_3	0.998	0.995	328.79 (< 0.001)	0.26
SWthf = 1.016·u_1 + 7.102·u_2 + 1.503·u_3	0.853	0.811	20.37 (0.0012)	1.20
WLaq ; no model resulted statistically significant. The data are summarized by descriptive statistics. Mean(WLaq) ± C.I.$_{(95\%,\ n=10)}$ = 10 ± 3 %; median 9.6%; range (min-max) 5.0-17.4%	NA	NA	NA	NA
WLthf = 19.62·u_1 + 10.50·u_2 – 50.85·u_3 – 12.06·u_1·u_2 + 128.71·u_1·u_3 + 73.27·u_2·u_3	0.890	0.752	6.34 (0.027)	4.33
PID = –0.46·u_1 + 1.64·u_2 + 0.45·u_3	0.878	0.837	24.8 (< 0.001)	0.33
VD = –1.01·u_1 + 5.94·u_2 – 0.37·u_3	0.834	0.787	17.6 (0.0018)	1.47

The definitive confirmation of the predictive ability of the models was obtained after collecting the data of replicates of the experiments corresponding to the composition of the reaction mixture [A: BA + GMA 0.788, B: surfactant 0.062, C: TMPT 0.15]. The experimental values obtained for SWaq, SWthf, WLaq, WLthf, PID, and VD, together with the predicted values

computed by the models for each response, are presented in Table 1-9. Based on these results, it can be concluded that the models were all reliable since the agreement between the predicted value and the experimental value was within the limits of the experimental error and none of the results of the validation experiments were significantly different from the predicted values. Therefore, the models were applicable for predicting the properties of the formulations prepared by using the compositions included in the experimental domain. In mixture design data analysis, one difficulty is that the relevance of the effects of the components cannot be directly deduced by observing the magnitude of the coefficients computed. The mixture models must be analyzed taking into consideration that a change in one component is accompanied by the simultaneous change in the other two components of the mixture since the overall composition of the mixture must respect the constrain A + B + C = 1. Several methods for estimating the effects of the components in a mixture have been reported[34], and in the present study, the approach described by Cafaggi and coworkers was chosen to owe to its simplicity[32]. Briefly, the effect of component i is computed as the difference between the responses at two points centered on the centroid of the experimental domain. The two points have a fixed difference in terms of component i. The other two components instead are kept at a constant ratio which corresponds to the composition of the mixture represented in the centroid of the experimental domain.

Table 1-10: Effects of the components on the characteristics of the polymer obtained: Y_{center} and Y_{change} are the responses computed by the models in the centroid of the experimental domain and in the point with coordinates changed by an increase of +0.02 in one component while keeping the other two at the constant ratio occurring in the centroid

Component change	**Effect = Y_{change} – Y_{center} (Effect % = 100* Effect/Y_{center})**				
	Swaq	SWthf	WLthf	PID	VD
u1: BA+GMA 0.725 → 0.745; (X2/X3 = 1.067)	3.344 - 2.877= 0.467 (+16%)	4.475-4.037 = 0.438 (+11%)	11.701-14.569= -2.868 (-20%)	0.929-0.729 = 0.2 (+27%)	2.960-2.454= 0.506 (+21%)
u2: SURFACTANT 0.128 → 0.148 (X1/X3 = 6.267)	1.980–2.877=- 0.897 (-31%)	3.235-4.037=-0.802 (-20%)	17.004-14.569= 2.435 (+17%)	0.468-0.729= -0.261 (-36%)	1.540-2.454 = -0.914 (-37%)
u3: TMPT 0.120 → 0.140 (X1/X2 = 5.875)	3.253 – 2.877 = 0.376 (+13%)	4.094-4.037 = 0.057 (1%)	13.912-14.569 = -0.657 (-5%)	0.650-0.729 = -0.079 (-11%)	2.509-2.454= 0.055 (+2%)

Table 1-11: Results of the validation of the models. The coordinates of the point selected for the validation experiments were: BA+GMA: 0.788%, Surfactant: 0.062%, TMPT: 0.15%. These coordinates correspond to coded upper level-bound pseudocomponents: u1: 0.08; u2: 0.92; u3: 0.00.

RESPONSE	VALUE MEASURED MEAN ± SD	VALUE PREDICTED BY THE MODEL VALUE COMPUTED ± CI(95%)	RELATIVE ERROR (%)
sWAQ%	4.3 ± 0.6 (2)	4.9 ± 0.3	14
sWTHF%	6.7 ± 0.6 (2)	7 ± 1	4
WLAQ%	9 ± 5 (2)	11 ± 3 (median 9.6)§	22
WLTHF%	6 ± 3 (2)	10 ± 7	67
PID MM	1.2 ± 0.1 (4)	1.5 ± 0.4	26
VD MM	4.7 ± 0.1 (4)	5 ± 2	12

Responses abbreviations: SWaq, swelling of the polymer in water; SWthf, swelling of the polymer in THF; WLaq, weight loss after polymer wetting with water; and WLthf, weight loss after polymer wetting with THF; PID, polymer throats internal diameter; VD, polymer voids diameter are measured in µm.

§ The WLaq response is computed as mean and median and compared with the data obtained in the validation experiments.

CI(95%), confidence interval computed at the 95% probability level.

n, the number of replicate measurements carried out independently from those used to build the model.

Relative error % = 100* (Value predicted – Value measured)/Value measured.

By applying this method, it has been possible to compute quantitatively the effects given in Table 1-4 which can be evaluated qualitatively as shown in Fig. 1-4a– 1-4e. Based on the results reported in Table 1-6 and on the study of the response surfaces plotted in Fig. 1-4a–1-4e, the following conclusions could be drawn. The SWaq and SWthf are affected primarily by the surfactant amount in the mixture (Table 1-8 and Fig. 1-4a, 1-4b). By increasing the surfactant by 0.02% the models showed a decrease in responses for both SWaq and SWthf

of about 31% and 20%, respectively. The effect of BA + GMA is also important and similar on either swelling, but to a lesser extent (+16% and +11% on SWaq and SWthf, respectively). The effect of TMPT is evidenced only on the swelling in THF, where the increase of TMPT causes an increase of about 13% in this polymer feature. As far as the weight loss in water is concerned, as evidenced by the experimental data, no significant changes are evident because of the changes in the mixture used for the polymerization.

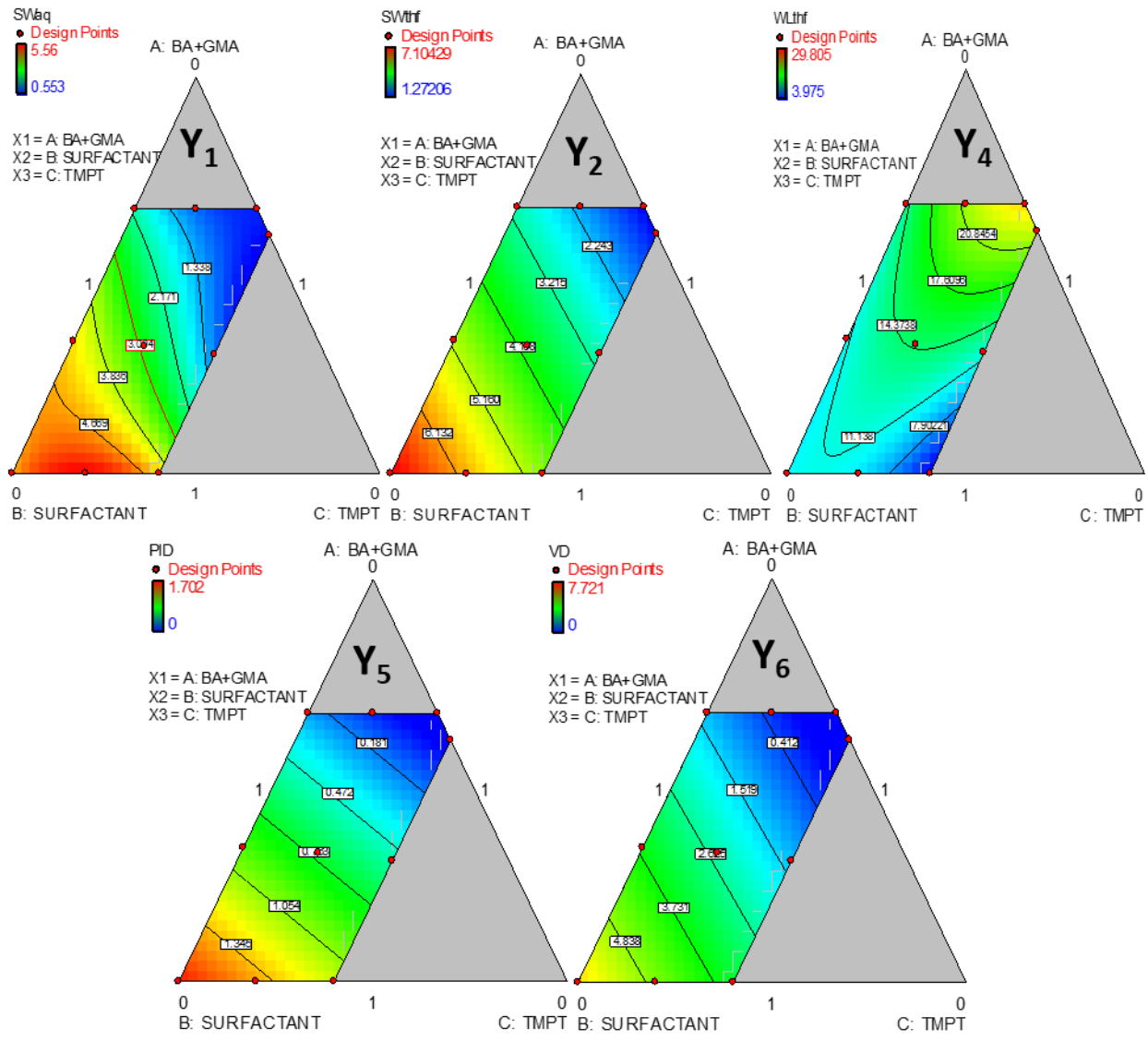

Figure 1-7: Response surfaces for the five statistically significant models computed and validated: 4a) Swelling in water (SWaq%), 4b) Swelling in THF (SWthf%), 4c) Weight loss in THF (SWthf%), 4d) Throats internal diameter (PID, µm), and 4e) Voids diameter (VD, µm).

The average WLaq is around 10% (median 9.6%). The fact that no model could be computed is due to the great scatter of the data around the mean with no evident tendency due to

changes in the mixture composition, Table 1-8. The weight loss in THF appears instead influenced by BA + GMA and by the surfactant amount to the same extent, although in opposite directions. The response decreases drastically as the BA + GMA amount increase in the mixture and the response increases instead if the surfactant amount increases (Fig. 1-4c). The throat internal diameters (PID, Fig. 1-4d) and void diameters (VD, Fig. 1- 4e) are affected in the same way by the changes in the composition of the polymerization mixture. The major effect is that of the amount of surfactant, followed by that of the amount of BA + GMA. When the amount of surfactant is increased, this brings to throats and voids with smaller diameters. The effect of increasing the amount of BA + GMA is to produce throats and voids with larger diameters. The effect of TMPT is measurable only on the throat internal diameters, where the tendency shown is that an increase in the amount of TMPT produces polymers with smaller throats.

3.2. Evaluation of polyHIPE as a material for enzyme immobilization

For this experiment, polyHIPE #6 has been chosen as a model material because of its low swelling in water and because of its regular SEM morphology. Filling the glass column with the emulsion before polymerization allowed us to achieve the polymerization directly in the column and, consequently, to slightly modify the procedure for the radical induction. To avoid a premature polymerization of the HIPE prior to the column filling, TEMED was not added directly to the emulsion (in the flask) but a “syringe-to-syringe” method was used to quickly transfer the radically initiated emulsion directly to the column (refer to the Experimental part). Approximately a 10 × 6 mm ID polyHIPE bed was obtained. For this experiment, we selected HRP since it is well known that this enzyme preserves its catalytic activity after immobilization on epoxy-functionalized materials[39-41]. The covalent immobilization of the HRP to the polyHIPE was accomplished by following a consolidated in situ procedure (see the Experimental part). The immobilization yield was determined spectrophotometrically by measuring the absorbance of the enzymatic solution before and after the immobilization procedure. For quantitation, a calibration curve was derived at 280 nm and a linear correlation was found ($y = 0.8562x - 0.0009$; $R^2 = 0.9996$). The immobilization yield was 24.13%, corresponding to 50 mg of an immobilized enzyme indicating the successful immobilization of HRP on the epoxy groups of the polyHIPE-based stationary phase. To verify that the enzymatic solution does not undergo a reduction in UV absorbance during the immobilization process, the same experiment was performed by fluxing the same HRP

solution through support without epoxy functionalities. After 24 h the enzyme absorbance was equal to 99.5% with respect to the initial absorbance.

3.3. Enzyme kinetic evaluation by an in-flow activity assay

Horseradish peroxidase is a typical peroxidase enzyme obtained from the roots of horseradish. Among all peroxidases, HRP is known to catalyze various oxidative transformations of organic compounds using H_2O_2 as an oxidative agent, such as the conversion of o-phenylenediamine (OPD) in 2,3-diaminophenazine. In this study, HRP was selected as a protein to be immobilized onto the polyHIPE monolithic column because, as a peroxidase, it is regarded as a highly selective and efficient biocatalyst. Moreover, HRP has some advantageous characteristic properties like a low price, significant resistance to organic solvents and a very wide number of substrates available on the market[42]. OPD was selected as an HRP chromogenic substrate because its oxidative conversion leads to obtain the product 2,3-diaminophenazine. 2,3-Diaminophenazine can be easily detected by using a UV-Vis detector at 441 nm[37]. Moreover, at 441 nm, OPD does not show any absorbance. For this reason, 441 nm was selected as the wavelength for the HPLC-UV-Vis analysis in the in-flow activity assay, Fig. 1-5. According to the conditions reported above, different OPD concentrations were injected into an HPLC-UV-Vis system and the monolithic polyHIPE HRP-column was used in the biocatalysis process. Fig. 1-5 shows the chromatograms obtained by injecting increasing substrate concentrations. As expected, the product peak areas increase with the substrate concentration. In order to evaluate the enzymatic kinetic, the reaction rate for each substrate concentration was calculated as follows:

$$v = \frac{peak\ area}{elution\ time}$$

where the elution time was assumed as the total time to elute the product. The relationship between the reaction rate and substrate concentration is shown in Fig. 1-6. This relation was expressed by the Michaelis–Menten equation that represents the kinetic profile of enzymatic reactions:

$$V = \frac{Vmax[OPD]}{Km + [OPD]}$$

where V is the reaction rate, Vmax is the maximum reaction rate, Km is the Michaelis–Menten constant and [OPD] is the substrate concentration expressed as mol L^{-1}. In order to

calculate the reaction kinetic values, such as Km and Vmax, this equation was expressed as a double reciprocal plot:

$$\frac{1}{V} = \frac{Km}{Vmax} \times \frac{1}{[OPD]} + \frac{1}{Vmax}$$

Thus, this equation is the graphic representation of this enzyme kinetic, where the slope is Km/Vmax, the y-intercept is 1/Vmax and the x-intercept is −1/Km. In this case, a curve y = 0.01688x + 0.00035 was achieved as shown in Fig. 1-7. Therefore, kinetic values were calculated as: Vmax = 2857.1 area per min; Km = 48.23 mM. These results showed good linearity and a correct outgoing for an enzymatic reaction. To date, the bioreactor has been used for approximately 50 bioconversions without loss of the initial catalytic activity confirming the high stability of the supported enzyme. Maintenance of their structural stability with functional efficiency and reproducibility provides an excellent base to further investigate the applicability of these supports in different fields.

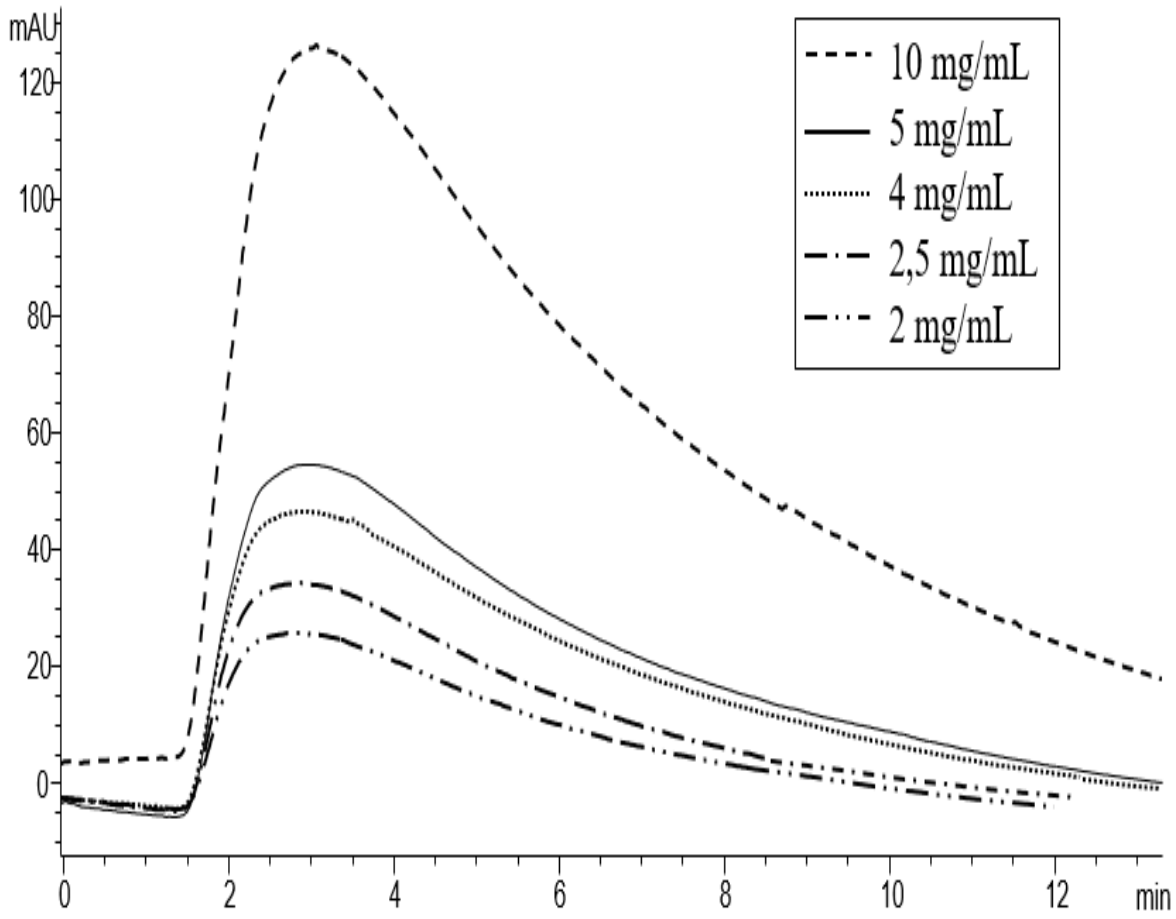

Figure 1-8: Chromatograms of OPD solution at different concentrations (mg/ml) in phosphate buffer at pH 7 (50 mM) as the mobile phase, detection at 441 nm

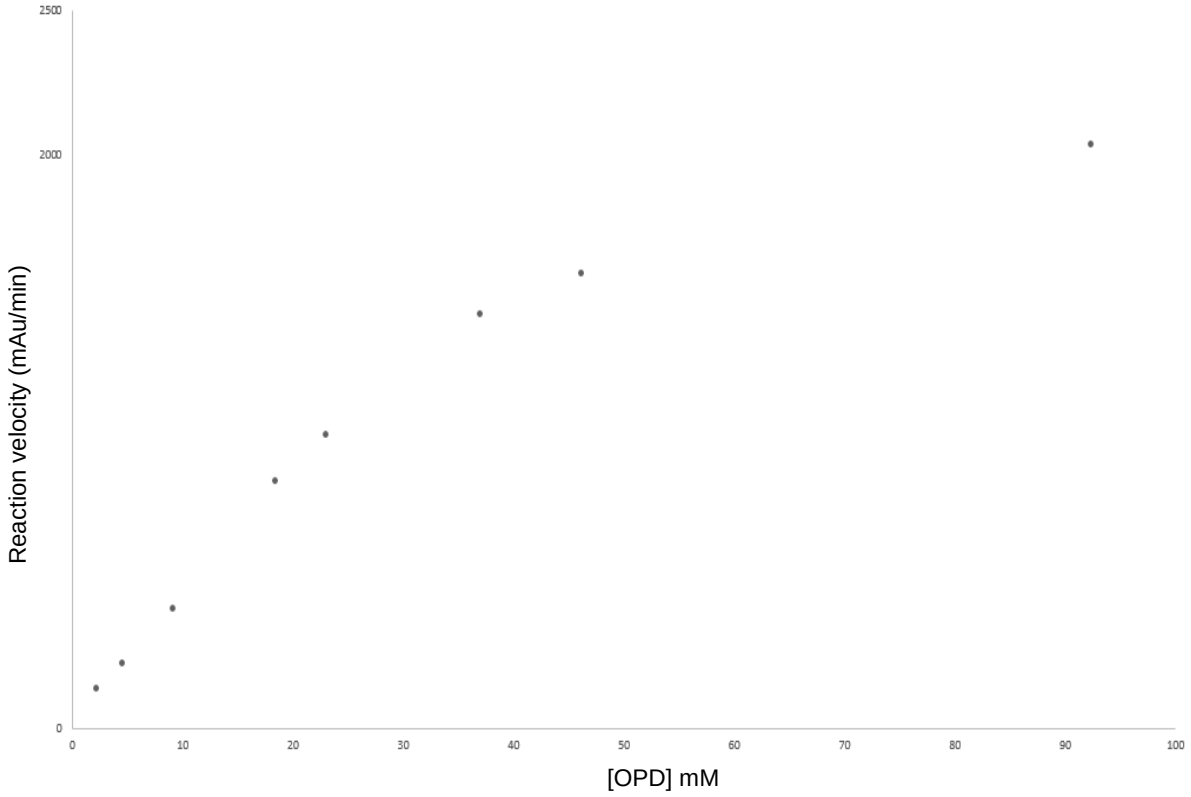

Figure 1-9: Relation between OPD concentration and reaction velocity. OPD concentrations were expressed as mM

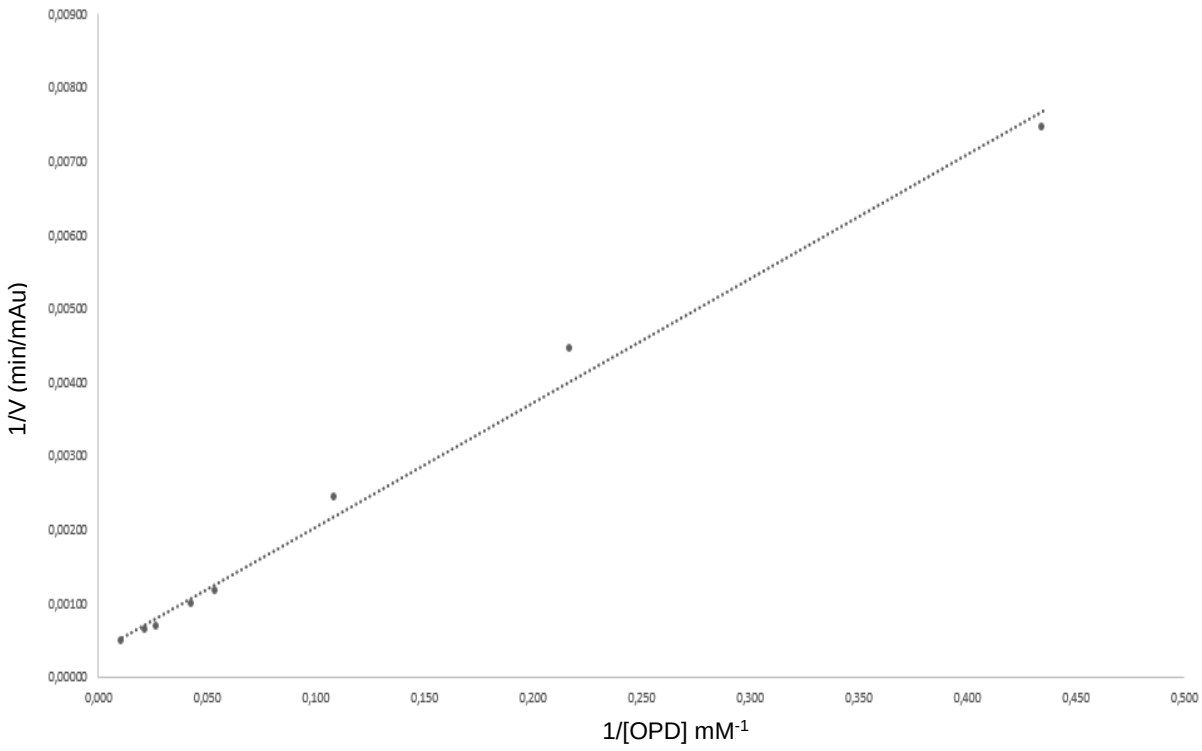

Figure 1-10: Double reciprocal plot of relation between OPD concentration (mM) and reaction velocity

4. Conclusions.

The synthesis of the polyHIPEs and method validation were performed by a design of experiment (DoE) approach. The prepared materials were physiochemically characterized and, most of them showed the typical interconnected pore structure of the polyHIPE. Among the obtained polymeric monoliths, one was selected for the chemical immobilization of a model enzyme on a pre-polymerization-filled chromatographic column. HRP, chemically immobilized into the polyHIPE, retained its catalytic activity. In conclusion, the special structure of polyHIPEs is well suited for in flow-applications. In fact, differently from particle-based supports, polyHIPE monolithic supports offer new possibilities since the diffusive limitations are minimized. Moreover, the highly interconnected channel network totally permeable for the eluent flow, allows us to reduce the backpressure of the system. The unique properties of these supports make them very attractive for bioconversion processes with the advantage to be realized with different functionalities and on different scales, e.g. from micro-analytical to industrial one. With the vast array of research on enzyme immobilization, this result paves the way for highly efficient and economically biotechnological processes in the field of biotransformation, diagnostics and pharmaceutical and food industries.

5. References

1. Bui, T. T.; Kim, Y. S.; Chun, H.; La, D. D.; Bhosale, S. V., Template synthesis of micro/mesoporous Cl-doped polypyrrole using vapor phase polymerization. *Materials Letters* **2017,** *192*, 80-83.
2. Tan, S. W.; Ebrahimi, A.; Langrish, T., Template-directed flower-like lactose with micro-meso-macroporous structure. *Materials & Design* **2017,** *117*, 178-184.
3. Karamessini, D.; Lainioti, G. C.; Deimede, V.; Kallitsis, J. K., Morphological control of porous membranes based on aromatic polyether/water soluble polymers. *Journal of Applied Polymer Science* **2017,** *134* (9).
4. Wei, X. B.; Gong, C. R.; Chen, X. J.; Fan, G. L.; Xu, X. H., Preparation of porous hollow silica spheres via a layer-by-layer process and the chromatographic performance. *Frontiers of Materials Science* **2017,** *11* (1), 33-41.
5. Xin, Y. R.; Xiong, Q. C.; Bai, Q. H.; Miyamoto, M.; Li, C.; Shen, Y. H.; Uyama, H., A hierarchically porous cellulose monolith: A template-free fabricated, morphology-tunable, and easily functionalizable platform. *Carbohydrate Polymers* **2017,** *157*, 429-437.
6. Schacht, K.; Vogt, J.; Scheibel, T., Foams Made of Engineered Recombinant Spider Silk Proteins as 3D Scaffolds for Cell Growth. *Acs Biomaterials Science & Engineering* **2016,** *2* (4), 517-525.
7. Cameron, N. R., High internal phase emulsion templating as a route to well-defined porous polymers. *Polymer* **2005,** *46* (5), 1439-1449.
8. Naranda, J.; Susec, M.; Maver, U.; Gradisnik, L.; Gorenjak, M.; Vukasovic, A.; Ivkovic, A.; Rupnik, M. S.; Vogrin, M.; Krajnc, P., Polyester type polyHIPE scaffolds with an interconnected porous structure for cartilage regeneration. *Scientific Reports* **2016,** *6*.
9. Du, F.; Sun, L.; Zhen, X.; Nie, H.; Zheng, Y.; Ruan, G.; Li, J., High-internal-phase-emulsion polymeric monolith coupled with liquid chromatography-electrospray tandem mass spectrometry for enrichment and sensitive detection of trace cytokinins in plant samples. *Analytical and Bioanalytical Chemistry* **2015,** *407* (20), 6071-6079.
10. Su, R.; Ruan, G.; Nie, H.; Xie, T.; Zheng, Y.; Du, F.; Li, J., Development of high internal phase emulsion polymeric monoliths for highly efficient enrichment of trace polycyclic aromatic hydrocarbons from large-volume water samples. *Journal of Chromatography A* **2015,** *1405*, 23-31.
11. Busby, W.; Cameron, N. R.; Jahoda, A. B. C., Tissue engineering matrixes by emulsion templating. *Polymer International* **2002,** *51* (10), 871-881.
12. Depardieu, M.; Kinadjian, N.; Backov, R., Integrative Chemistry: Advanced functional cellular materials bearing multiscale porosity. *The European Physical Journal Special Topics* **2015,** *224* (9), 1655-1668.
13. Pierre, S. J.; Thies, J. C.; Dureault, A.; Cameron, N. R.; van Hest, J. C. M.; Carette, N.; Michon, T.; Weberskirch, R., Covalent enzyme immobilization onto photopolymerized highly porous monoliths. *Advanced Materials* **2006,** *18* (14), 1822-+.
14. Sears, N. A.; Dhavalikar, P. S.; Cosgriff-Hernandez, E. M., Emulsion Inks for 3D Printing of High Porosity Materials. *Macromolecular Rapid Communications* **2016,** *37* (16), 1369-1374.
15. Lumelsky, Y.; Lalush-Michael, I.; Levenberg, S.; Silverstein, M. S., A Degradable, Porous, Emulsion-Templated Polyacrylate. *Journal of Polymer Science Part a-Polymer Chemistry* **2009,** *47* (24), 7043-7053.
16. Hu, Y.; Gao, H.; Du, Z.; Liu, Y.; Yang, Y.; Wang, C., Pickering high internal phase emulsion-based hydroxyapatite–poly (ε-caprolactone) nanocomposite scaffolds. *Journal of Materials Chemistry B* **2015,** *3* (18), 3848-3857.
17. Zhu, Y.; Zhang, R.; Zhang, S.; Chu, Y.; Chen, J., Macroporous Polymers with Aligned Microporous Walls from Pickering High Internal Phase Emulsions. *Langmuir* **2016,** *10.1021/acs.langmuir.6b00794*.
18. Liu, H.; Wang, C., Chitosan scaffolds for recyclable adsorption of Cu(II) ions. *Rsc Advances* **2014,** *4* (8), 3864-3872.
19. Oh, B. H. L.; Bismarck, A.; Chan-Park, M. B., High Internal Phase Emulsion Templating with Self-Emulsifying and Thermoresponsive Chitosan-graft-PNIPAM-graft-Oligoproline. *Biomacromolecules* **2014,** *15* (5), 1777-1787.

20. Kimmins, S. D.; Cameron, N. R., Functional porous polymers by emulsion templating: recent advances. *Advanced Functional Materials* **2011,** *21* (2), 211-225.
21. Silverstein, M. S., PolyHIPEs: Recent advances in emulsion-templated porous polymers. *Progress in Polymer Science* **2014,** *39* (1), 199-234.
22. Brusotti, G.; Calleri, E.; Milanese, C.; Catenacci, L.; Marrubini, G.; Sorrenti, M.; Girella, A.; Massolini, G.; Tripodo, G., Rational design of functionalized polyacrylate-based high internal phase emulsion materials for analytical and biomedical uses. *Polymer Chemistry* **2016,** *7* (48), 7436-7445.
23. Yin, D.; Guan, Y.; Gu, H.; Jia, Y., Polymerized high internal phase emulsion monolithic material: a novel stationary phase of thin layer chromatography. *Rsc Advances* **2017,** *7* (12), 7303-7309.
24. Livshin, S.; Silverstein, M. S., Enhancing Hydrophilicity in a Hydrophobic Porous Emulsion-Templated Polyacrylate. *Journal of Polymer Science Part a-Polymer Chemistry* **2009,** *47* (18), 4840-4845.
25. Rane, A. A.; Christman, K. L., Biomaterials for the Treatment of Myocardial Infarction. *Journal of the American College of Cardiology* **2011,** *58* (25), 2615-2629.
26. Pyun, J.; Tang, C. B.; Kowalewski, T.; Frechet, J. M. J.; Hawker, C. J., Synthesis and direct visualization of block copolymers composed of different macromolecular architectures. *Macromolecules* **2005,** *38* (7), 2674-2685.
27. Ruan, G.; Wu, Z.; Huang, Y.; Wei, M.; Su, R.; Du, F., An easily regenerable enzyme reactor prepared from polymerized high internal phase emulsions. *Biochem Biophys Res Commun* **2016,** *473* (1), 54-60.
28. Yücel, Y.; Demir, C.; Dizge, N.; Keskinler, B., Lipase immobilization and production of fatty acid methyl esters from canola oil using immobilized lipase. *Biomass and Bioenergy* **2011,** *35* (4), 1496-1501.
29. Pollard, D. J.; Woodley, J. M., Biocatalysis for pharmaceutical intermediates: the future is now. *Trends Biotechnol* **2007,** *25* (2), 66-73.
30. Datta, S.; Christena, L. R.; Rajaram, Y. R., Enzyme immobilization: an overview on techniques and support materials. *3 Biotech* **2013,** *3* (1), 1-9.
31. Calleri, E.; Cattaneo, G.; Rabuffetti, M.; Serra, I.; Bavaro, T.; Massolini, G.; Speranza, G.; Ubiali, D., Flow-Synthesis of Nucleosides Catalyzed by an Immobilized Purine Nucleoside Phosphorylase from Aeromonas hydrophila: Integrated Systems of Reaction Control and Product Purification. *Advanced Synthesis & Catalysis* **2015,** *357* (11), 2520-2528.
32. Cafaggi, S.; Leardi, R.; Parodi, B.; Caviglioli, G.; Bignardi, G., An example of application of a mixture design with constraints to a pharmaceutical formulation. *Chemometrics and Intelligent Laboratory Systems* **2003,** *65* (1), 139-147.
33. de Aguiar, P. F.; Bourguignon, B.; Khots, M. S.; Massart, D. L.; Phan-Than-Luu, R., D-optimal designs. *Chemometrics and Intelligent Laboratory Systems* **1995,** *30* (2), 199-210.
34. Cornell, J. A., *Experiments with mixtures: designs, models, and the analysis of mixture data*. John Wiley & Sons: 2011; Vol. 403.
35. Calleri, E.; Massolini, G.; Lubda, D.; Temporini, C.; Loiodice, F. C.; Caccialanza, G., Evaluation of a monolithic epoxy silica support for penicillin G acylase immobilization. *J Chromatogr A* **2004,** *1031* (1-2), 93-100.
36. Calleri, E.; Temporini, C.; Perani, E.; Stella, C.; Rudaz, S.; Lubda, D.; Mellerio, G.; Veuthey, J. L.; Caccialanza, G.; Massolini, G., Development of a bioreactor based on trypsin immobilized on monolithic support for the on-line digestion and identification of proteins. *J Chromatogr A* **2004,** *1045* (1-2), 99-109.
37. Iacono, M.; Heise, A., Stable poly(methacrylic acid) brush decorated silica nano-particles by ARGET ATRP for bioconjugation. *Polymers* **2015,** *7* (8), 1427-1443.
38. Cameron, N. R.; Sherrington, D. C.; Albiston, L.; Gregory, D. P., Study of the formation of the open cellular morphology of poly(styrene/divinylbenzene) polyHIPE materials by cryo-SEM. *Colloid and Polymer Science* **1996,** *274* (6), 592-595.
39. Topcular, C.; Ayhan, H., Immobilisation of horseradish peroxidase onto monodisperse poly(glycidyl methacrylate) microspheres. *J Biomater Sci Polym Ed* **2007,** *18* (5), 595-607.
40. Abad, J. M.; Velez, M.; Santamaria, C.; Guisan, J. M.; Matheus, P. R.; Vazquez, L.; Gazaryan, I.; Gorton, L.; Gibson, T.; Fernandez, V. M., Immobilization of peroxidase glycoprotein on gold electrodes modified with mixed epoxy-boronic Acid monolayers. *J Am Chem Soc* **2002,** *124* (43), 12845-53.

41. Kumar, V.; Misra, N.; Goel, N. K.; Thakar, R.; Gupta, J.; Varshney, L., A horseradish peroxidase immobilized radiation grafted polymer matrix: a biocatalytic system for dye waste water treatment. *RSC Advances* **2016,** *6* (4), 2974-2981.
42. Gao, X.; Huang, S.; Dong, P.; Wang, C.; Hou, J.; Huo, X.; Zhang, B.; Ma, T.; Ma, X., Horseradish peroxidase (HRP): a tool for catalyzing the formation of novel bicoumarins. *Catalysis Science & Technology* **2016,** *6* (10), 3585-3593.

CHAPTER 2

Polymeric IMERs for Biocatalysis

Not completely published results.

The experimental section was partially taken from the below-reported work.

Development of an integrated chromatographic system for ω-transaminase-IMER characterization useful for flow-chemistry applications

Corti, M.[a], Rinaldi, F.[a], Monti, D.[b], Ferrandi, E.E.[b], Marrubini, G.[a], Temporini, C.[a], Tripodo, G.[a], Kupfer, T.[c], Conti, P.[d], Terreni, M.[a], Massolini, G.[a], Calleri, E.[a]

[a]Department of Drug Sciences, University of Pavia, Viale Taramelli 12, Pavia, 27100, Italy

[b]Istituto di Chimica del Riconoscimento Molecolare, CNR, Via M. Bianco 9, Milan, 20131, Italy

[c]Merck KGaA, Frankfurter Straße 250, Darmstadt, 64293, Germany

[d]Department of Pharmaceutical Sciences, University of Milan, Via Mangiagalli 25, Milan, 20133, Italy

*Journal of Pharmaceutical and Biomedical Analysis, **2019**, 169, 260-268*

1. Introduction

Enzymes are increasingly used as biocatalysts for the production of fine chemicals and pharmaceutical products[1-3]. In industrial processes, the enzyme should be easily separated from the product and have acceptable stability in order to be reused. These needs can be accomplished via immobilization of the enzyme onto solid support that can be used in batch but also under continuous flow conditions. Flow reactors can be used for different scopes: analytical scale synthesis (e.g. for screening purposes and rapid optimization of the reaction conditions), lab-scale synthesis (e.g. for pilot studies) or large-scale synthesis (e.g., industrial production of active pharmaceutical ingredients, APIs). Biocatalyzed reactions performed in a flow system can benefit from improved mass transfer, excellent temperature control and, importantly, continuous substrate feed and product removal, thus limiting the possible substrate/product inhibition of enzyme activity[4, 5]. The implementation of new biocatalytic processes can be a challenging procedure, which may require several stages of characterization and evaluation prior to scale-up[6]. In recent years, analytical IMER-based platforms have found several applications in drug discovery with a special emphasis on enzyme inhibitor screening and on-line digestion for proteins characterization[7-10]. However, the potentiality of IMERs for substrate screening and reaction optimization studies on analytical scale, as prototypes for biosynthetic purposes, has not been fully exploited[11, 12]. Stereoselective biotransformations are among the different classes of reactions that have been investigated using continuous flow technology. In particular, asymmetric catalysis has come to the forefront as a highly economical and efficient strategy for the generation of chiral compounds, whereby achiral starting materials are transformed directly into enantio-enriched products[13-15]. It has been recognized that ω-transaminases (ω-TAs) represent an attractive option for the synthesis of chiral amines, which are valuable building blocks for the preparation of APIs that span a range of therapeutic areas[14, 16]. Transaminases are pyridoxal 5′-phosphate (PLP)-dependent enzymes that transfer an amino group from an amino donor (e.g., D- or L-alanine, isopropylamine) to a prochiral ketone substrate, thereby creating a CN bond as well as establishing a key stereogenic center in a single step. At present, more than 60 (S)- and (R)-selective ω-TAs have been identified, mainly from bacterial and fungal strains[17]. However, some challenges inherent to transaminase-catalyzed processes, such as reaction equilibrium and stereoselectivity, still remain to be tackled before developing large-scale processes[18]. In this context, the use of ω-TAs-based IMERs in a continuous flow mode can be useful for the production of chiral amines; two examples of such applications have been reported[19, 20]. In Ref. 19, E. coli cells containing overexpressed (R)-selective ω-transaminase and the cofactor Pyridoxal-5′-phosphate (PLP) were immobilized on methacrylate beads and used in the asymmetric synthesis of some chiral amines under flow conditions combining a catch and release strategy. Differently, in Ref. 20, homemade monolithic silica support was prepared in a heat-shrinkable Teflon tube and used for the immobilization of transaminase. The reactor was used for the in-flow kinetic resolution of a chiral amine. In this work, we developed a reliable analytical approach for substrate

screening and reaction optimization studies, using a new bioreactor based on ATA-117, an (R)-selective ω-transaminase [17-20]. For enzyme immobilization, a polymerized high internal phase emulsion was prepared, and a monolithic polymeric column was produced in-house. Indeed, according to literature, polyHIPE-based materials exhibit good performances in enzyme immobilization and in in-flow synthesis procedures[21-23]. For reaction monitoring over time, the bioreactor was inserted in a bidimensional chromatographic system where the reaction mixture can be directly transferred to the analytical column for separation and direct quantification of the product and unreacted substrate. The activity of the bioreactor was determined by setting an on-column enzymatic assay using a model transamination reaction (production of acetophenone). The synthesized and characterized bioreactor was then applied for the in-flow synthesis of the chiral amine (R)-1-methyl-3-phenylpropylamine as intermediate for the synthesis of the antihypertensive drug dilevalol. The enantiomeric excess of the reactions was checked by HPLC with a method developed on purpose. To improve the conversion, diverse strategies were considered including the use of different amino donors. This work underlines the role that the proposed analytical platform can play to enable fast and reliable definition of the best reaction conditions for the manufacture of chiral amines interesting as pharmaceutical building blocks using immobilized enzymes in flow chemistry reactions.

2. Experimental section

2.1. Chemicals

ATA-117 (R)-amine transaminase from *Arthobacter* sp. KNK168 (GenBank: BAK39753.1) was overexpressed and purified by "Istituto di Chimica del Riconoscimento Molecolare, CNR" of Milan. The enzyme was immobilized on an epoxy-functionalized polyHIPE-based monolithic column (6.6 × 10 mm). Glycine, (R)-methylbenzylamine (MBA), sodium pyruvate, pyridoxal 5-phosphate (PLP) hydrate, acetophenone, D-alanine, 4-phenyl-2-butanone, 1-methyl-3-phenylpropylamine (MPPA), N-(2,4-dinitro-5-fluorophenyl)-L-alaninamide (Marfey's reagent), pyruvate decarboxylase, isopropylamine, acetonitrile, methanol and trifluoroacetic acid (TFA) were from Sigma-Aldrich (St. Louis, MO, USA). Potassium dihydrogen phosphate and sodium acetate were purchased from Carlo Erba Reagents (Cornaredo, Italy), while ammonium sulfate and ammonium chloride were from Merck KGaA (Darmstadt, Germany). Water was obtained from a Milli-Q® Integral purification system (Merck KGaA, Darmstadt, Germany).

2.2. Cloning and overexpression of the ATA-117 gene in *E. coli* BL21(DE3)

The codon-optimized ATA117 gene was synthesized and cloned into the pUC57 vector obtaining pUC-ATA117opt by BaseClear (Leiden, The Netherlands). The ATA117 gene was then amplified using pUC-ATA117opt as a template and primers ATA117fw (GAAGGAGATATACATATGGCGTTCAGTGCCGATACC)/ATA117rv(GTGATGGTGGTGATGATG ATACTGCACCGGGGTTAAAAG) that include 18 nt of overlap with the ends of the pETite vector (Lucigen, WI, USA) for the subsequent cloning into the pETite plasmid in frame with a 6xHis tag sequence. The PCR amplification was carried out on 50 µL reaction mixtures containing 10 ng of plasmid DNA, dNTPs (0.2 mM each), primers (1 µM each), 4 U of XtraTaq Pol and 5 µL of the XtraTaq buffer (both from Genespin, Italy). The PCR conditions were as follows: 95 ◦C for 2 min, followed by 35 cycles at 94 ◦C for 30 s, 55 ◦C for 30 s, 72 ◦C for 1 min, and then 72 ◦C for 10 min. PCR products were cloned into the pETite vector and transformed into the E. coli Hi control 10G using the Expresso T7 Cloning and Expression kit from Lucigen. The resulting plasmid pETiteATA117opt was purified and transformed into E. coli BL21(DE3). The obtained transformants were grown in LB supplemented with 30 µg/mL kanamycin (LBkan30) medium (50 mL) overnight and then inoculated in 0.5 L LB kan30 at 37 ◦C and 220 rpm. When the OD600 reached 0.6–1, gene expression was induced by the addition of 1 mL of 0.5 M IPTG solution in water and the culture was shifted to 30 ◦C and 220 rpm and grown for further 16 h. Then cells were harvested by centrifugation (5000 rpm for 30 min), resuspended in 20 mL of wash buffer and disrupted by sonication. Wash buffer consisted of potassium phosphate buffer (pH 7.0; 20 mM), NaCl (500 mM) and imidazole (20 mM). For protein purification, clear cell lysates containing soluble protein were subsequently incubated with Nickel Sepharose 6 Fast Flow agarose resin (Ni-NTA) (GE Healthcare, Italy) for 1 h

at 4 ◦C and the mixture was then loaded onto a glass column (10 × 110 mm). The resin was subsequently washed with 10 mL of wash buffer and His-tagged ATA117 was eluted using a 3 step gradient (10 mL washing buffer containing 100, 200, and 300 mM imidazole, respectively) and dialyzed against potassium phosphate buffer (pH 8; 50 mM), at 4 ◦C. The protein content was measured using the Bio-Rad Protein Assay according to the Bradford method and the protein purity was verified by SDS-PAGE analysis (12% T, 2.6% C). Transaminase activity was assayed by spectrophotometrically measuring the formation of acetophenone at 245 nm (ε =3.66 mM–1 cm^{-1})[24] and 20 °C on a Jasco V-530 UV/VIS spectrophotometer (Easton, MD, USA) after adding 10–50 µL of purified transaminase to the enzyme assay solution, which consisted of sodium pyruvate (2.5 mM), (R)-(−)-methylbenzylamine (2.5 mM) in potassium phosphate buffer (pH 8.0 or pH 7.0; 50 mM) and DMSO (0.25%, v/v)in 0.5 mL total volume. One unit of activity is defined as the enzyme activity that produces 1 µmol of acetophenone per minute under the assay conditions described above.

2.3. Preparation of the monolithic support

The preparation of a monolithic polymeric column was carried out by the preparation of a suitable polyHIPE material. The corresponding high internal phase emulsion (HIPE) was prepared by following a well-established procedure[21, 25-27]. Therefore, the oil phase of the emulsion was prepared by mixing butyl acrylate (BA, 4.30 mL), glycidyl methacrylate (GMA, 1.72 mL), trimethylolpropane triacrylate (TMPT, 0.96 mL), and Synperonic PE/L 121 (1.02 mL). The aqueous phase was achieved by simply dissolving 272 mg of potassium persulfate (KPS) in 32 mL of degassed double deionized water. The water phase was added drop-by-drop to the oil one under continuous stirring (provided by an overhead mechanical stirrer equipped with a D-shaped Teflon paddle) at 200 rpm. When the water phase was completely added to the oil one, the stirring was increased up to 400 rpm and the system was maintained under continuous stirring and under continuous nitrogen flow for 1 h until a white, paste-like emulsion was achieved. Then, 272 µL of tetramethylethylenediamine (TEMED) were added and mixed with the biphasic system. The mixed material was rapidly transferred into an Omnifit® empty glass (6.6 mm ID, 150 mm) column where the HIPE was allowed to polymerize at room temperature for 24 h. To remove the non-crosslinked portions, the obtained column was washed by flushing several solvents using an HPLC pump. The solvent used during the washing procedure were, in order, MeOH (14 mL), water (14 mL), and THF (14 mL). Before the immobilization step, the obtained monolith (6.6 mm ID, 10 mm) (Fig. 2-1) was stored in THF at room temperature.

Figure 2-11: PolyHIPE-based monolithic column achieved by the in-situ polymerization of the corresponding emulsion in an Omnifit® empty glass column.

2.4. Immobilization of ATA-117 on the monolithic support

Enzyme immobilization was carried out following an in situ procedure[28] by flushing in a recycling system an ATA-117 solution through the monolithic support using an HPLC quaternary pump. Before flushing the enzyme solution, the epoxy monolithic column was conditioned with phosphate buffer (pH 7.5; 50 mM) at 0.3 mL/min for 20 min. The enzyme solution was prepared by diluting the transaminase solution (11.68 mg/mL) in ammonium sulfate (1.875 M) in phosphate buffer (pH 7.5; 50 mM) to a final concentration of 2.34 mg/mL (10 mL). During the immobilization procedure, the column was backflushed every 20 min and the flow-rate was maintained constant (0.3 mL/min) for 24 h. The back-flushing procedure was used during the in-situ immobilization step in order to obtain a homogeneous enzyme density in the column. Then, an end-capping process was performed by flushing through the support 10 mL of a glycine solution (1 M) in phosphate buffer (pH 7.5; 50 mM). Therefore, the gained bioreactor was evaluated in terms of immobilization yield and catalytic activity. In order to assess the amount of immobilized enzyme onto the monolithic support, a spectrophotometric assay was carried out at 280 nm. A calibration curve for ATA-117 quantification was calculated (calibration range 0.0365 mg/mL–0.584 mg/mL). The curve ($y = 0.7512x – 0.0125$) showed a good linearity as expressed by $R^2 = 0.9986$. Therefore, the spectrophotometric assay was carried out on the enzyme solution used for the immobilization procedure before and after the 24 h. The amount of the immobilized enzyme was estimated by the difference between the two enzyme concentrations, leading to an immobilization yield of 19.93% corresponding to approximately 2.68 mg of the enzyme. When not in use, the ATA-117-IMER was stored at 4 °C in phosphate buffer (pH 7.5; 50 mM).

2.5. Chromatography

2.5.1. Apparatus

Chromatographic experiments were performed with three modular systems. System 1 and System 2 were used for assembling the column-switching set-up reported in Fig. 2-2. System 1 consisted of an Agilent HP-1100 (Palo Alto, CA, USA) pump (pump 1) and an HP-1100 thermostat, delivering the reaction mixture. Pump 1 was directly connected to the bioreactor (ATA-117-IMER) and to a 6-way switching valve (V) containing a 20 µL loop. System 2 consisted of an Agilent HP-1100 (Palo Alto, CA, USA) pump (pump 2) connected through V to the chromatographic column (LiChospher® 100 RP18, 250 × 4.0 mm, 5 µm). The systems were controlled by an HPLC ChemStation (RevisionA.04.01). In this integrated system, the reaction mixture is re-circulated through the bioreactor (System 1, V in position a). After switching V to position b, the analytes (products and unreacted substrates) loaded in the 20 µL loop are directly pumped by System 2 to the analytical column for reaction monitoring. System 3 was used for ee determination and consisted of an Agilent HP-1100 system (Palo Alto, CA, USA) with a Rheodyne sample valve (20 µL loop) equipped with an

HP-1100 diode-array detector and a Zorbax Eclipse XDB C18-Agilent analytical column (150 × 4.6 mm I.D., 5 µm).

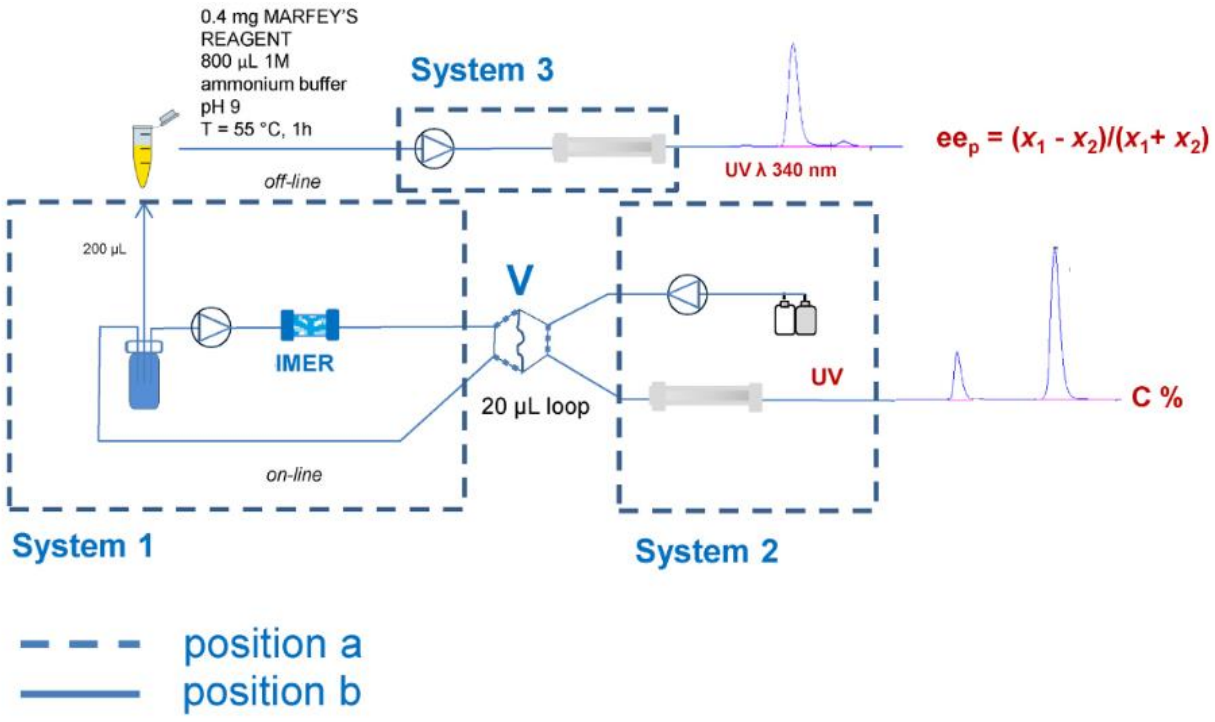

Figure 2-12: Analytical platform developed by on-line coupling the IMER (system 1) with the analytical column (system 2). The platform comprised also system 3 correspondings to the derivatization procedure and chromatographic conditions applied for the off-line evaluation of the enantiomeric excess.

2.5.2. Chromatographic methods

2.5.2.1. In-flow activity assay

The catalytic activity of the immobilized ATA-117 was evaluated by an in-flow activity assay based on the standard reaction reported in Fig. 2-3. A solution (9 mL) consisting of (R)-methylbenzylamine (MBA, 10 mM), sodium pyruvate (10 mM) and pyridoxal 5 -phosphate (PLP, 0.1 mM) in phosphate buffer (pH 7; 50 mM) was prepared and flushed at 0.5 mL/min through the IMER as shown in Fig. 2-2. For reaction monitoring, 20 µL reaction mixture was diverted to the analytical column. The chromatographic conditions applied for reaction monitoring consisted of isocratic elution using water containing TFA (0.1%, v/v)- acetonitrile containing TFA (0.1%, v/v) (50:50, v/v). The flow-rate was 1 mL/min and the detector was set at 254 nm. The column selected was a LiChrospher® 100 RP18, 250 × 4.0 mm, 5 µm (Agilent Technologies, Palo Alto, CA, USA). The enzyme activity was evaluated by the formation of acetophenone over time.

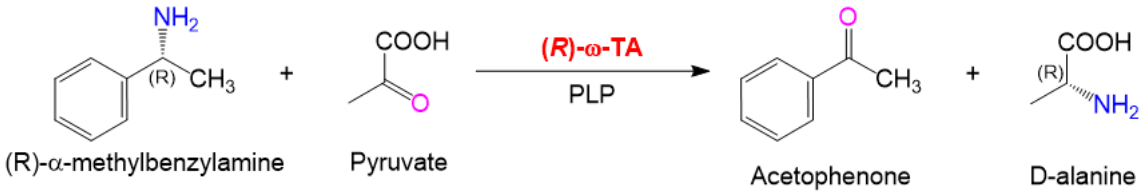

Figure 2- 13: Oxidative deamination of (R)-methylbenzylamine and reductive amination of Pyruvate catalyzed by ATA-117, with the consequent synthesis of Acetophenone and D-alanine

2.5.2.2. In-flow synthesis of and (R)-1-methyl-3-phenylpropylamine

The synthesis of (*R*)-1-methyl-3-phenylpropylamine (MPPA) was carried out by the transamination of 4-phenyl-2-butanone (Fig. 2-4). The reaction mixture was prepared by mixing D-alanine (D-ala) or isopropylamine (IPA) as the amino donor, 4-phenyl-2-butanone as an amino acceptor in different concentrations. In all experiments, the reaction mixture contained PLP 0.1 mM in a phosphate buffer (PB) 75 mM, pH 8. In this case, the chromatographic conditions for monitoring the synthesis process consisted in an isocratic elution of a binary mobile composed by water containing TFA (0.1%, v/v)-acetonitrile containing TFA (0.1%, v/v) (50:50, v/v) at 1 mL/min as flow rate and the detector was set at 254 nm. The stationary phase used was a Zorbax Eclipse XDB C18-Agilent (150 × 4.6 mm I.D., 5 µm, 80 Å pore size). The enzyme activity was evaluated by the formation of MPPA over time.

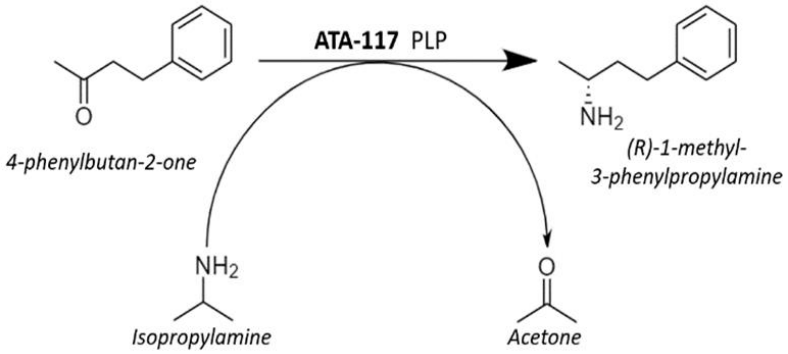

Figure 2-14: Transamination reaction for the production of (R)-1-methyl-3-phenylpropylamine catalyzed by ATA-117

2.5.2.3. Enantiomeric excess determination

In order to establish the enantiomeric excess of the produced chiral amine, an off-line derivatization procedure was set up. Nα-(2,4-dinitro-5-fluorophenyl)-L-alaninamide (Marfey's reagent) was used as a derivatization agent. The derivatization reaction (Fig. 2-5) was performed by dissolving in a vial 0.4 mg of Marfey's reagent[29] in 800 µL of ammonium

buffer (pH 9; 1 M). 200 µL of the reaction mixture were then added to the Marfey's reagent solution. The mixtures were heated at 55 °C for 1 h. In order to calculate the enantiomeric excess, 20 µL of the solution were injected in System 3. The two diastereoisomers were separated using an isocratic elution of a binary mobile phase acetate buffer (pH 5; 20 mM)-acetonitrile (60–40, v/v). The flow-rate was 0.8 mL/min and the detection was set at 340 nm.

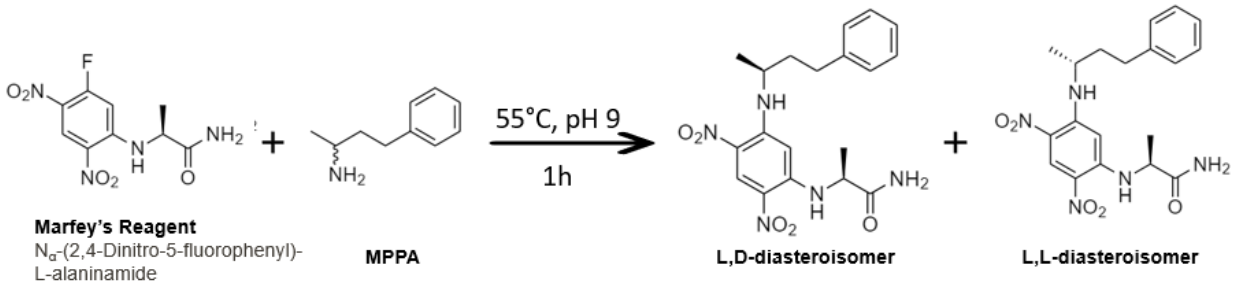

Figure 2-15: Derivatization reaction with Marfey's reagent, with the consequent production of two diastereoisomers

2.5.2.4. Data processing

Conversion percentages were calculated as C% = [product concentration/(product concentration + substrate concentration)] × 100 where product and substrate concentrations were calculated from the calibration curves. The product enantiomeric excess was calculated as follows: $ee_p = (x_1 - x_2)/(x_1 + x_2)$; where x_1 and x_2 denote the areas of the two diastereoisomers separated on the analytical column.

2.6. Quantitative analysis

For quantitation, three different calibration curves were obtained. For both reaction products (acetophenone, and MPPA), a 10 mM stock solution was prepared in phosphate buffer (pH 7; 50 mM) and five dilutions were prepared in the same solvent. Each solution was injected in triplicate. The chromatographic conditions used for the calibration curves are reported in paragraph 2.5.2. The calibration ranges were 0.05 mM – 10 mM for acetophenone and 0.1 mM – 2.5 mM for MPPA. The lowest level of the calibration curve of acetophenone corresponds to 0.5% conversion, while the lowest level for MPPA corresponds to a 1% conversion. The highest level of the two curves corresponds to 100% conversion. The calibration curve equation of MPPA was $y = (241.6 \pm 0.6)x + (0.4 \pm 0.7)$, with a correlation coefficient $R^2 = 0.99998$, demonstrating excellent fitting. The slope is highly significant ($p < 0.0001$) and the intercept is not significant ($p = 0.5450$). The calibration curve equation of acetophenone was $y = (9053 \pm 170)x + (1210 \pm 875)$, with a determination coefficient $R^2 = 0.9989$, demonstrating satisfactory fitting. The slope is highly significant ($p < 0.0001$)

and the intercept is not significant ($p = 0.2608$). For the calibration curves, each standard solution was injected in triplicate. The precision of the methods was estimated calculating the RSD% of the three replicates. In all cases, a RSD% lower than 3.5% at the lower limit of the linear range was obtained (maximum RSD%, 2.5% for MPPA, and 1.1% for acetophenone).

3. Results and Discussion

In this work, the development of an IMER based on an (*R*)-selective ω-transaminase for reaction optimization on an analytical scale, is described. The most appealing benefits offered by analytical IMERs technology are the low sample consumption and the possibility of connecting the reactors to different separation and detection systems. In addition, the high enzyme-to-substrate ratio, achievable with these systems, can significantly improve reaction efficiency and shorten the reaction times required to rapidly screen different reaction conditions/substrate specificity in view of preparative applications.

3.1. Bioreactor preparation

The monolithic column was prepared by the exploitation of polyHIPE technology. BA was selected as a backbone monomer due to its high hydrophobicity and glass transition temperature (Tg) leading to a good resistance of the final material to produce in-flow resistant support. TMPT was selected as a tri-arm crosslinker agent in order to provide a high crosslinking density with a consequent increase of the mechanical resistance of the final material. The functional monomer selected was the epoxy-bearing GMA, because the epoxy group can be easily exploited for a post-production immobilization of proteins (such as enzymes) by the covalent interaction OF this functional group with nucleophilic moieties of the macromolecule (such as lysine residues). The polymerization reaction was initiated by the redox initiator KPS/TEMED. Indeed, KPS is an effective radical initiator for free radical polymerizations, but for this mechanism, a temperature higher than 60°C is required. This temperature is not compatible with emulsions that are thermodynamically unstable systems. For this reason, TEMED was added in order to allow a polymerization step occurring at room temperature[25]. The polyHIPE column functionalized with epoxy groups was used for the covalent immobilization of the enzyme following an in situ procedure. This support exhibits a hierarchical porous structure composed of two levels of porosity, namely voids and throats (Fig. 2-6). This highly interconnected network was achieved by a specific HIPE starting composition and the corresponding monolith has been already tested for in-flow applications and for the immobilization of an active macromolecule[21]. This specific polyHIPE material has been already characterized in a previous work[21] and the average diameter of voids and throats was measured as 2.4 ± 0.7 µm and 0.7 ± 0.2 µm respectively. Therefore, Purified ATA-117 was immobilized on the monolithic polyHIPE following the immobilization protocol described in paragraph 2.4. The amount of immobilized enzyme, as estimated

spectrophotometrically, was 2.68 mg corresponding to an immobilization yield of 19.93%. The amount of immobilized enzyme per unit column volume was 7.88 mg/ml.

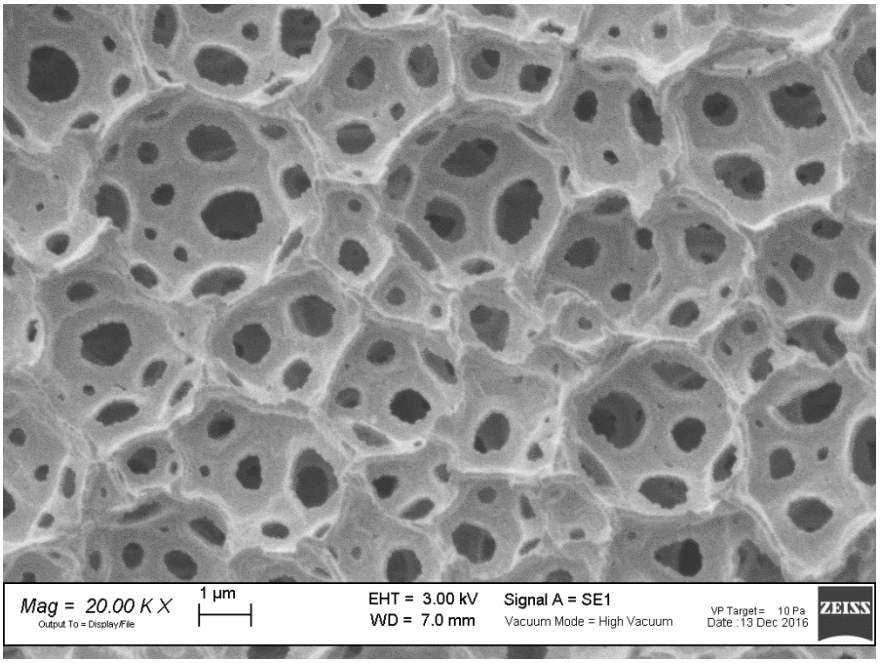

Figure 2-16: Scanning electron microscopy image acquired using a Zeiss EVO MA10 instrument (Carl Zeiss, Germany) on a gold-sputtered sample. The image reported was taken from the internal side of a sample of monolithic material used as polyHIPE-based column

3.2. Bioreactor characterization and stability

Evaluation of the enzyme activity after immobilization was the next step. The activity of the ATA-117-IMER was assayed by submitting the bioreactor to an in-flow activity assay (production of acetophenone, see Fig. 2-3) based on the conversion of the model substrate (*R*)-α-methylbenzylamine and using the column switching set-up (Fig. 2-2). The experimental conditions are detailed in paragraph 2.5.2.1. The reaction mixture was prepared as described above, and the product of this reaction, acetophenone, was quantified over time by an HPLC method developed on purpose. A typical chromatogram is reported in Fig. 2-8A. A conversion percentage of approximately 90% was obtained after 21 h allowing the equilibrium conditions (Fig. 2-8B). The initial rate of the reaction was estimated from the slope of the curve at the beginning of the reaction, from 0 to 4 h (Fig. 2-8B). This assay was also used to test the stability of the bioreactor over time. Transaminase IMER retained the initial catalytic activity over 35 reactions in 4 months. A variation percentage of less than ± 5% has been considered as nonsignificant and linked to the

experimental variability. After one year from the bioreactor preparation, the long-term stability was evaluated using the same assay and a loss of activity (15%) was measured.

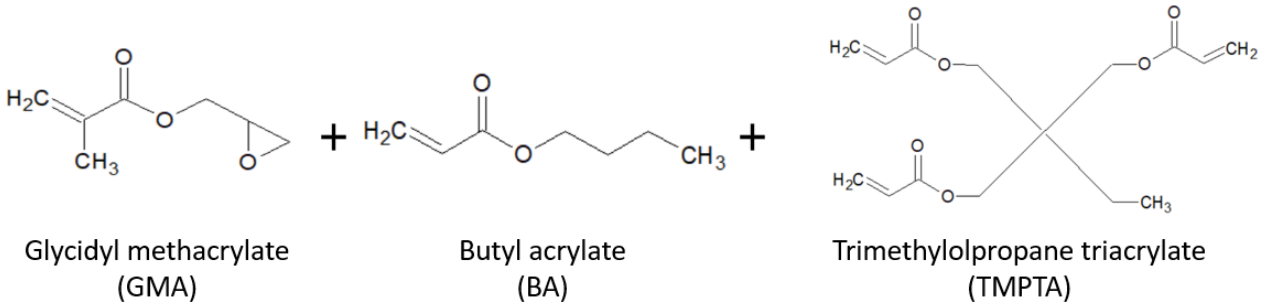

Glycidyl methacrylate (GMA) | Butyl acrylate (BA) | Trimethylolpropane triacrylate (TMPTA)

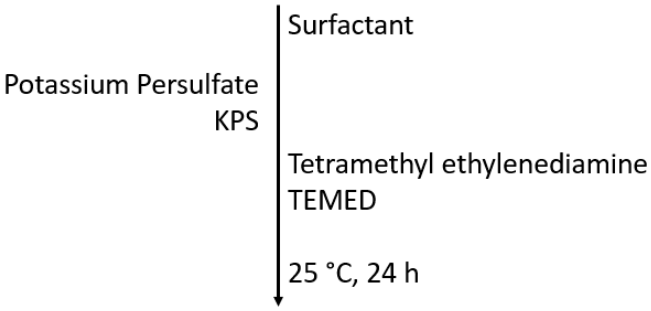

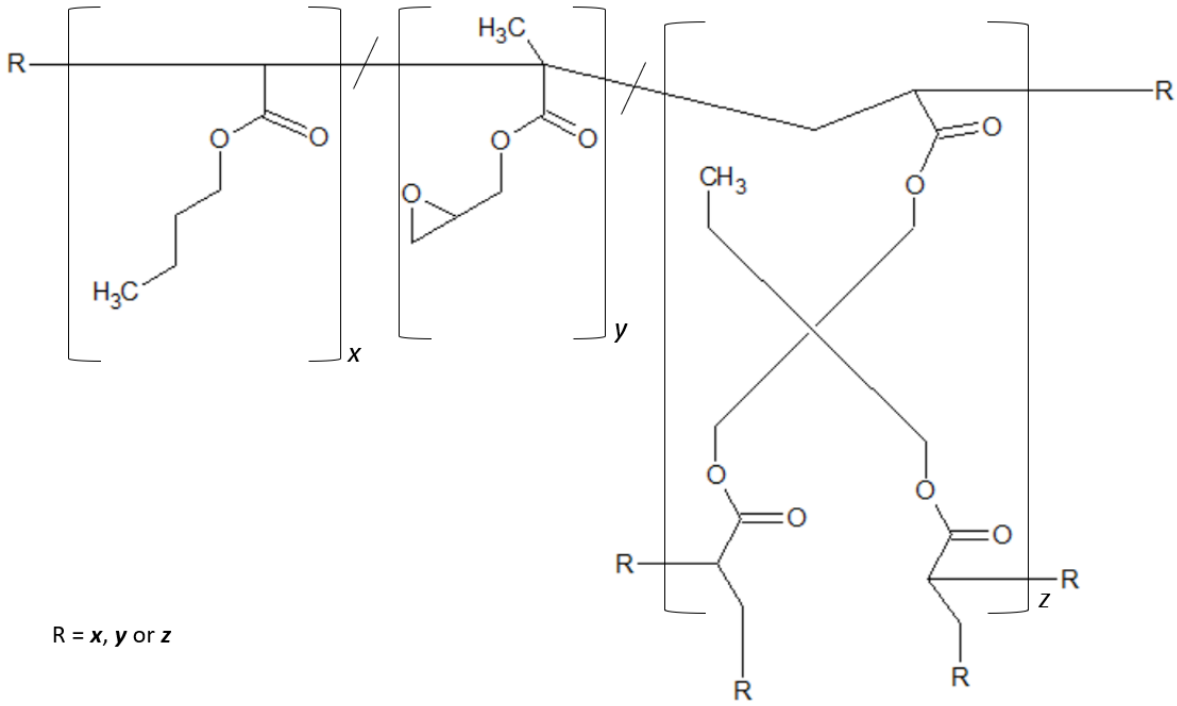

Figure 2-17: Schematic representation of the polymerization reaction

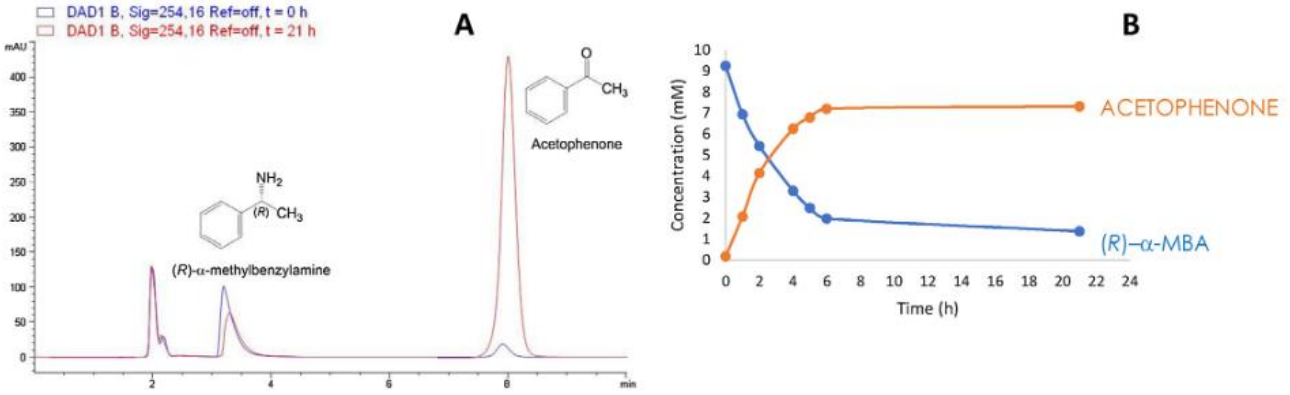

Figure 2-18: A) representative chromatograms for the in-flow activity assay. Results of the reaction monitoring at 0 (blue) and 21 h (red) are reported. B) Monitoring overtime of the in-flow activity assay. Calculated concentrations of substrate and product are reported

3.3. Bioreactor applications: in-flow synthesis of (R)-1-methyl-3-phenylpropylamine (MPPA)

The synthesis of enantio-enriched amines can be achieved by asymmetric synthesis starting from the prochiral ketones. This is an attractive approach since a theoretically 100% yield can be obtained. The ATA-117-IMER was used to study the synthesis of MPPA, a precursor of dilevalol [the (R,R)-isomer of labetalol] from the corresponding ketone (Fig. 2-4 and Fig 2-9). As the starting amino donor, the commonly used D-alanine was firstly chosen. This stereoselective synthesis was already described using the free enzyme in solution[30].

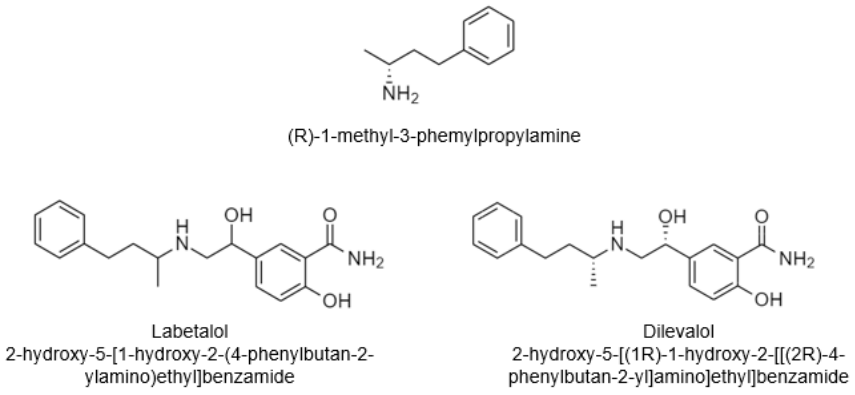

Figure 2-19: MPPA is the intermediate for the synthesis of dilevalol, the (R, R)-isomer of labetalol

When the experimental conditions applied comprised ketone 10 mM and D-ala 100 mM (ratio 10/1), the maximum conversion rate was calculated as 4.97% at 24 hours. The low conversion yield calculated (less than 10%) is not surprising since organic synthesis by ω-transaminases suffers from an unfavorable reaction equilibrium, especially in the asymmetric synthesis of amines from an amino acid as an amino donor. In fact, to maximize the productivity of ω-transaminases it is necessary to shift the equilibrium by process control strategies such as the *in situ* removing of the product, or the use of cascade reactions[17]. Therefore, the experimental conditions were further modified in order to shift the reaction equilibrium, this can be easily carried out with the chromatographic platform. First, soluble pyruvate decarboxylase (140 µg enzyme) was added to the reaction mixture to remove pyruvate co-product. The advantage of using pyruvate decarboxylase is that it does not require recycling of cofactor and the byproducts formed are highly volatile, therefore they can be easily removed[30]. However, in the considered conditions, the conversion yield did not improve significantly.

As a second strategy, isopropylamine (IPA) was considered as an alternative amino donor and it was added to the mixture in the same molar ratio as D-alanine (10:1). The molar ratio was then increased up to 30:1 in other experiments. IPA as an amino donor is very interesting because of the simple removal of the acetone co-product.

The three reaction mixtures were prepared in phosphate buffer (pH 8; 75 mM), PLP (0.1 mM) and the temperature was set at 50 °C. The experiments were carried out in the recycling system described above at 0.3 mL/min for 24 h. The amount of produced amine was monitored over time by an HPLC method developed on purpose and the ee determination was performed as well. Representative chromatograms of the reaction monitoring are presented in Fig 2-10. In order to compare the different conditions (Fig. 2-11), all the reactions were monitored at a fixed time (24 h).

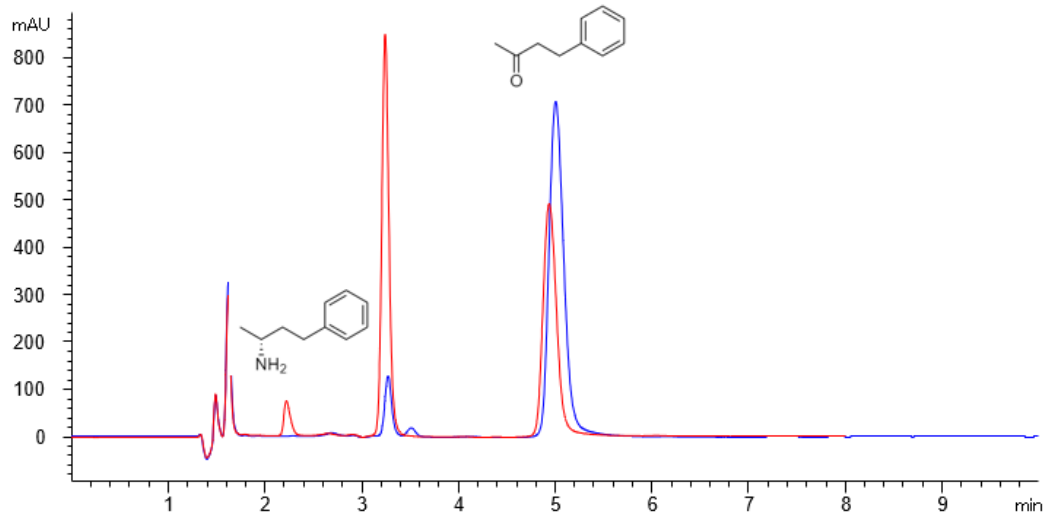

Figure 2-20: Representative chromatograms for the in-flow synthesis of (R)-1-methyl-3-phenylpropylamine starting from 4-phenyl-2-butanone. Results of the reaction monitoring at 0 (blue) and 24 h (red) are reported.

A significant increase in the conversion yield was obtained by using isopropylamine as the amino donor (13.52% conversion yield). An increase in the molar ratio between the amino-donor and the prochiral ketone from 1:10 to 1:30 allowed reaching a 29.21% conversion yield in 24 h.

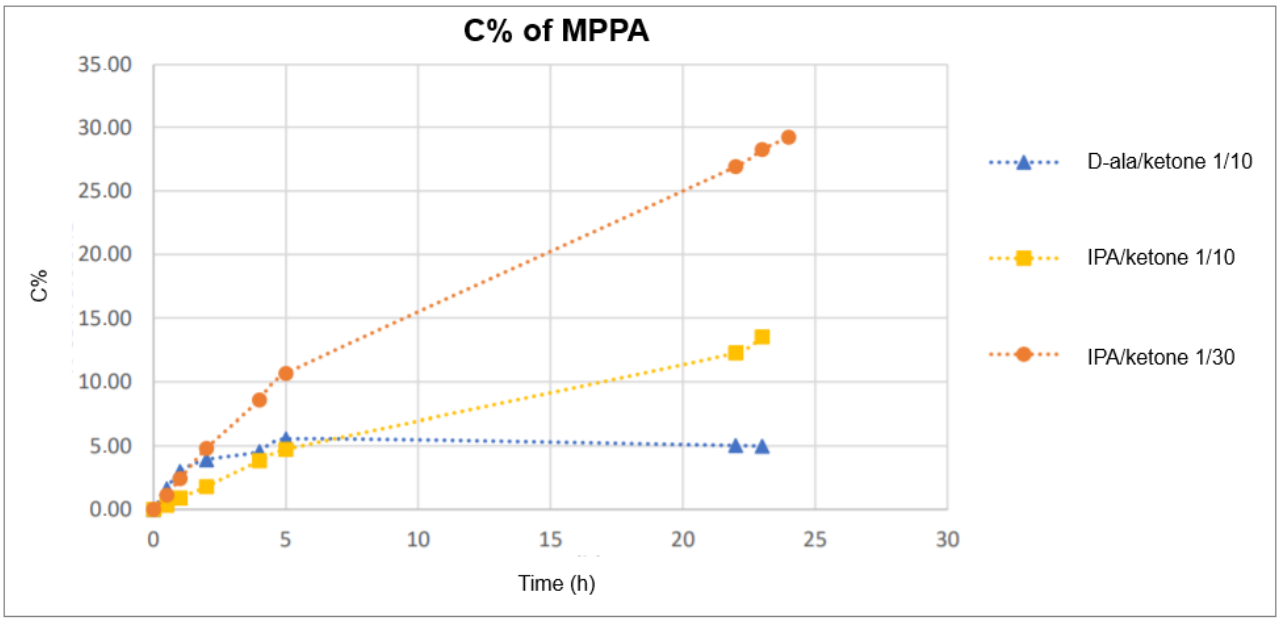

Figure 2-21: Comparison of the different donor/acceptor ratios applied for the synthesis of MPPA. In this graph, the conversion percentage calculated overtime is reported for every experimental condition.

Enantioselective reactions are the result of the competition between different possible diastereomeric reaction pathways, through diastereomeric transition states when

the prochiral substrate complexed to the chiral catalyst reacts with the corresponding reagent. At 24 h the ee was determined for the obtained chiral amine. An enantiomeric excess of 99% was reached for MPPA. Representative chromatograms of the ee determination are presented in (Fig. 2-12). The same reactions were performed in batch conditions. The conditions were: pH 8, 75 mM phosphate buffer, 0.1 mM PLP, T = 50 °C and isopropylamine/prochiral ketone ratio (30:1) in a 9 mL reaction mixture. An established amount of enzyme was added to the reaction mixture to provide a 0.259 mg/mL concentration of ATA-117. In these experiments, a maximum conversion yield (approximately 10%) was obtained after 24 h for MPPA. The ee was also measured and no significant variation in respect to the in-flow experiments was observed.

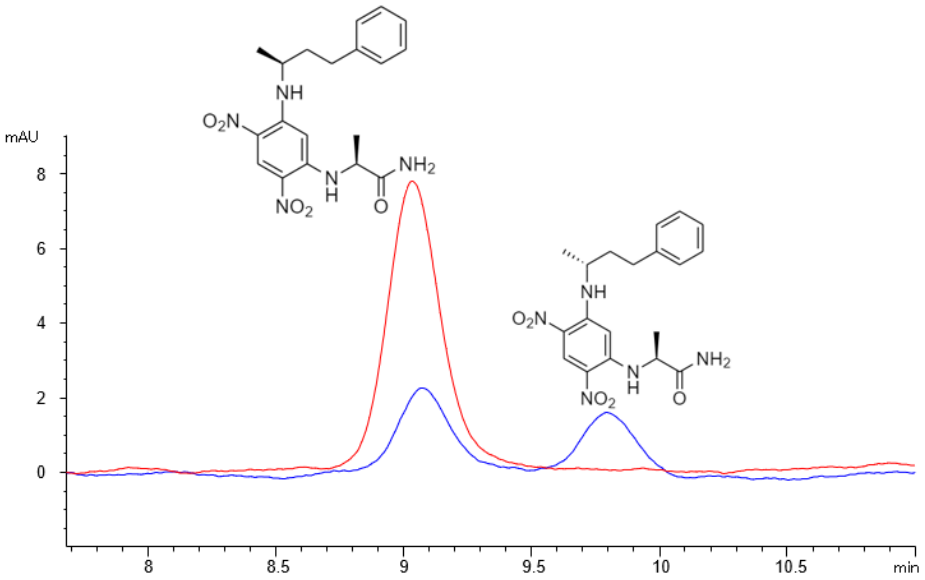

Figure 2-22: Representative chromatograms for the enantiomeric excess determination in the production of (R)-1-methyl-3-phenylpropylamine starting from 4-phenyl-2-butanone. Chromatograms of the reaction mixture at 24 h (red) compared to the racemic amine (blue), both after derivatization.

4. Conclusions

An integrated platform for the asymmetric synthesis of chiral amines was developed using polyHIPE technology. In particular, in this work, a polymeric enzyme reactor (IMER) was achieved by the immobilization of a ω-transaminase on a polyHIPE-based monolith. Moreover, this work underlines the contribution that an analytical platform can give to derive the best reaction conditions, achieving interesting conversion yields, for the manufacture of chiral amines as important pharmaceutical building blocks. Indeed, an on-line reaction monitoring and enantiomeric excess determination were performed by the development of suitable analytical methods. The integrated platform developed can be easily applied in the optimization of other specific substrates to be converted or to characterize other ω-transaminases with different specificities.

5. References

1. Woodley, J. M., New opportunities for biocatalysis: making pharmaceutical processes greener. *Trends Biotechnol* **2008,** *26* (6), 321-7.
2. Busacca, C. A.; Fandrick, D. R.; Song, J. J.; Senanayake, C. H., The Growing Impact of Catalysis in the Pharmaceutical Industry. *Advanced Synthesis & Catalysis* **2011,** *353* (11-12), 1825-1864.
3. Truppo, M. D., Biocatalysis in the Pharmaceutical Industry: The Need for Speed. *ACS Med Chem Lett* **2017,** *8* (5), 476-480.
4. Sheldon, R. A.; Woodley, J. M., Role of Biocatalysis in Sustainable Chemistry. *Chem Rev* **2018,** *118* (2), 801-838.
5. Bernal, C.; Rodriguez, K.; Martinez, R., Integrating enzyme immobilization and protein engineering: An alternative path for the development of novel and improved industrial biocatalysts. *Biotechnol Adv* **2018,** *36* (5), 1470-1480.
6. Tamborini, L.; Fernandes, P.; Paradisi, F.; Molinari, F., Flow Bioreactors as Complementary Tools for Biocatalytic Process Intensification. *Trends Biotechnol* **2018,** *36* (1), 73-88.
7. Naldi, M.; Tramarin, A.; Bartolini, M., Immobilized enzyme-based analytical tools in the -omics era: Recent advances. *J Pharm Biomed Anal* **2018,** *160*, 222-237.
8. Kecskemeti, A.; Gaspar, A., Particle-based immobilized enzymatic reactors in microfluidic chips. *Talanta* **2018,** *180*, 211-228.
9. Fang, S. M.; Wang, H. N.; Zhao, Z. X.; Wang, W. H., Immobilized enzyme reactors in HPLC and its application in inhibitor screening: A review. *J Pharm Anal* **2012,** *2* (2), 83-89.
10. Ma, J.; Zhang, L.; Liang, Z.; Zhang, W.; Zhang, Y., Monolith-based immobilized enzyme reactors: recent developments and applications for proteome analysis. *J Sep Sci* **2007,** *30* (17), 3050-9.
11. Calleri, E.; Cattaneo, G.; Rabuffetti, M.; Serra, I.; Bavaro, T.; Massolini, G.; Speranza, G.; Ubiali, D., Flow-Synthesis of Nucleosides Catalyzed by an Immobilized Purine Nucleoside Phosphorylase from Aeromonas hydrophila: Integrated Systems of Reaction Control and Product Purification. *Advanced Synthesis & Catalysis* **2015,** *357* (11), 2520-2528.
12. Giulia, C.; Rabuffetti, M.; Speranza, G.; Kupfer, T.; Peters, B.; Massolini, G.; Ubiali, D.; Calleri, E., Synthesis of Adenine Nucleosides by Transglycosylation using Two Sequential Nucleoside Phosphorylase-Based Bioreactors Coupled On-Line to an HPLC System for Reaction Monitoring. *ChemCatChem* **2017,** *9*.
13. Kelly, S. A.; Pohle, S.; Wharry, S.; Mix, S.; Allen, C. C. R.; Moody, T. S.; Gilmore, B. F., Application of ω-Transaminases in the Pharmaceutical Industry. *Chemical Reviews* **2018,** *118* (1), 349-367.
14. Mathew, S.; Yun, H., ω-Transaminases for the Production of Optically Pure Amines and Unnatural Amino Acids. *ACS Catalysis* **2012,** *2* (6), 993-1001.
15. Ghislieri, D.; Turner, N. J., Biocatalytic Approaches to the Synthesis of Enantiomerically Pure Chiral Amines. *Topics in Catalysis* **2014,** *57* (5), 284-300.
16. Truppo, M. D.; Rozzell, J. D.; Moore, J. C.; Turner, N. J., Rapid screening and scale-up of transaminase catalysed reactions. *Org Biomol Chem* **2009,** *7* (2), 395-8.
17. Ferrandi, E. E.; Monti, D., Amine transaminases in chiral amines synthesis: recent advances and challenges. *World J Microbiol Biotechnol* **2017,** *34* (1), 13.
18. Tufvesson, P.; Lima-Ramos, J.; Jensen, J. S.; Al-Haque, N.; Neto, W.; Woodley, J. M., Process considerations for the asymmetric synthesis of chiral amines using transaminases. *Biotechnol Bioeng* **2011,** *108* (7), 1479-93.
19. Andrade, L. H.; Kroutil, W.; Jamison, T. F., Continuous flow synthesis of chiral amines in organic solvents: immobilization of E. coli cells containing both omega-transaminase and PLP. *Org Lett* **2014,** *16* (23), 6092-5.
20. Biggelaar, L.; Soumillion, P.; Debecker, D., Enantioselective Transamination in Continuous Flow Mode with Transaminase Immobilized in a Macrocellular Silica Monolith. *Catalysts* **2017,** *7*, 54.
21. Tripodo, G.; Marrubini, G.; Corti, M.; Brusotti, G.; Milanese, C.; Sorrenti, M.; Catenacci, L.; Massolini, G.; Calleri, E., Acrylate-based poly-high internal phase emulsions for effective enzyme immobilization and activity retention: From computationally-assisted synthesis to pharmaceutical applications. *Polymer Chemistry* **2018,** *9* (1), 87-97.

22. Wang, M.; Zhu, Y.; Zhang, S.; Chen, J., Enzyme immobilized millimeter-sized polyHIPE beads with easy separability and recyclability. *Reaction Chemistry and Engineering* **2019,** *4* (6), 1136-1144.
23. Zhu, L. L.; Zhu, C. T.; Xiong, M.; Jin, C. Q.; Sheng, S.; Wu, F. A.; Wang, J., Enzyme immobilization on photopatterned temperature-response poly (N-isopropylacrylamide) for microfluidic biocatalysis. *Journal of Chemical Technology and Biotechnology* **2019,** *94* (5), 1670-1678.
24. Ferrandi, E. E.; Previdi, A.; Bassanini, I.; Riva, S.; Peng, X.; Monti, D., Novel thermostable amine transferases from hot spring metagenomes. *Appl Microbiol Biotechnol* **2017,** *101* (12), 4963-4979.
25. Brusotti, G.; Calleri, E.; Milanese, C.; Catenacci, L.; Marrubini, G.; Sorrenti, M.; Girella, A.; Massolini, G.; Tripodo, G., Rational design of functionalized polyacrylate-based high internal phase emulsion materials for analytical and biomedical uses. *Polymer Chemistry* **2016,** *7* (48), 7436-7445.
26. Calleri, E.; Tripodo, G.; Massolini, G. In *Functional materials with nano-micro sized internal structure for biomedical applications*, AIP Conference Proceedings, 2018.
27. Corti, M.; Calleri, E.; Perteghella, S.; Ferrara, A.; Tamma, R.; Milanese, C.; Mandracchia, D.; Brusotti, G.; Torre, M. L.; Ribatti, D.; Auricchio, F.; Massolini, G.; Tripodo, G., Polyacrylate/polyacrylate-PEG biomaterials obtained by high internal phase emulsions (HIPEs) with tailorable drug release and effective mechanical and biological properties. *Materials Science and Engineering C* **2019,** *105*.
28. Calleri, E.; Massolini, G.; Lubda, D.; Temporini, C.; Loiodice, F. C.; Caccialanza, G., Evaluation of a monolithic epoxy silica support for penicillin G acylase immobilization. *J Chromatogr A* **2004,** *1031* (1-2), 93-100.
29. Guillarme, D.; Bonvin, G.; Badoud, F.; Schappler, J.; Rudaz, S.; Veuthey, J. L., Fast chiral separation of drugs using columns packed with sub-2 microm particles and ultra-high pressure. *Chirality* **2010,** *22* (3), 320-30.
30. Koszelewski, D.; Lavandera, I.; Clay, D.; Rozzell, D.; Kroutil, W., Asymmetric Synthesis of Optically Pure Pharmacologically Relevant Amines Employing ω-Transaminases. *Advanced Synthesis & Catalysis* **2008,** *350*, 2761-2766.

CHAPTER 3

Biomedical Applications

Polyacrylate/polyacrylate-PEG biomaterials obtained by high internal phase emulsions (HIPEs) with tailorable drug release and effective mechanical and biological properties

Corti, M.[a], Calleri, E[a]., Perteghella, S.[a], Ferrara, A.[b], Tamma, R.[c], Milanese, C.[d], Mandracchia, D.[e], Brusotti, G.[a], Torre, M.L.[a], Ribatti, D.[c], Auricchio, F.[b], Massolini, G.[a], Tripodo, G.[a]

[a]Department of Drug Sciences, University of Pavia, Viale Taramelli 12-14, Pavia, 27100, Italy

[b]Department of Civil Engineering and Architecture, University of Pavia, Via Adolfo Ferrata 3, Pavia, 27100, Italy

[c]Department of Basic Medical Sciences, Neurosciences, and Sensory Organs, University of Bari Medical School, Piazza Giulio Cesare 11, Bari, 70100, Italy

[d]C.S.G.I. - Department of Chemistry, Physical-Chemistry Section, University of Pavia, Viale Taramelli 16, Pavia, 27100, Italy

[e]Department of Pharmacy-Drug Sciences, University of Bari "Aldo Moro", Via Orabona 4, Bari, 70125, Italy

*Material Science & Engineering C, **2019**, 105 110060*

The paper focuses on the preparation of polyacrylate based biomaterials designed as patches for dermal/transdermal drug delivery using materials obtained by the high internal phase emulsion (HIPE) technique. In particular, butyl acrylate and glycidyl methacrylate were selected, respectively, as backbone and functional monomer while two different crosslinkers, bifunctional or trifunctional, were used to form the covalent network. The influence of PEG on the main properties of the materials was also investigated. The obtained materials show a characteristic and interconnected internal structure as confirmed by SEM studies. From an industrial point of view, an interesting feature of this system is that it can be shaped as needed, in any form and thickness. The physiochemically characterized materials showed tailorable curcumin (model of hydrophobic drugs) drug release, effective mechanical properties, and cell viability and resulted neither pro nor anti-angiogenic as demonstrated in vivo by the chick embryo chorioallantoic membrane (CAM) assay. Based on these results, the obtained polyHIPEs could be proposed as devices for dermal/transdermal drug delivery and/or for the direct application on wounded skin.

1. Introduction

Polymer-based drug delivery systems have been widely explored in medicine in the last twenty years[1, 2]. Three-dimensional porous scaffolds (3D) represent the first class of biomaterials applied in biotechnological fields such as controlled delivery of drugs in long-term therapies and cell growth supports[3]. 3D porous scaffolds are considered as polymer-based materials with an internally interconnected structure[4]. Biomaterial-based scaffolds may be formulated also as fibers[5] or hydrogels synthesized by the cross-linking of hydrophilic polymeric structures[4, 6-8]. Lately, even classical drug delivery systems (DDSs) were formulated from new biocompatible building blocks leading to more sustainable systems to provide a controlled release involving different drug delivery technologies[8]. According to the literature, many different approaches were proposed to achieve biomaterial-based scaffolds such as freeze-drying[9], salt leaching[10], gas foaming[11], supercritical fluid[12], melt molding[13], electro spinning[13], and thermally induced phase separation[13]. The High Internal Phase Emulsion (HIPE) technique is emerging as a valid tool, also in the pharmaceutical field, by emulsion-templating of polymeric materials. HIPEs are typically water in oil (W/O) emulsions with an internal to external phase volume ratio higher than 0.70 (meaning >70% v/v of internal phase). By the polymerization of the external phase of a HIPE (or by using a pre-synthesized polymer) and the subsequent removal of the internal phase, a porous polymeric material with a high degree of internal interconnections, defined polyHIPE (polymerized high internal phase emulsion), could be achieved[14, 15]. In theory, all the known polymerization techniques such as, e.g., free radical polymerization[16], step-growth[17], atom transfer radical polymerization[18] or ROMP[19], could be used to polymerize the external phase, thus enormously increasing the versatility of the HIPE technique. After polymerization of the external phase, the internal phase leave the place to cavities (typically named “voids”) that are reciprocally interconnected through secondary pores or channels (throats) leading to an open-porous/highly-interconnected structure. Both voids and throats are considered as macropores[16]. These interconnecting pores are generated by the rupture (contraction) of the polymeric film during the polymerization step[20]. According to the literature, many synthetic conditions can influence the polyHIPEs internal structure such as the kind and concentration of surfactants[21], the volume of internal phase[16] and the effect of other stabilizers (particles in the “Pickering” type HIPE[22]). Due to their chemical and process versatility, polyHIPEs systems are increasingly applied as templates for porous materials with tailorable properties and structures[23]. Important applications of polyHIPEs are in: cosmetic and food industry[24], chromatography[25],

3D printing[26], catalysis[27], enzyme immobilization[28], electrode material of supercapacitors[29] and absorption of warfare chemical agents[30]. PolyHIPEs may also be proposed for biomedical application (i.e. tissue engineering or drug delivery system) by the synthesis of biodegradable and biocompatible emulsion-templated materials. In literature, different strategies have been shown to achieve biomaterials-based polyHIPEs such as hydrogel-based polyHIPEs[31] or by using biocompatible building blocks[32]. For example, in 2009 Lumelsky and co-workers produced a polyHIPE suitable for tissue engineering using t-butyl acrylate as principal backbone monomer[33]. Other works suggest the use of polyacrylate (biocompatible materials widely used for biomedical application[34]) for the development of polyHIPEs suitable for biomedical purposes[28, 35]. While the application of polyHIPE-based biocompatible scaffolds in tissue engineering is reported in the literature[36, 37], at the best of our knowledge, the use of polyHIPE-based materials for the preparation of drug delivery systems is not described. This work is specifically aimed at establishing the main behaviors of acrylate-based polyHIPEs for drug delivery applications since a so conceived drug delivery system (DDS) would benefit from the possibility to co-deliver hydrophobic drugs and biotechnological molecules through direct conjugation to the functional moieties of the designed polyHIPEs. These behaviors were evaluated on different materials obtained by using butyl acrylate as the monomer forming the polymeric backbone, glycidyl methacrylate as a functional monomer bearing epoxy groups for post-production derivatization, e.g., with hydrophilic biomolecules and two different crosslinker, one tri-functional and one bifunctional to evaluate their effect on the mechanical behaviors of the final materials. Furthermore, a PEG mono-methacrylate was introduced in the formulation with the aim to modify the hydrophilic behaviors of the material surfaces (internal and external) and to evaluate its influence on the internal structure of the corresponding polyHIPEs or on the drug release properties of the material.

2. Experimental section

2.1. Materials

Trimethylolpropane triacrylate (TMPT), Butyl acrylate (BA), Potassium persulfate (KPS), Glycidyl methacrylate (GMA), PEG methacrylate (PEGMA, Mn 360 as from vendor specifics), 1,6-Hexanediol dimethacrylate (HDMA), *N*,*N*,*N*′,*N*′-Tetramethylethylendiamine (TEMED), Monobasic potassium phosphate (KH_2PO_4), Dibasic sodium phosphate (Na_2HPO_4) NaCl, KCl, tetrahydrofuran (THF), absolute ethanol (EtOH), methanol (MeOH), acetonitrile (CH_3CN), acetic acid, 3-(4,5-dimethylthiazol-2-yl)-2,5-diphenyl-tetrazolium bromide (MTT), dimethyl sulfoxide, 30 mL Syringe PP/PE without needle luer lock tip and female luer coupler in polypropylene were from Sigma-Aldrich (Milan, Italy). Synperonic PE/L 121® was kindly provided by Croda Italiana Spa. The water used in this study was double deionized water (DDW), obtained by a Milli-q system from Millipore. All reagents used for cell culture were purchased from Euroclone (Milan, Italy).

2.2. Apparatus

2.2.1. Scanning electron microscopy

SEM images were acquired on gold-sputtered samples using a Zeiss EVO MA10 instrument (Carl Zeiss, Oberkochen, Germany).

2.2.2. High performance liquid chromatography

Chromatographic analysis were carried out using an Agilent technology HP-1100 HPLC instrument (Palo Alto, CA-USA) equipped with a quaternary pump, a Rheodyne injection valve (20 µl), a degasser, an UV–Vis detector set at 420 nm, a thermostat oven (25 ± 0.5 °C) and an Agilent Technologies LiChrospher 100 RP-18 5 µm (250 × 4 mm ID) column. The chromatographic conditions applied were: isocratic elution of a mobile phase composed by water: acetonitrile (55/45 v/v) containing 5% acetic acid at 0.8 ml/min as flow rate. To quantify the unknown CUR amount in the sample, a calibration curve ($y = 52{,}606\,x - 374.78$; $R^2 = 0.9992$) was performed by the injection of standard solutions of CUR in THF at known concentrations (calibration range 0,002 g/L–0,2 g/L). All the injections were conducted in triplicate for six CUR concentration within the indicated range.

2.2.3. Mechanical characterization

Tensile tests were performed by using an MTS Insight Testing System device (MTS System Corporation) equipped with a 250 N load-cell, two pneumatic grips, and a video

extensometer (model ME-46 Messphysik, Fürstenfeld, Austria). For compression tests, the MTS system was equipped with a 10 kN load-cell and two compression plates, whereas the video extensometer was not used due to the specimen shortness.

2.2.4. 3D printing

The dog-bone and cylindrical molds were printed in-home with the Objet260 Connex3 3D printer (Stratasys).

2.3. Methods

2.3.1. PolyHIPE synthesis

The monolithic materials were prepared by the radical polymerization of W/O emulsions characterized by a large volume of the internal phase. For the different compositions refer to Table 3-1.

2.3.2. HIPEs preparation

Table 3-12: Composition parameters for the prepared HIPEs

Sample	Oil phase			Water phase	
	BA/GMA/Surfactant (mL)	TMPTA (mL)	HDMA (mL)	DDW (mL)	PEGMA (mL)
3.2	4.5/1.8/0.5	1.2	/	31	1
3.5	4.5/1.8/0.5	1.2	/	31.25	0.75
3.7	4.5/1.8/0.5	/	1.2	32	/
3.8	4.5/1.8/0.5	/	1.2	31.25	0.75
3.10	4.5/1.8/0.5	/	1.4	32	/
3.11	4.5/1.8/0.5	/	0.8	32	/
3.12	4.5/1.8/0.5	/	1.2	31	1
3.14	4.5/1.8/0.5	/	1.0	31	1
3.15	4.5/1.8/0.5	/	1.4	30.80	1.2
3.16	4.5/1.8/0.5	/	0.8	31	1

In this work, HIPEs were prepared following a previously reported procedure[28, 35]. Briefly, the oil phase was prepared by mixing in a two-necks round bottom glass flask butyl acrylate (BA) and glycidyl methacrylate (GMA), backbone and functional lipophilic monomers,

respectively. Synperonic PE/L 121 was used as a polymeric surfactant and an established amount of crosslinker (trimethylolpropanetriacrylate [TMPTA] or 1,6-hexandioldimethacrylate [HDMA]) were added (see Table 3-1 for the samples' composition). The water phase was achieved by dissolving 272 mg of potassium persulfate (KPS), as a radical initiator, in the presence or not of PEGMA (see Table 3-1), in nitrogen degassed double distilled water (DDW). The water phase was added drop by drop into the round bottom flask using a dropping funnel. During this procedure, the system was maintained under continuous stirring (300 rpm) provided by an overhead mechanical stirrer and under a constant nitrogen flow. After the whole internal aqueous phase was added to the oil phase (20 min drop by drop), the stirring was increased up to 400 rpm for 1 h under nitrogen until a white highly viscous biphasic system (high internal phase emulsion) was achieved.

2.3.3. PolyHIPEs preparation; polymerization step

In order to polymerize the external phase of the HIPEs (to obtain the polyHIPEs), the emulsions were transferred in a PE Syringe connected by a female luer coupler to a second syringe pre-filled with 272 µL of TEMED, Fig. 3-1. Using a "syringe-to-syringe" method, HIPEs and TEMED were mixed by an alternate extrusion from one syringe to the other until (12 extrusion processes). The optimal number of extrusions was visually established by using a monomer-soluble dye instead of the radical initiator until the color uniformity of the emulsion was reached. The mixed material was then rapidly transferred onto different supports: PTFE (Teflon), glass or PMMA (Plexiglas). The materials were then modeled as a thin layer, by using a homemade plastic casting blade to control the thickness of the final polymer.

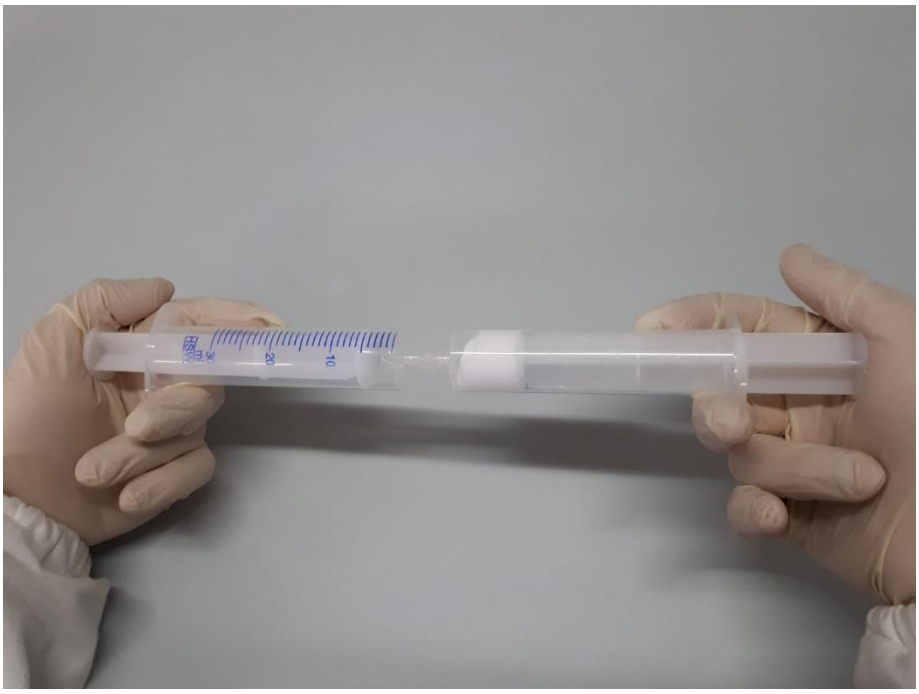

Figure 3-23: The used “syringe-to-syringe” method for HIPEs and TEMED mixing. The redox initiator TEMED was placed in the left syringe while HIPE was in the right one.

For all materials, the polymerization was carried out for 24 h at room temperature. The monoliths were then washed in order to remove the not crosslinked materials, initiators and water phase. For the washing procedure, the polymerized and crosslinked materials were placed in a 200 mL beaker and different solvents such as DDW (two × 100 mL), MeOH (two × 100 mL), EtOH (two × 100 mL) and, eventually, THF (one step) were used. The materials not subjected to the final washing step in THF were used for the characterizations in terms of swelling and weight loss in water and organic solvents. After the washing step, the materials were placed in an oven at 45 °C for 24 h to remove residual solvents.

2.3.4. Swelling (SW) and weight loss (WL) studies in water and THF

All dried materials, obtained as above described, not subjected to the THF last washing step, were studied in terms of solvent uptake (THF) and extractable matter in both water and organic solvents. Weighed polymeric monoliths (10–15 mg) were selected and their initial weight was registered (Ws). These polyHIPE samples were placed in a beaker containing 20 mL of water or THF for 24 h. Thereafter, the monoliths were rapidly paper blotted on the surface and the weight of the wet polyHIPEs (Wfw) was registered. Finally, the materials were dried in an oven at 40 °C (24 h was a suitable time to reach a constant weight) and their final weights were registered as Wfd. For water uptake (swelling) studies, THF only pre-washed samples were used. The swelling and weight loss values of each sample were calculated using the equations below. All determinations were performed in

triplicate. Weight loss % (WL) and swelling (SW) were calculated according to the following equations (the equation terms were defined in the above text):

$$WL = \frac{Ws - Wfd}{Ws} \times 100 \qquad SW = \frac{Wfw - Wfd}{Wfd}$$

2.3.5. SEM analysis

Scanning electron microscopy analyses were conducted on gold-sputtered samples in order to assess the presence of the typical “open-cell” polyHIPE internal structure. SEM images were acquired from different sides, such as upper, lower and internal sides and those from the internal side were used for the voids and throats (internal pores) evaluation.

2.3.6. Drug loading of curcumin (CUR)

PolyHIPEs 3.2, 3.5, 3.7, 3.8, 3.11, 3.12, 3.14 and 3.16 were selected to be loaded with curcumin (CUR). For each sample, 200 mg of washed and dried material was weighted. Therefore, a 10 mg/mL CUR solution in THF was prepared and the weighted material was placed into 2 mL of this solution for 24 h. Then, the loaded polyHIPEs were oven-dried in mild conditions at 45 °C for 3 h and afterward in a vacuum desiccator for 12 h to remove the remaining solvent. All these procedures occurred in the dark to avoid the photodegradation of CUR.

2.3.7. Drug release studies

A Phosphate Buffer Saline pH 7.4 (PBS) was prepared with NaCl 8 g, KCl 0.2 g, Na_2HPO_4 1.44 g and KH_2PO_4 0.24 g per 1 L of buffer. For the in vitro release studies, a 3% (w/v) polysorbate 80 solution in PBS pH 7.4 was prepared and used as releasing buffer to assure the sink conditions. For each loaded material, 21 small monoliths (≈10 mg) were sampled and each one was placed in 50 mL of release buffer. Therefore, 1 ml of buffer was sampled for 7 established time intervals (every sample was conducted in triplicate) corresponding to 30 min, 1 h, 2 h, 4 h, 6 h, 8 h, 24 h, 48 h, 72 h, and 120 h. All procedures were carried out in the dark and at 37 °C. The filtered release solutions, at the established time intervals, were then injected in an HPLC/UV–Vis system. To evaluate the complete CUR dissolution in the release medium (sink conditions), the same amount of curcumin loaded in the samples was put in 50 mL of release buffer and the solution concentration estimated by HPLC as reported in paragraph 2.2.

2.3.8. Tensile mechanical testing

Dog-bone specimens (type V according to ASTM D638 standard) were prepared for some polyHIPE material compositions. In particular, proper dog-bone dimes were printed in-home with the Objet260 Connex3 3D printer (Stratasys) using a Vero-Stratasys photopolymer resin (see Fig. 3-2).

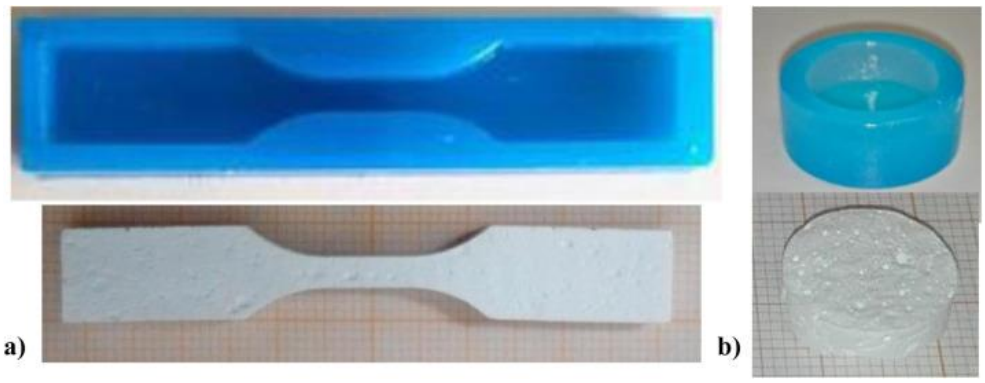

Figure 3-24: 3D molds in photopolymer resin and corresponding polyHIPEs specimens; a) Dog-bone specimen (type V according to ASTM D638 standard) for tensile tests; b) cylindrical specimens (12 mm of diameter and 4 mm of height, ratio 3:1) for compression experiments

Tensile tests were performed in ambient conditions of temperature and relative humidity using an MTS Insight Testing System device (MTS System Corporation) equipped with a 250 N load-cell, two pneumatic grips, and a video extensometer (model ME-46 Messphysik, Fürstenfeld, Austria). All specimens were loaded at a constant cross-head speed of 1 mm/min until specimen break. Strain and stress were computed as $\varepsilon = (l - l_0)/l_0$, and $\sigma = F/A_0$, respectively, with l and l_0 the current and initial gauge lengths, F the applied load, A_0 the initial cross-sectional area. Tensile properties were determined from the stress/strain plots according to the ASTM D-638 standard. In particular, the tensile strength was identified as the stress at the breakpoint, and the Young modulus was computed as the slope of the initial linear portion of the stress/strain curve. Moreover, the strain at the breakpoint was also identified.

2.3.9. Compression mechanical testing

Cylindrical specimens (12 mm of diameter and 4 mm of height, ratio 3,1) were prepared for some polyHIPE material compositions. In particular, cylindrical dimes in photopolymer resin were printed again using the Objet 260 Connex 3D printer (see Fig. 3-2). For compression tests, the MTS system was equipped with a 10 kN load-cell and two compression plates, whereas the video extensometer was not used due to the specimen shortness. All

specimens were compressed at a cross-head speed of 1 mm/min until the crash of the two plates. Strain and stress were computed as $\varepsilon = (l - l_0)/l_0$, and $\sigma = F/A_0$, respectively, with l and l_0 the current and initial height of the specimen, F the applied load, A_0 the initial cylinder section area. The compressive properties were determined from the stress/strain plots according to the ASTM D-1621 standard. In particular, after correcting for zero strain, the compressive modulus was computed as the slope of the linear region and the compressive strength as the stress at the yield point or the stress at 10% strain, if such deformation occurs before the yield point, or in the absence of such a yield point. Finally, the stress at crush point (i.e., crush strength) was identified.

2.3.10. Cell culture

Human fibroblasts were obtained from informed donors subjected to skin biopsy. Skin samples were enzymatically digested (0.125% trypsin and 1% collagenase); obtained fibroblasts were cultured in Dulbecco's Modified Eagle's Medium High Glucose (DMEM-HG), 10% fetal bovine serum (FBS), L-glutamine (1.8 mM), penicillin (100 IU/mL), streptomycin (100 µg/mL) and amphotericin B (2.5 µg/mL). The culture medium was refreshed 2 times per week until cell subconfluence. For this experiment, we considered cells cultured until third culture passage.

2.3.11. Cytotoxicity tests

To evaluate the biocompatibility of scaffolds (sample ID: 3.2, 3.5, 3.7, 3.8, 3.10, 3.11, 3.14, 3.15, 3.16), we considered two types of cytotoxicity assay: extract, namely indirect (the material-conditioned medium was used for cell culture), and direct contact cytotoxicity assays. All the samples were sterilized by autoclaving at 121 °C for 20 min before cell testing. Human fibroblasts were seeded in 96-well plates (10,000 cells/cm^2). After 24 h, media were discarded and 100 µL of samples were added for 24 h of incubation. For indirect method, suitable to detect the effect of soluble substances released by polymeric supports, we previously incubated the scaffolds (2 mg/mL and 4 mg/mL) in culture medium (DMEM-HG with 10% FBS) for 24 h at 37 °C, 5% CO_2; after this time each extract supernatant sample were incubated with fibroblasts for 24 h. For direct contact method, scaffolds were shattered in small pieces (0.5 mm^2) and co-incubated (24 h, 37 °C and 5% CO_2) with fibroblasts at two concentrations: 2 mg/mL and 4 mg/mL. After cell exposure to extracts and scaffolds, viability was evaluated adding 100 mL of 3-(4,5-dimethylthiazol-2-yl)-2,5-diphenyl-tetrazolium bromide (MTT) solution (0.5 mg/mL) in each well. MTT solution was removed after 3 h of incubation and obtained formazan crystals were dissolved with 100 ml of DMSO.

Optical density (OD) of the DMSO solution was measured on a microplate reader (Synergy HT, BioTek, UK) at 570 nm and 670 nm (reference wavelength). Cell viability (%) was calculated as follows: 100 × (ODs/ODc), where ODs represents the OD mean value of tested sample and ODc is the OD mean value of untreated cells (control). Each condition was tested in triplicate.

2.3.12. Chick embryo chorioallantoic membrane (CAM) assay

Fertilized White Leghorn chicken eggs (20 per group) were incubated at 37 °C at constant humidity. On day 3, a square window was opened in the shell, and 2 to 3 mL of albumen were removed to allow detachment of the developing CAM from the shell. The window was sealed with a glass, and the eggs were returned to the incubator. On day 8, eggs were treated with 1 mm^3 fragment of polyHIPEs samples (sterilized by autoclaving at 121 °C for 20 min) or a gelatin sponge soaked with 50 ng vascular endothelial growth factor (VEGF), used as a positive control was placed on the top of the growing CAM, as previously described[38]. CAMs were examined daily until day 12 and photographed *in ovo* with a stereomicroscope equipped with a camera system (Olympus Italia, Rozzano, Italy). On day 12, the angiogenic response was evaluated by image analysis. Briefly, microscopic images obtained from the stereomicroscope were converted in gray-scale and analyzed using the Aperio Positive Pixel Count algorithm embedded in the ImageScope (Leica Biosystems, Nussloch, Germany). The algorithm input parameters were initially set to obtain the identification of pixels related to the blood vessels as strong positive and to the background as medium and weak positive and tuned to minimize non-specific pixel recognition as strong positive. The algorithm output is composed of the number of strong positive pixels (Nsp), the number of medium positive pixels (Np), the number of weak positive pixels (Nwp). A morphometric value is then defined and calculated by the algorithm as *Number of strong positive pixels* (%) = $Nsp/Np + Nwp + NspX100$. Statistical significance between the stimulated, normal and inhibited experimental groups was assessed by one-way Anova followed by Tukey multiple comparison post-test. The statistical analysis and graph plotting were performed with the Graph Pad Prism 5.0 statistical package (GraphPad Software, San Diego, CA, USA).

2.3.13. Statistical analysis

For cytotoxicity tests: results obtained from each cytotoxicity assay (direct and indirect) were processed by a multifactor ANOVA, considering sample formulation and concentration as fixed factors, and the viability % as dependent variables. The differences between groups

were analyzed with the posthoc LSD's test for multiple comparisons. Unless differently specified, data are expressed as mean ± standard deviation. The statistical significance was fixed at $p < 0.05$. For chick embryo chorioallantoic membrane (CAM) assay: data from different experimental groups were compared by one-way analysis of variance (ANOVA) with $p < 0.05$ at 99% level of confidence (GraphPad Prism v. 4.00 GraphPad Software, Inc., San Diego, CA). Bonferroni post-tests were used for post hoc contrast.

3. Result and discussion

3.1. PolyHIPEs preparation and characterization

Here, we set up the preparation of new materials based on polyacrylate/polyacrylate-PEG produced by the high internal phase emulsion technique to provide materials with a suitable internal structure to be exploited for biomedical applications. In particular, the new materials are intended to be applied to the skin as wound dressings and/or for the controlled release of hydrophobic active principles. The essentially hydrophobic nature of the polyacrylate network was tailored by using a bifunctional crosslinker instead of a trifunctional one (to soften the network increasing its flexibility) and/or by introducing into the network hydrophilic portions of PEG monoacrylate (to make a more hydrophilic network so increasing the amount of incoming water). With these premises, we stabilized an 80% v/v water phase into 20% v/v of oil phase (monomers and surfactant) getting a W/O emulsion by using a low HLB surfactant chemically belonging to PEO-PPO-PEO family [poly(ethylene oxide)-poly(propylene oxide)-poly(ethylene oxide)], see Table 3-1 for samples composition. These surfactants, commercially known as, e.g., Symperonic® are biocompatible and miscible with the oil (monomers) phase. A so structured emulsion falls within the category of high internal phase emulsions (HIPEs) which we previously explored to produce materials for different biomedical applications[28, 35]. In the present study, we are substantially modifying the chemical composition of the previously prepared polyHIPEs by using a bifunctional crosslinker to improve the materials flexibility and PEG chains to increase the hydrophilicity of the butyl acrylate-based materials. An example of a bent polyHIPE obtained by using the bifunctional crosslinker HDMA is shown in Fig. 3-3. Please note that this sample was swollen in THF before bending, in the same conditions the polyHIPEs obtained by the tri-functional crosslinker broke after approximately 50° bending.

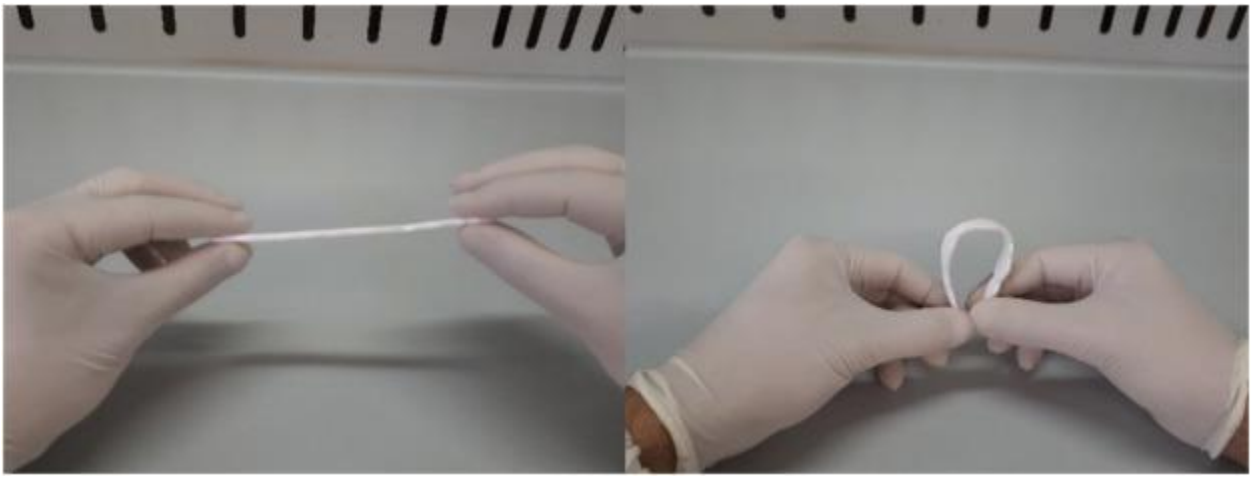

Figure 3-25: Images showing the flexibility of a representative polyHIPE sample (3.11) obtained the bifunctional crosslinker HDMA (this sample was preventively swelled in THF).

As the first set of experiments, we allowed the HIPEs emulsion to polymerize by casting them on surfaces made from different materials. It was aimed at evaluating the influence of the casting surface on properties such as swelling or weight loss of the polymerized emulsions. We used glass, plexiglass (polyacrylate) or Teflon as the casting bases. The rationale for this choice arises from the different wettability of the emulsion with regard to the casting base other than they are widely used as building materials for e.g. tubes, plates, supports of industrial interest. The contact angle between the emulsion and the surfaces was not evaluated because the emulsion is cream-like so the measurement would not be accurate. Thus, we assumed that the surfaces had comparable roughness. In this way, we thought that the different affinity (in terms of hydrophobic interactions) between the HIPE and the surfaces could lead to unpredictable size pore formation at the interface emulsion/surface depending on their affinity. This would affect the water uptake, by increase or reduction of the polyHIPEs pore size or, for the same reason, the weight loss. In Table 3-2 are summarized the main results obtained from this study. These results clearly indicate that there are no significant differences in terms of SW or WL between materials obtained by casting and polymerizing them on different surfaces. Only for samples 3.2, 3.8 and 3.16, it looks like the SWaq is increasing in the order Plexiglas > Glass > Teflon but, in general, considering the experimental error, the values can be considered aligned. It would predict the obtainment of polyHIPEs with similar structure independently from the material used for the emulsion deposition. On the other side, samples 3.12, 3.14 and 3.16 showed low SW values in both water and THF. This behavior could not be simply explained by linking it to the composition, thus further studies were carried out.

Table 3-13: Weight loss (WL) and swelling (SW) in water (aq) or tetrahydrofuran (THF) of HIPE samples cast on Teflon (A), Glass (B) or Plexiglass (C). All samples were tested in triplicate. Mean ± SD

Sample	***Surface material***	*WLaq*	*SWaq*	WL_{THF}	SW_{THF}
3.2	A	10.10 ± 0.98	1.69 ± 0,03	6.60 ± 0.28	2.35 ± 0.05
	B	7.29 ± 0.11	2.22 ± 0.14	2.90 ± 0.62	3.93 ± 0.12
	C	6.01 ± 0.56	3.05 ± 0.03	6.01 ± 0.56	4.03 ± 0.69
3.5	A	6.04 ± 0.53	3.10 ± 0.28	4.66 ± 0.36	5.26 ± 0.20
	B	15.72 ± 2.75	2.53 ± 0.25	8.54 ± 1.08	3.91 ± 0.20
	C	1.54 ± 0.30	3.27 ± 0.07	6.25 ± 1.31	5.18 ± 0.34
3.7	A	5.83 ± 1.51	0.98 ± 0.27	8.08 ± 1.57	6.24 ± 0.45
	B	8.37 ± 0,05	3.77 ± 1.55	4,17 ± 1,41	7,35 ± 0,01
	C	2.03 ± 0.85	1.73 ± 0.06	1.48 ± 0.59	7.30 ± 0.12
3.8	A	1.74 ± 0.32	0.57 ± 0.15	1.16 ± 0.19	5.23 ± 0.38
	B	1.33 ± 0.41	1.26 ± 0.40	1.52 ± 0.72	5.71 ± 0.11
	C	2.46 ± 0.15	1.45 ± 0.24	1.68 ± 0.87	4.71 ± 0.33
3.11	A	7.62 ± 0.52	2.73 ± 0.08	5.92 ± 0.09	9.13 ± 0.02
	B	1.61 ± 0.77	4.67 ± 0.01	3.15 ± 0.20	9.04 ± 0.15
	C	2.97 ± 1.87	1.84 ± 0.88	5.09 ± 0.24	8.95 ± 0.56
3.12	A	3.84 ± 0.58	1.20 ± 0.09	2.12 ± 0.88	1.08 ± 0.36
	B	2.77 ± 0.54	0.29 ± 0.03	2.66 ± 0.29	0.38 ± 0.02
	C	1.48 ± 0.01	1.04 ± 0.04	1.00 ± 0.34	1.73 ± 0.24
3.14	A	3.50 ± 0.30	0.39 ± 0.04	0.55 ± 0.15	1.81 ± 0.67
	B	5.22 ± 0.01	0.71 ± 0.04	4.02 ± 0.06	0.80 ± 0.01
	C	6.10 ± 0.79	0.68 ± 0.02	6.07 ± 0.79	0.96 ± 0.08
3.16	A	1.06 ± 0,31	1.4 ± 0.07	2.54 ± 0.35	1.41 ± 0.11
	B	9.06 ± 3,21	1.58 ± 0.11	3.90 ± 1.44	1.01 ± 0.09
	C	6.29 ± 0.79	2.29 ± 0.27	2.79 ± 1.34	1.86 ± 0.14

We focused our attention on the SEM characterization of the polyHIPEs obtained on Teflon because it is the less chemically reactive support among the tested and gave materials macroscopically well-formed.

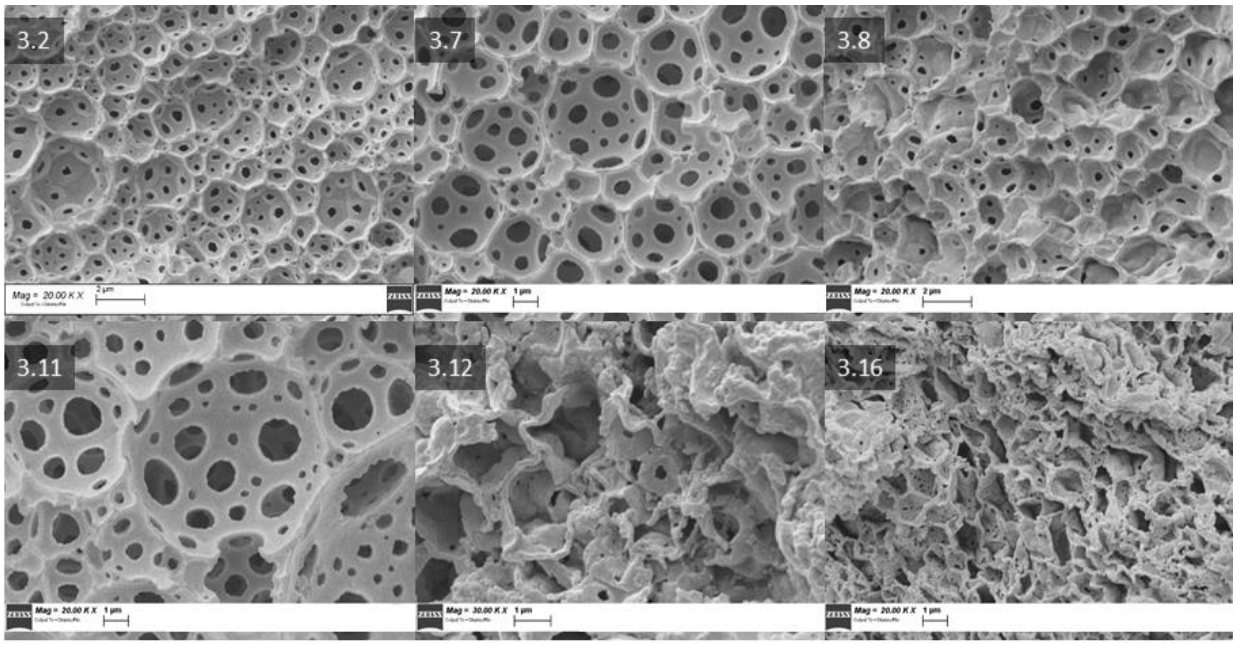

Figure 3-26: SEM pictures of representative polyHIPEs samples

From the SEM studies, Fig. 3-4, what mostly affects the polyHIPEs internal morphology seems to be the presence or not of PEGMA. In particular, sample 3.11 does not contain any PEG and, apart from the void dimensions, also the throats (the holes inside the voids), look larger and more numerous than in the other samples. The sample 3.16 has the same composition than 3.11 plus PEGMA and shows more collapsed voids with smaller and less numerous throats. The main polyHIPE structure is still maintained. Samples 3.8 and 3.12 have the same monomers composition but different amounts in PEGMA, being 0.75 mL in 3.8 and 1.0 mL in 3.12. The higher amount of PEGMA leads to a more collapsed structure (3.12). Even more evident is the morphologic difference between samples 3.7 and 3.8, the only difference is that 3.8 has PEG while 3.7 not. It is also to be noted that the kind of used crosslinker had a marked effect on the structure, in fact, samples 3.2 and 3.5 (see Fig. 3-5 for sample 3.5), both containing PEGMA, respectively 0.75 mL and 1.0 mL, but from the trifunctional crosslinker do not show any particular collapse due to the PEG presence even if the throats resulted less numerous and smaller than the counterpart 3.7 without PEG. It could be supposed that the tri-arm crosslinker, such as TMPT, can lead to void walls more structured than those formed by using the bifunctional crosslinker HDMA. This would in part compensate for the softening action of PEG. To further corroborate this assumption, PEGMA amount was reduced from 1 mL in sample 3.12 to 0.75 mL in sample 3.8 (both crosslinked with HDMA); this led to a more coherent structure similar to the samples 3.2 and 3.5 both crosslinked with TMPT. In conclusion, PEGMA has an evident effect on the

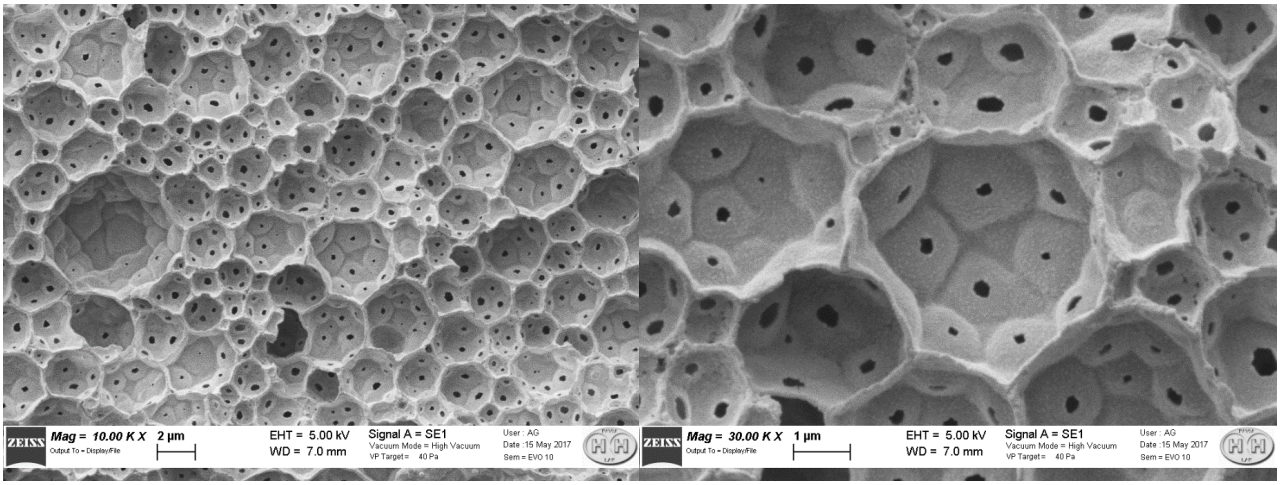

Figure3- 27: SEM pictures of sample 3.5.

polyHIPEs internal structure; the actual amount in the monomers' composition allows precise control of the internal structure.

3.2. Drug loading and release

One of the main aims of this study was to evaluate these materials as drug delivery system for the controlled topical delivery of bioactive molecules. In this context, we selected curcumin as a model active molecule with numerous applications, i.e., in wound healing, cancer treatment, and anti-inflammatory activity[39]. Curcumin is a highly hydrophobic drug as several molecules of pharmaceutical interest are, such as steroidal drugs and different antibiotics. Curcumin would benefit from its loading into a partially hydrophobic matrix because it should spread inside the material and would be released when in sink conditions. To perform the release studies, curcumin has been loaded into the polyHIPEs by solvent (THF) soaking thus, the whole amount of loaded CUR was found into the material and was for all the samples 5% w/w. THF was chosen because of its affinity toward polyacrylates, its simple removal, and low toxicity if compared to other volatile solvents such as chlorinated. The results from drug release studies are shown in Fig. 3-6. From a first view, the release curves are split into two main groups. The first group formed by most of the samples, namely 3.2, 3.5, 3.7, 3.8 and 3.11, shows a complete (100%) release in the 100–140 h time range (sample 3.7 reached 100% release in 140 h). The release rate shows a moderate burst effect at the beginning of the experiment (mostly due to the drug adsorbed on the matrix surface) and an almost constant release rate up to the complete release. The second group of curves,

comprised samples 3.12, 3.14 and 3.16, does not show a complete release if not a remarkable burst effect in the first hours of the experiment.

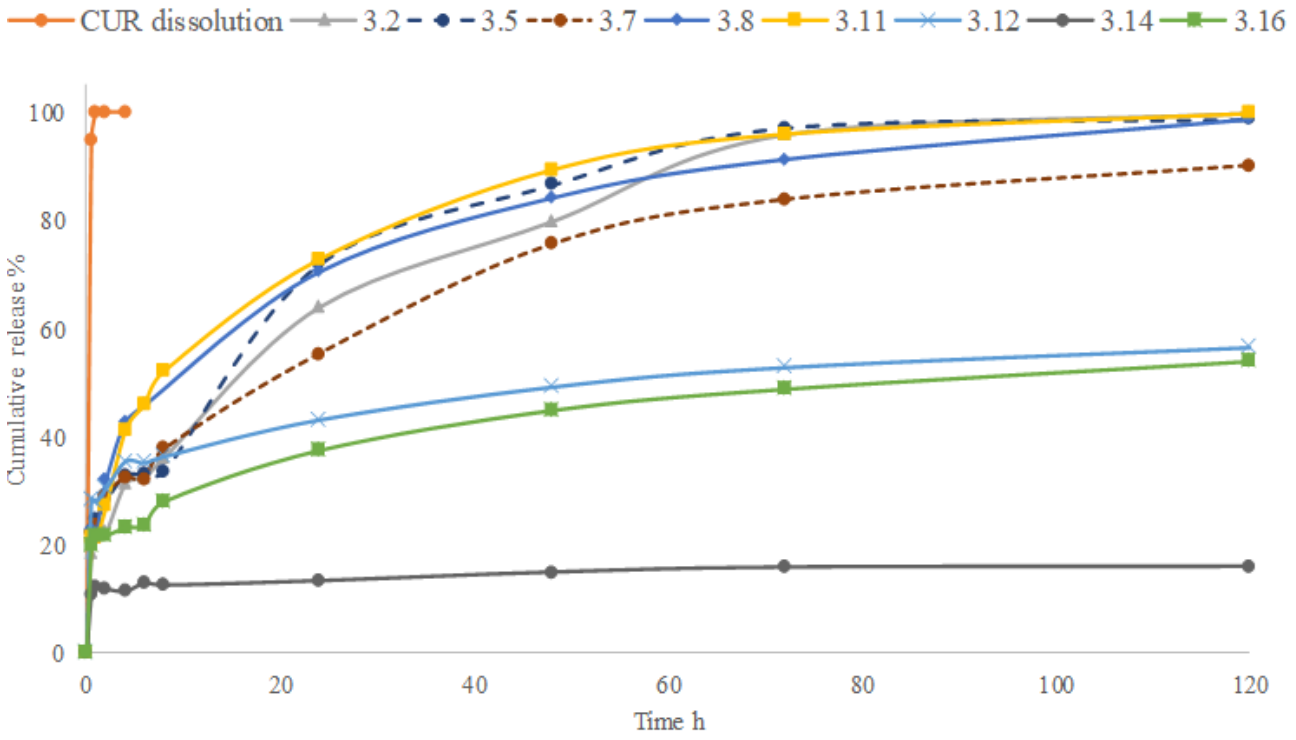

Figure 3-28: Curcumin release studies from the prepared polyHIPEs, CUR dissolution curve indicates that sink conditions are maintained along with the experiment. All the samples had the same drug loading (5% w/w).

Now it is possible to link together the results from swelling, SEM and drug release studies. In particular, samples 3.12, 3.14 and 3.16 are those for which the main behaviors are affected by the presence of PEGMA in the water phase and, even, by its amount. Introducing 1 mL of PEGMA in the composition led to i) low swelling in water and THF ii) a void structure with small or no throats iii) reduced drug release. As known, both concentration and Mw (that here was maintained constant) of PEG could affect the main behavior of an emulsion. In particular, Papouts and co-workers found that: “For molecular weights below Mw 1000, the polymer serves to modify the water-oil interface with an increase in electrical conductivity. With large chains comparable to the droplet size or larger, the structure of the microemulsion is altered.”[40], in our study we used a PEGMA with an Mw of 2000 Da. It could be supposed that the PEG, above an established concentration, affected the emulsion formation or stability in a way that does not allow the throat formation upon polymerization or reduced it in a significant manner. On the other side, since PEGMA enters the polyHIPE composition (being a methacrylate), it could change the monomer film microenvironment not allowing the polymeric film contraction (due to PEG softening behaviors) that is necessary

for throat formation. In fact, in literature, it is reported that throat formation is due to volume contraction during the conversion of monomers to polymer[41]. These assumptions could well explain the structure we found from SEM which shown closed or almost closed throats within the voids of samples 3.12, 3.14 and 3.16. It would also explain the low swelling and incomplete drug release.

3.3. Mechanical testing on polyHIPE materials

Tensile and compression tests were performed on specimens of selected polyHIPEs samples in order to investigate the impact of the material composition on mechanical properties. The selection was accomplished to investigate samples with the bifunctional crosslinker or with the tri-arm crosslinker as well as samples with or without PEG. In particular, four material compositions were selected, namely 3.2 (not tested for tensile test) and 3.5 (tri-arm crosslinker/PEG), 3.7 (bifunctional crosslinker) and 3.8 (bifunctional crosslinker/PEG). Results are summarized in Table 3-3 for tensile and compression tests, respectively. Reported moduli, strength and strain data are the corresponding average values among successful tests.

Table 3-14: Tensile and compression tests on selected polyHIPEs

Sample	*Tensile modulus [MPa]*	*Tensile strength [MPa]*	*Deformation at break [%]*	*Compressive modulus [MPa]*	*Compressive strength [MPa]*	*Crush strength [MPa]*
3.2	15.2 ± 3.8	0.49 ± 0.12	6.08 ± 1.2	4.69 ± 0.31	0.40 ± 0.04	58.8 ± 22.4
3.5	-	-	-	2.88 ± 0.18	0.33 ± 0.04	33.1 ± 0.1
3.7	42.0 ± 0.4	0.87 ± 0.13	6.09 ± 1.7	4.82 ± 1.37	0.41 ± 0.10	41.25 ± 16.2
3.8	16.5 ± 4.5	0.91 ± 0.14	19.50 ± 0.9	2.00 ± 0.33	0.24 ± 0.02	56.15 ± 9.5

On one hand, our results evidence that in tension the considered polyHIPE samples have the typical behavior of a brittle material, i.e., specimens break without a significant deformation (see Fig. 3-7). In particular, the tensile modulus is lower in samples containing PEG (i.e., 3.5, and 3.8) than in the one without PEG (3.7). Accordingly, we can say that the presence of PEG in the material composition reduces significantly the stiffness of the considered polyHIPEs. Then, the presence of PEG seems to affect the deformation at the break of samples. For example, considering samples with bifunctional crosslinker, the deformation at break is higher for the sample containing PEG (3.8) than for the sample without PEG (3.7) suggesting that the presence of PEG makes the polyHIPEs more deformable.

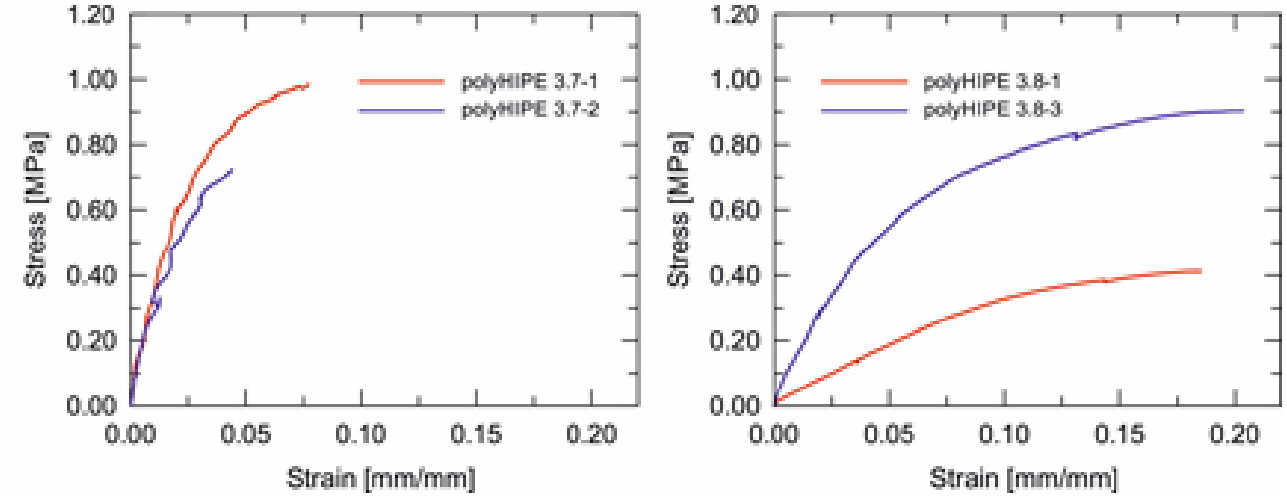

Figure 3-29: Representative tensile test curves for polyHIPE samples.

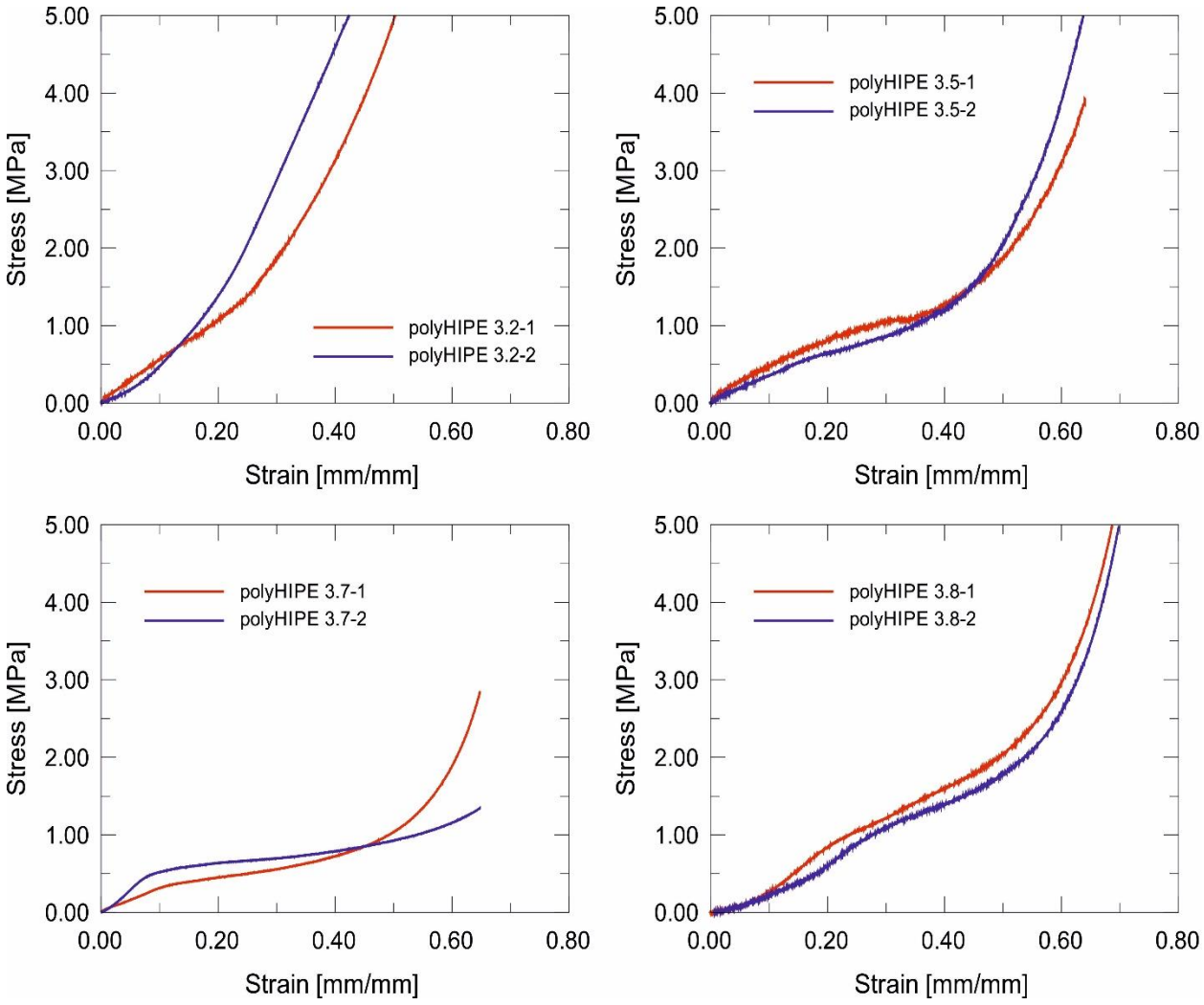

***Figure 3-30**: Representative compression test curves for polyHIPE samples*

On the contrary, the presence of PEG has no influence on the ultimate tensile strength as shown by the similar values obtained for samples 3.8 and 3.7. Finally, the kind of used crosslinker seems to affect the material tensile strength as suggested by the lower value obtained for the sample 3.5 containing tri-arm crosslinker rather than bifunctional crosslinker. On the other hand, our results evidence, in compression, a softer behavior. The typical stress-strain plot has three regions, namely, initial linear region, plateau region, and bulk compression region (see Fig. 3-8). Again, our results evidence that polyHIPE compressive properties are strongly affected by the presence of PEG. For example, with respect to bifunctional crosslinker samples (i.e., 3.7 and 3.8), the compressive modulus is lower for the sample containing PEG (3.8) than for the sample without PEG (3.7). On the contrary, reducing the amount of PEG in tri-arm crosslinker samples (i.e., 1.00 mL for sample 3.2 vs 0.75 mL for sample 3.5) a strong reduction of the compressive modulus is observed (see Table 3-3). Although the presence of PEG has an effect in reducing the compressive modulus at a parity of crosslinker, such a difference is not remarkable as for tensile tests. Finally, it is worth noting that, samples 3.2 and 3.5 partially recover the compressive deformation when compressive plates are moved after the end of the test (see Fig. 3-9). On the contrary, samples 3.7 and 3.8 remain crushed, respectively.

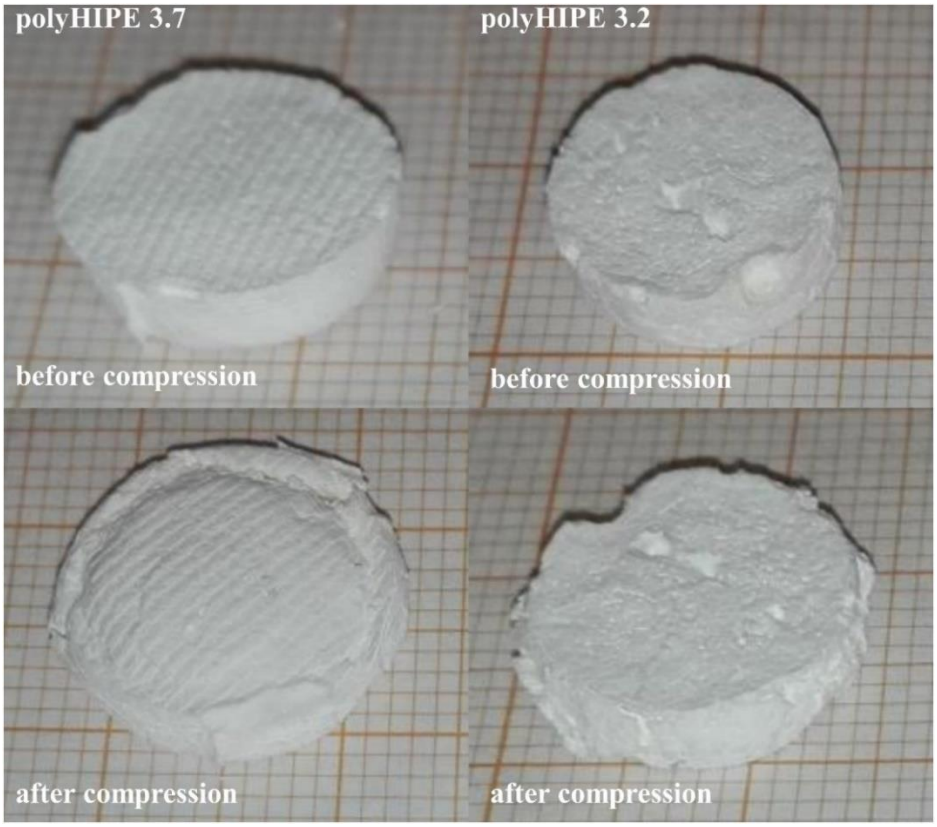

Figure 3-31: Representative samples 3.7 and 3.2 before (upper images) and after (lower images) the compression test. To be noted the partial recovery of the initial shape by the sample 3.2

Some works on mechanical characterizations of acrylate-based polyHIPEs are available in the literature. For example, Jerenc et al. prepared polyHIPEs from monomers such as glycidyl methacrylate (GMA), ethylene glycol dimethacrylate (EGDMA) and 2-ethylhexyl acrylate (EHA). Depending on the relative amount of the monomers, they found different mechanical behaviors either in elongation or compression[42]. In particular, they noted differences in dependence of the EHA amount since by increasing its amount to 5% w/w the tensile modulus, as well as the compressive modulus, are reduced accounting this effect to an increased free volume as a consequence of EHA introduction in the composition. In the evaluation of mechanical characteristics of polyHIPEs, even the internal morphology must be taken into account as evidenced by the previous study and by other authors after filling different polyHIPEs with hydroxyapatite[43]. Both the cited papers link the varied mechanical behaviors of polyHIPEs with their porosity but also with their morphology that, as shown in Fig. 3-4, may change greatly depending on the composition. The dependence of tensile properties on the kind of crosslinker was explored by Caldwell et al. in 2012[44]. They used as crosslinkers the trimethylolpropane triacrylate (TMPTA, the same tri-arm crosslinker we are using in our study) and the dipentaerythritol penta/hexa-acrylate (DPEHA). From the tensile test studies, they found that the polyHIPEs obtained with the DPEHA were stiffer than those from TMPTA, so confirming our findings[44]. This is obviously due to the higher crosslinking density gained by using multi-arm crosslinkers that confers higher stiffness at the final material. Returning to our results, while tensile tests indicated that the polyHIPE samples we tested resulted in tendentially brittle materials, the compression data pointed on materials with a certain softness. It looks contradictory but, as mentioned before, the internal structure of the polyHIPE must be accounted as one of the major contributors to the final mechanical properties as well as the chemical composition. If we think at the polyHIPEs internal structure, we might think at a deflated ball which thickness of the walls can still sustain the main structure. Thus, if the hypothetical ball (the voids in the polyHIPE) is stretched, then it will break upon elongation involving the contiguous voids that will break consequently. When compressed, the walls of the voids will bend in the direction of the applied force and their flexibility will allow some recovery of the original shape.

3.4. Cytocompatibility studies on fibroblasts

Cytotoxicity test on fibroblasts showed a certain variability among the samples, Fig. 3-10. The highest viability values were found for samples 3.7, 3.14, 3.15 or 3.16. The last three samples were formed in the presence of PEGMA and by using the bifunctional crosslinker

but it is also true that samples 3.14 and 3.16 showed a not complete drug release probably related to their internal structure. No significant difference was found among these samples when the experiment was performed as a direct or indirect test at 2 or 4 mg/mL. The two samples crosslinked with the trifunctional reagent, 3.2 and 3.5, showed the lowest cell viability, being the direct method results worse than those from the indirect method. For these two samples also the sample concentration played an important role. In particular, sample 3.5 showed viability lower than 40% in the direct method at 4 mg/mL. Interestingly, sample 3.10 that is similar in composition to samples 3.15 and 3.16, resulted in cell viability close to 60%. While sample 3.11 shown high cell viability in the indirect method and still high cell viability for the direct method at 2 mg/mL. This sample does not show the PEGMA in its composition. In literature, there are not many examples of cell compatibility studies of polyHIPE materials on selected cell lines. One recent paper shows the cell viability of HeLa cells upon incubation with a medium conditioned with the poyHIPE material (indirect method) developed in the study. The authors stated that "…the polyHIPE leachates had a limited impact on the viability of the cells; each composition remained greater than 70% viable and were therefore considered non-toxic"[37]. Their finding perfectly fits with our results obtained from the indirect method. The only difference between the two studies is that we performed the test on human fibroblasts primary cells (healthy cells) while the authors of the referenced paper used immortalized tumor cells.

3.5. Angiogenesis studies by the in vivo chick embryo CAM assay

As another biological characterization, we performed angiogenesis studies by the in vivo chick embryo CAM assay. This is a well-established method to evaluate the pro or anti-angiogenic the potential of various substances, both in solution or solid form through their direct application to the CAM surface. Since chick embryo at the time of the experiment does not possess a yet developed immune system it is not subject to immune response. On the other side, if a well known angiogenic growth factor such as VEGF soaked in a gelatin sponge and applied on the CAM surface, four days after the application, numerous new-formed blood vessels converge toward the sponge, confirming the pro-angiogenic activity of the molecule. On the contrary, when an anti-angiogenic molecule is applied the pre-formed blood vessels around the substance will disappear. From Fig. 3-11, it is clear that the applied materials do not have any detectable activity on the CAM vessels, neither pro-angiogenic nor anti-angiogenic.

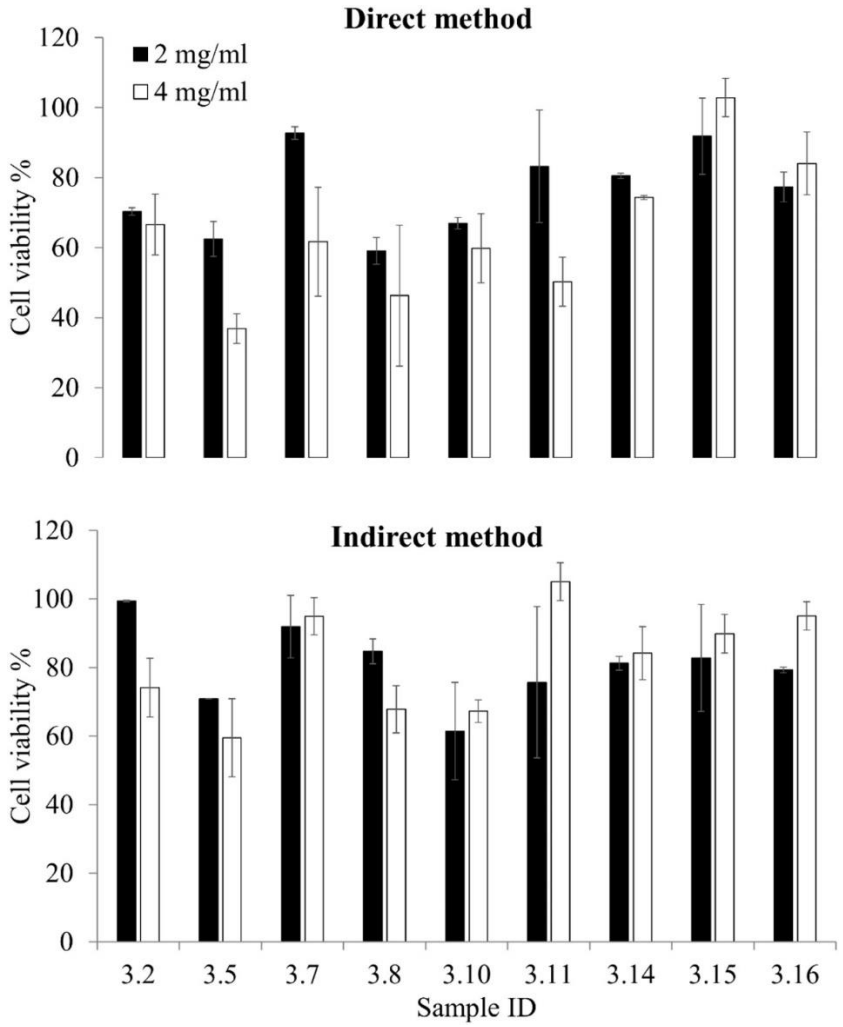

Figure 3-32: Fibroblasts viability for the prepared polyHIPEs by direct contact of the materials with the cells (direct method) or by conditioning the culture medium with the materials (indirect method), at two different concentrations 2 or 4 mg/ml

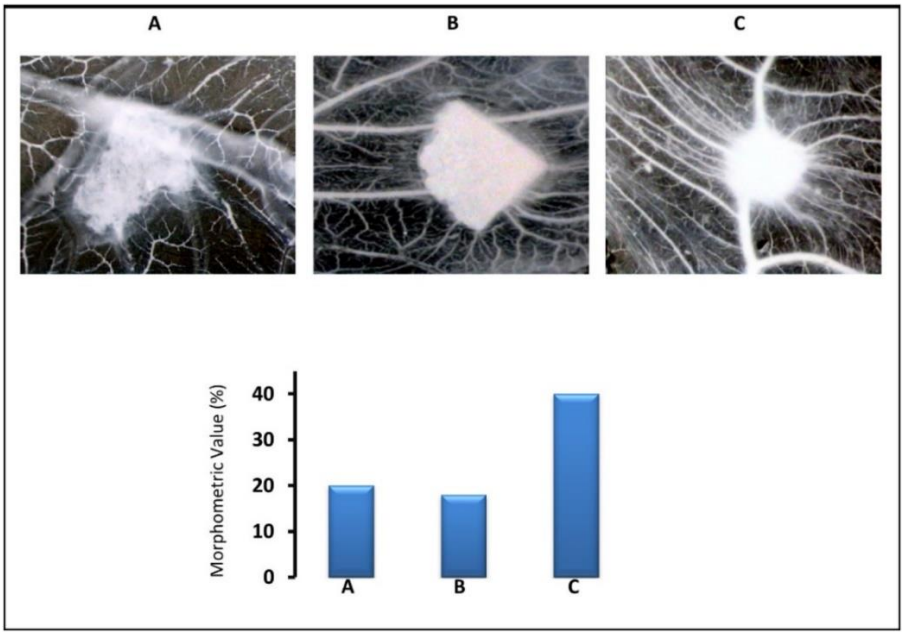

Figure 3-33: Samples 3.7 (A) or 3.11 (B), and VEGF (positive control) (C) tested by CAM assay

Thus, considering an angiogenic point of view, these materials can be considered inert, as the number of blood vessels around the samples is significantly less numerous as compared to the positive control. Considering that the prepared materials are thought for the dermal delivery of hydrophobic drugs it would be a great advantage applying on the skin a material that does not show any kind of angiogenic activity. If a particular angiogenic activity would be required by a specific application, a growth factor or, on the contrary, an anti-angiogenic substance could be added to the final formulation. As conclusive remarks, based on the collected data, we can assume that PEGMA has an important effect on the emulsion stability and in the monomer film contraction during polymerization. It leads to pore interconnections less numerous and smaller with respect to the samples without PEGMA. Probably, the softening effect of PEG on the main structure also induced some collapsing of the structure itself. The samples 3.7 and 3.11, both obtained from the bifunctional crosslinker, exhibited a controlled release of curcumin up to 5 days and remarkable cell compatibility.

4. Conclusions

Due to the growing interest in porous materials formed by the polyHIPE technique, this paper focuses on the specific use of these materials for drug delivery applications. At the best of our knowledge, this is among the first examples in literature in which a polyHIPE based biomaterial is used as a DDS. The most engineering aspects are being assessed, such as the obtainment of materials with well-reproducible thickness, shape and actual dimensions. In fact, the prepared samples showed tailorable features in terms of drug release depending on the internal structure. The possibility to easily sterilize these materials by thermal treatments, the good cytocompatibility and the results obtained from the in vivo chick embryo CAM assay showing that the prepared polyHIPEs are neither pro nor anti-angiogenic are fundamental to think at a direct application on wounded tissues after, e.g., the loading of antimicrobial drugs and biological molecules such as growth factors.

5. References

1. Langer, R., Where a pill won't reach. *Sci Am* **2003,** *288* (4), 50-7.

2. Mandracchia, D.; Piccionello, A. P.; Pitarresi, G.; Pace, A.; Buscemi, S.; Giammona, G., Fluoropolymer Based on a Polyaspartamide containing 1, 2, 4-Oxadiazole Units: A Potential Artificial Oxygen (O2) Carrier. *Macromolecular bioscience* **2007,** *7* (6), 836-845.

3. Rath, S. N.; Arkudas, A.; Lam, C. X.; Olkowski, R.; Polykandroitis, E.; Chroscicka, A.; Beier, J. P.; Horch, R. E.; Hutmacher, D. W.; Kneser, U., Development of a pre-vascularized 3D scaffold-hydrogel composite graft using an arterio-venous loop for tissue engineering applications. *J Biomater Appl* **2012,** *27* (3), 277-89.

4. Garg, T.; Goyal, A. K., Biomaterial-based scaffolds--current status and future directions. *Expert Opin Drug Deliv* **2014,** *11* (5), 767-89.

5. Hutmacher, D.; Bowlin, G. L., Nano-fiber scaffold science and tissue engineering. Foreword. *J Biomater Sci Polym Ed* **2008,** *19* (5), 541-2.

6. Pitarresi, G.; Tripodo, G.; Triolo, D.; Fiorica, C.; Giammona, G., Inulin vinyl sulfone derivative cross-linked with bis-amino PEG: new materials for biomedical applications. *Journal of Drug Delivery Science and Technology* **2009,** *19* (6), 419-423.

7. Dispenza, C.; Tripodo, G.; LoPresti, C.; Spadaro, G.; Giammona, G., Synthesis, characterisation and properties of alpha,beta-poly(N-2-hydroxyethyl)-DL-aspartamide-graft-maleic anhydride precursors and their stimuli-responsive hydrogels. *Reactive & Functional Polymers* **2009,** *69* (8), 565-575.

8. Tripodo, G.; Chlapanidas, T.; Perteghella, S.; Vigani, B.; Mandracchia, D.; Trapani, A.; Galuzzi, M.; Tosca, M. C.; Antonioli, B.; Gaetani, P.; Marazzi, M.; Torre, M. L., Mesenchymal stromal cells loading curcumin-INVITE-micelles: A drug delivery system for neurodegenerative diseases. *Colloids and Surfaces B-Biointerfaces* **2015,** *125*, 300-308.

9. Abd-Khorsand, S.; Saber-Samandari, S., Development of nanocomposite scaffolds based on TiO2 doped in grafted chitosan/hydroxyapatite by freeze drying method and evaluation of biocompatibility. *Int J Biol Macromol* **2017,** *101*, 51-58.

10. Hu, C.; Tercero, C.; Ikeda, S.; Nakajima, M.; Tajima, H.; Shen, Y.; Fukuda, T.; Arai, F., Biodegradable porous sheet-like scaffolds for soft-tissue engineering using a combined particulate leaching of salt particles and magnetic sugar particles. *J Biosci Bioeng* **2013,** *116* (1), 126-31.

11. Nam, Y. S.; Yoon, J. J.; Park, T. G., A novel fabrication method of macroporous biodegradable polymer scaffolds using gas foaming salt as a porogen additive. *J Biomed Mater Res* **2000,** *53* (1), 1-7.

12. Kankala, R. K.; Zhang, Y. S.; Wang, S. B.; Lee, C. H.; Chen, A. Z., Supercritical Fluid Technology: An Emphasis on Drug Delivery and Related Biomedical Applications. *Adv Healthc Mater* **2017,** *6* (16).

13. Raeisdasteh Hokmabad, V.; Davaran, S.; Ramazani, A.; Salehi, R., Design and fabrication of porous biodegradable scaffolds: a strategy for tissue engineering. *J Biomater Sci Polym Ed* **2017,** *28* (16), 1797-1825.

14. Silverstein, M. S., PolyHIPEs: Recent advances in emulsion-templated porous polymers. *Progress in Polymer Science* **2014,** *39* (1), 199-234.

15. Kimmins, S. D.; Cameron, N. R., Functional porous polymers by emulsion templating: recent advances. *Advanced Functional Materials* **2011,** *21* (2), 211-225.

16. Pulko, I.; Krajnc, P., High internal phase emulsion templating--a path to hierarchically porous functional polymers. *Macromol Rapid Commun* **2012,** *33* (20), 1731-46.

17. David, D.; Silverstein, M. S., Porous polyurethanes synthesized within high internal phase emulsions. *Journal of Polymer Science Part A: Polymer Chemistry* **2009,** *47* (21), 5806-5814.

18. Gurevitch, I.; Silverstein, M. S., Nanoparticle-based and organic-phase-based AGET ATRP polyHIPE synthesis within pickering HIPEs and surfactant-stabilized HIPEs. *Macromolecules* **2011,** *44* (9), 3398-3409.

19. Kovačič, S.; Kren, H.; Krajnc, P.; Koller, S.; Slugovc, C., The Use of an Emulsion Templated Microcellular Poly (dicyclopentadiene-co-norbornene) Membrane as a Separator in Lithium-Ion Batteries. *Macromolecular rapid communications* **2013,** *34* (7), 581-587.

20. Cameron, N. R.; Sherrington, D. C., High internal phase emulsions (HIPEs)—Structure, properties and use in polymer preparation. In *Biopolymers liquid crystalline polymers phase emulsion*, Springer: 1996; pp 163-214.

21. Barbetta, A.; Cameron, N. R., Morphology and surface area of emulsion-derived (PolyHIPE) solid foams prepared with oil-phase soluble porogenic solvents: Span 80 as surfactant. *Macromolecules* **2004,** *37* (9), 3188-3201.

22. Ikem, V. O.; Menner, A.; Horozov, T. S.; Bismarck, A., Highly permeable macroporous polymers synthesized from pickering medium and high internal phase emulsion templates. *Advanced Materials* **2010,** *22* (32), 3588-3592.

23. Yang, X.; Tan, L.; Xia, L.; Wood, C. D.; Tan, B., Hierarchical Porous Polystyrene Monoliths from PolyHIPE. *Macromol Rapid Commun* **2015,** *36* (17), 1553-8.

24. Lissant, K., *Emulsions and emulsion technology*. CRC Press: 1974; Vol. 3.

25. Su, R.; Ruan, G.; Nie, H.; Xie, T.; Zheng, Y.; Du, F.; Li, J., Development of high internal phase emulsion polymeric monoliths for highly efficient enrichment of trace polycyclic aromatic hydrocarbons from large-volume water samples. *Journal of Chromatography A* **2015,** *1405*, 23-31.

26. Sears, N. A.; Dhavalikar, P. S.; Cosgriff-Hernandez, E. M., Emulsion Inks for 3D Printing of High Porosity Materials. *Macromolecular Rapid Communications* **2016,** *37* (16), 1369-1374.

27. Depardieu, M.; Kinadjian, N.; Backov, R., Integrative Chemistry: Advanced functional cellular materials bearing multiscale porosity. *The European Physical Journal Special Topics* **2015,** *224* (9), 1655-1668.

28. Tripodo, G.; Marrubini, G.; Corti, M.; Brusotti, G.; Milanese, C.; Sorrenti, M.; Catenacci, L.; Massolini, G.; Calleri, E., Acrylate-based poly-high internal phase emulsions for effective enzyme immobilization and activity retention: From computationally-assisted synthesis to pharmaceutical applications. *Polymer Chemistry* **2018,** *9* (1), 87-97.

29. Hu, W.; Xie, F.; Li, Y.; Wu, Z.; Tian, K.; Wang, M.; Pan, L.; Li, L., Hierarchically Porous Carbon Derived from PolyHIPE for Supercapacitor and Deionization Applications. *Langmuir* **2017,** *33* (46), 13364-13375.

30. Wright, A. J.; Main, M. J.; Cooper, N. J.; Blight, B. A.; Holder, S. J., Poly High Internal Phase Emulsion for the Immobilization of Chemical Warfare Agents. *ACS Appl Mater Interfaces* **2017,** *9* (37), 31335-31339.

31. Kulygin, O.; Silverstein, M. S., Porous poly (2-hydroxyethyl methacrylate) hydrogels synthesized within high internal phase emulsions. *Soft Matter* **2007,** *3* (12), 1525-1529.

32. Christenson, E. M.; Soofi, W.; Holm, J. L.; Cameron, N. R.; Mikos, A. G., Biodegradable fumarate-based polyHIPEs as tissue engineering scaffolds. *Biomacromolecules* **2007,** *8* (12), 3806-3814.

33. Lumelsky, Y.; Lalush-Michael, I.; Levenberg, S.; Silverstein, M. S., A Degradable, Porous, Emulsion-Templated Polyacrylate. *Journal of Polymer Science Part a-Polymer Chemistry* **2009,** *47* (24), 7043-7053.

34. Dumitriu, S., *Polymeric biomaterials, revised and expanded*. Crc Press: 2001.

35. Brusotti, G.; Calleri, E.; Milanese, C.; Catenacci, L.; Marrubini, G.; Sorrenti, M.; Girella, A.; Massolini, G.; Tripodo, G., Rational design of functionalized polyacrylate-based high internal phase emulsion materials for analytical and biomedical uses. *Polymer Chemistry* **2016,** *7* (48), 7436-7445.

36. Streifel, B. C.; Lundin, J. G.; Sanders, A. M.; Gold, K. A.; Wilems, T. S.; Williams, S. J.; Cosgriff-Hernandez, E.; Wynne, J. H., Hemostatic and Absorbent PolyHIPE-Kaolin Composites for 3D Printable Wound Dressing Materials. *Macromol Biosci* **2018,** *18* (5), e1700414.

37. McGann, C. L.; Streifel, B. C.; Lundin, J. G.; Wynne, J. H., Multifunctional polyHIPE wound dressings for the treatment of severe limb trauma. *Polymer (United Kingdom)* **2017,** *126*, 408-418.

38. Ribatti, D.; Nico, B.; Vacca, A.; Presta, M., The gelatin sponge-chorioallantoic membrane assay. *Nature Protocols* **2006,** *1* (1), 85-91.

39. Pulido-Moran, M.; Moreno-Fernandez, J.; Ramirez-Tortosa, C.; Ramirez-Tortosa, M. C., Curcumin and health. *Molecules* **2016,** *21* (3).

40. Papoutsi, D.; Lianos, P.; Brown, W., Interaction of Polyethylene Glycol with Water-in-Oil Microemulsions. 3. Effect of Polymer Size and Polymer Concentration. *Langmuir* **1994,** *10* (10), 3402-3405.

41. Cameron, N. R., High internal phase emulsion templating as a route to well-defined porous polymers. *Polymer* **2005,** *46* (5), 1439-1449.

42. Jerenec, S.; Šimić, M.; Savnik, A.; Podgornik, A.; Kolar, M.; Turnšek, M.; Krajnc, P., Glycidyl methacrylate and ethylhexyl acrylate based polyHIPE monoliths: Morphological, mechanical and chromatographic properties. *Reactive and Functional Polymers* **2014,** *78*, 32-37.

43. Lee, A.; Langford, C. R.; Rodriguez-Lorenzo, L. M.; Thissen, H.; Cameron, N. R., Bioceramic nanocomposite thiol-acrylate polyHIPE scaffolds for enhanced osteoblastic cell culture in 3D. *Biomater Sci* **2017,** *5* (10), 2035-2047.

44. Caldwell, S.; Johnson, D. W.; Didsbury, M. P.; Murray, B. A.; Wu, J. J.; Przyborski, S. A.; Cameron, N. R., Degradable emulsion-templated scaffolds for tissue engineering from thiol–ene photopolymerisation. *Soft Matter* **2012,** *8* (40), 10344-10351.

GENERAL CONCLUSIONS AND PERSPECTIVES

In this project, the development of a versatile and adjustable acrylate-based polymeric structure has been described. The synthesis of polymeric materials was carried out by using water-in-oil high internal phase emulsions as a template for the macroporous structure. In order to obtain biocompatible materials, we selected acrylate monomers. Therefore, we selected butyl acrylate as the backbone monomer, glycidyl methacrylate as the functional monomer and trimethylolpropane triacrylate as the crosslinker agent. During the first year of the Ph.D. project, the synthetic procedure was established, and validation of this protocol was provided by the application of a Design of Experiment approach. Indeed, materials features (namely swelling in water and THF, mass loss in water and THF, throats and voids diameter) were modeled using D-optimal mixture design. Therefore, a correlation between the applied synthetic conditions and final properties was demonstrated. After the evaluation of acrylate-based polyHIPE materials to be used for the binding of enzymes in an active form (we used HRP as a model enzyme) and successfully applied under flow conditions, the second year of this project was focused on the development of suitable supports for the production of in-flow bioreactors. Therefore, a polymeric LC-stationary phase was synthesized by developing a polyHIPE-based monolithic column. Then, a suitable macromolecule of pharmaceutical interest was selected to be immobilized into the developed polyHIPE column. In this context, the research group of Pharmaceutical Analysis Laboratory (PAL) of the University of Pavia was involved in a Cariplo Foundation project, called “Bioflow” aimed at the development of bioreactors for the in-flow biocatalyzed synthesis of APIs. Therefore, ATA-117, an (R)-selective ω-transaminase was selected. The so obtained bioreactor was applied for the in-flow synthesis of phenylpropanolamine as a pharmaceutical interest building block, i.e. 1-methyl-3-phenylpropylamine (MPPA). MPPA is an intermediate for the production of dilevalol, the (R, R)-isomer of labetalol, an already commercially available antihypertensive drug. Another important aim of this project was the evaluation of the potentialities of acrylate-based polyHIPEs to be used in biomedical applications. For this purpose, some modifications of starting HIPE compositions were considered and polymeric materials in flatforms were produced. In particular, the effect of PEG methacrylate on the main properties of the final polyHIPEs was investigated. Therefore, one of the main aims of the third year was the preparation of polyacrylate based biomaterials as drug delivery systems by using polyHIPE technology. The obtained polyHIPE materials showed tailorable curcumin (selected as a model of hydrophobic drugs) drug release and cell compatibility (evaluated on human fibroblasts). Based on these results,

the developed polyHIPEs could be proposed as devices for future production of drug delivery systems.

In conclusion, we demonstrated that polyHIPE technology is a valuable technique for the production of porous polymers showing a well-defined and hierarchical network of pores. The potential of these polymeric materials was explored in different fields leading to the synthesis of valuable solid supports. Indeed, it was possible to produce:

1. Laboratory-scale transaminase-IMER for the synthesis of chiral amines as building blocks of pharmaceutical interest by using a polyHIPE-based monolithic column. Moreover, by the exploitation of the ease of curing polyHIPEs in different shapes and dimensions, these materials seem to be appealing even for a scale-up of the biocatalytic process.
2. Biocompatible polyHIPE-based scaffolds for hydrophobic bioactive molecules loading and their release in an aqueous medium in order to provide controlled local drug delivery systems using curcumin as a model lipophilic molecule.

We also highlighted the extreme versatility of this kind of material. Indeed, by little modifications of the starting emulsion compositions, we were able to produce polyHIPEs in different shapes and showing easily tailorable properties. The results obtained and reported in this work are paving the way for future studies aimed at the development of high performance, active and smart materials. Indeed, we demonstrated that polyHIPE technology is an efficient method for the synthesis of polyacrylate-based supports to be exploited in several application fields including pharmaceutical, biomedical and many others.